Production of η and η' Mesons on Nucleons and Nuclei

B. Krusche[1] and C. Wilkin[2]

[1] Department of Physics, University of Basel, CH-4056 Basel, Switzerland
[2] Physics and Astronomy Department, UCL, Gower Street, London WC1E 6BT, UK

October 29, 2014

arXiv:1410.7680v1 [nucl-ex] 28 Oct 2014

Abstract

The production of η and η' mesons in photon- and hadron-induced reactions on free and quasi-free nucleons and on nuclei is reviewed. The extensive database on $\gamma N \to \eta N$, for both proton and neutron targets, is described in detail and its implications for the search for $N^\star$ resonances much heavier than the dominant $S_{11}(1535)$ discussed. Though less is currently known about the production of the η' or of $\eta\pi$ pairs, these also offer tantalizing prospects in the search for the missing isobars. The more limited data available on pion-induced production are still necessary ingredients in the partial wave analysis discussed.

The production of the η-meson in pp and pn collisions shows once again the strong influence of the $S_{11}(1535)$ isobar, which is in contrast to the relatively weak behaviour seen near threshold for η' production. This difference is reflected in the important final state interaction effects of the η in nuclei that may even lead to this meson being "bound" in some systems. The evidence for this is reviewed for both γA and pA collisions. The inclusive photoproduction of η, η', and $\eta\pi$ pairs from nuclei provides further information regarding the production mechanism and the interaction of the η and η' with nuclei and the $\eta\pi$ pairs may even allow access to low mass ηA systems that are forbidden in direct single-meson photoproduction.

1 Introduction

Although the isovector π and the isoscalar η and η' represent the non-strange members of the fundamental pseudoscalar meson nonet, their interactions with nucleons are dramatically different. The s-wave πN interactions are very weak and at only a few MeV above threshold the p-wave, driven by the $\Delta(1232)$ isobar, starts to dominate. In complete contrast, the S_{11} $N^*(1535)$ resonance sits very close to the ηN threshold, which means that the s-wave ηN interaction is extremely strong and its effects are felt in many of the phenomena discussed in this review. Finally, there is far less unambiguous evidence for isobars that have large decay widths into the $\eta' N$ channel so that one would expect the near-threshold behaviour of η' production to be very different from that of the η, and this is precisely what one finds.

This review is concerned with the production of η and η' mesons with both photons and hadronic probes. Earlier articles have surveyed various aspects of the field [1, 2, 3, 4, 5], but possibly with not such a wide remit. Our primary thrust will be to discuss physics phenomena rather than the details of theoretical models. The first part of this survey is concerned with *elementary reactions*, by which we mean production reactions that involve only a single nucleon. It is immediately apparent here that the sad lack of secondary pion beams in the world compared to the richness of possibilities offered at

electron machines means that the vast majority of the new data in this field were obtained with photon (or electron) beams. This imbalance has, of course, to be reflected in our review.

Because of its large mass and isoscalar nature, the ηN system has a very important role to play in the search for the *missing* $N^\star$ ($I = \frac{1}{2}$) isobars. This search would be simpler if one had a complete set of measurements of the $\pi^- p \to \eta n$ reaction, because there is here only one isospin channel. In photoproduction there are contributions from both isoscalar and isovector photons (plus interference terms) so that an experimental programme involving (quasi-free) neutrons is completely essential to resolve some of the ambiguities. Nevertheless, the rich collection of photoproduction data, both current and under analysis, involving both polarized photons and nucleons, means that these results largely dominate the partial wave analyses. Though there are data also on the photoproduction of both the η' and $\eta\pi$ pairs from nucleons, these have yet to have their full impact on the search for heavy nucleon isobars.

Once the η meson has been produced, it interacts very strongly with nucleons and this is seen in its photoproduction off light nuclei but possibly even more clearly in nucleon-nucleon or nucleon-nucleus reactions. The interaction is so strong, and attractive that it might even lead to the formation of quasi-bound states of an η meson with a nucleus. The evidence for this is reviewed in both electromagnetic and hadronic reactions. The searches above threshold suggest that such a state might exist for a light nucleus such as ${}^{3}_{\eta}$He, though no evidence for this is found from other decay channels looking in the bound state region.

Though the beam intensities can be very strong, and one is not hindered by the suppression associated with the fine structure constant, proton-induced reactions have a serious problem with the enormous total hadronic background. This is especially troublesome if one cannot trigger on a clean η signal and there have been few experiments with heavier nuclei. On the other hand, the selection rules in coherent (γ, η) reactions strongly hinder most direct searches for mesic nuclei but this will not be the case for the $(\gamma, \eta\pi)$ reactions that can be measured on nuclei as well as nucleons.

Much less is known about the production and interaction of the η' meson. Photon-induced transparency measurements suggest that the interaction with nucleons is weakly attractive but data from $pp \to pp\eta'$ near threshold find little indication for any significant $\eta' p$ interaction. This point is very relevant in the discussion of possible quasi-bound states of an η' with a nucleus.

2 Elementary reactions

In this section we summarize the basic properties of the production of η and η' mesons from free and quasi-free nucleons using photon and pion beams. Production reactions off the proton can be studied with the free protons contained in hydrogen targets. But, in the case of photon-induced reactions, the disentanglement of the isospin composition of the reaction amplitudes requires also measurements off neutrons. This is only possible in quasi-free kinematics with neutrons bound in light nuclei, in particular the deuteron. Therefore we discuss here reactions with both free protons and also quasi-free nucleons from light nuclei, when the aim is the study of the elementary cross section for neutrons.

2.1 Production in γN reactions

Photon-induced reactions have cross sections that are typical for electromagnetic interactions and are thus much smaller than those for reactions induced by hadrons via the strong force. However, over the last two decades a large effort has been made to study meson production reactions with real (tagged photons) or virtual (electron scattering) photon beams with experiments at modern electron-accelerator facilities. Experiments such as Crystal Barrel/TAPS [6, 7] at ELSA [8] in Bonn (Germany), the CLAS detector at Jlab in Newport News [9] (USA), the GRAAL facility at ESRF in Grenoble [10] (France),

the Crystal Ball/TAPS setup [7, 11] at MAMI [12] in Mainz (Germany), the LEPS facility at SPring-8 in Osaka [13] (Japan), and the GeV-γ experiment at LNS at Tohoku University [14] in Sendai (Japan) have dominated this research. A short overview of these experiments is given in [5].

As a consequence of these efforts, for many final states the precision of the results from electromagnetic production reactions may now be as good or even better than those from hadron beams. This is particularly true for the production of η and η' mesons. As a side remark, for these two mesons photon-induced production off protons (which is a very 'clean' production reaction) even becomes important for the investigation of (rare) meson decays. Recent results from this programme at MAMI for η mesons include measurements of the slope parameter for the Dalitz plot of the $\eta \to 3\pi^0$ decay [15, 16], of the η transition form factor from the $\eta \to e^+e^-\gamma$ Dalitz decay [17], and of the rare $\eta \to \pi^0\gamma\gamma$ decay [18]. Programmes for the study of rare η' decays are under way at ELSA and at MAMI.

In the meantime, the GRAAL experiment has been shut-down and the CLAS detector has stopped data taking and is under preparation for the Jlab 12-GeV upgrade (though many observables measured by CLAS for different reactions are still under analysis and will only become available over the next few years). Programmes for the measurement of single and double polarization observables are still under way at the ELSA and MAMI facilities, where the emphasis is gradually shifting towards the neutron target. These two experiments will fill the gap in the data base for photoproduction reactions with more than one neutral particle (nucleon or meson) in the final state.

The experimental approaches at these laboratories were in general different (and complementary), especially for the reactions discussed in this review ($\gamma N \to N\eta$, $\gamma N \to N\eta'$, $\gamma N \to N\eta\pi$). The main features of the facilities that are most important for the experiments discussed here are:

- The CEBAF Large Acceptance spectrometer (CLAS) [9] was housed in Hall B of the Thomas Jefferson National Accelerator Facility in Newport News. This experiment was optimized for the detection of charged particles (protons, charged pions,...) using a magnetic field. The resolution for the momenta of charged particles was thus superior to the other experiments. Neutral particles, such as neutrons or mesons decaying into photons, could only be identified via missing-mass analysis (only a small fraction of the total solid angle at forward angles was equipped with an electromagnetic calorimeter and this provided only a very restricted acceptance for photons). This experiment therefore achieved excellent performance for final states with not more than one neutral particle but could not measure final states with neutral meson production off neutrons or pairs of neutral mesons (e.g. $\pi^0\pi^0$ or $\pi^0\eta$). The maximum electron beam energy was 6 GeV; linearly and circularly polarized beams and longitudinally and transversely polarized targets have been used.

The other experiments avoided magnetic spectroscopy and employed electromagnetic calorimeters with (almost) 4π coverage for the detection of photons, charged hadrons (protons, charged pions,...), and neutrons. For these experiments the reaction identification is based on combined invariant and missing-mass analyses (kinematic fitting is often used for the proton target).

- Crystal Barrel/TAPS at ELSA: the combination of the Crystal Barrel (CBB, CsI(Tl) scintillators) [6] detector with the TAPS calorimeter (BaF_2 scintillators) [7] provides a device that can detect and identify photons and recoil nucleons over almost the full solid angle. However, in the configuration used up to now, only a small part of the calorimeter (at laboratory polar angles below 30°) provided trigger information, because only this part (TAPS forward detector and CBB forward plug) was equipped with photomultipliers. The main part of the CBB was read out by photodiodes, which did not deliver timing and trigger information. Additional trigger information was derived from a detector for charged particle identification that surrounded the target. Thus, for measurements with a free proton target, the recoil proton provided the trigger. Measurements off quasi-free neutrons were so far only possible for high-multiplicity final states

(such as $\eta \to 3\pi^0 \to 6\gamma$ or $\eta' \to \pi^0\pi^0\eta \to 6\gamma$), for which the probability of some photons hitting the calorimeter at small angles is sufficiently large. Currently the CBB is undergoing an upgrade (readout with Avalanche Photodiodes) which will eliminate this restriction. The maximum electron beam energy is 3.5 GeV; linearly and circularly polarized beams are available and transversely and longitudinally polarized targets have been used.

- Crystal Ball/TAPS at MAMI: The detector setup is very similar to that at ELSA, also covering almost 4π with the Crystal Ball (CBM, NaI scintillators) [11] and using TAPS as a forward wall (the TAPS calorimeter has been split into two parts, allowing simultaneous experiments at ELSA and MAMI). Since the Crystal Ball modules are equipped with photomultipliers, this detector can trigger on photons over the full solid angle covered. It is thus capable of also measuring reactions with low photon multiplicities off quasi-free neutrons such as $\gamma n \to n\eta \to n\gamma\gamma$. The maximum electron beam energy is 1.5 GeV; polarized beams and polarized targets are available.

- The GRAAL experiment: The central detector component [10] was also an electromagnetic calorimeter constructed from BGO modules (covering polar angles from 25° to 155°) combined with forward detectors (wire chambers, time-of-flight hodoscopes from plastic scintillators, lead-scintillator sandwich) used mainly for recoil nucleon detection. In contrast to the previous experiments, which all used bremsstrahlung beams, GRAAL located at the ESRF in Grenoble, used laser backscattering. The maximum photon energy was 1.5 GeV; linearly and circularly polarized photon beams were available, but no polarized targets were used.

- The BGO-OD experiment at ELSA: This experiment [19] is still in the setup phase. It is mentioned here because experiments to search for η' mesic states have been suggested for this unique facility [20]. The main components are the BGO calorimeter, previously used in the GRAAL experiment, and a dipole magnet (and tracking detectors) at forward angles. It will thus combine an almost 4π coverage for photons with magnetic spectrometry for forward-going charged particles. These features allow an efficient detection of neutral mesons, using invariant-mass analysis for their photon decays, together with high-resolution momentum spectrometry for recoil protons.

The main motivation for the study of photon-induced meson production off nucleons is the investigation of the excitation spectrum of the nucleon, which is one of the most important testing grounds for Quantum Chromodynamics (QCD) in the non-perturbative regime (see [21] for a recent summary). In the past, most information about excited nucleon states was gained from pion scattering; even today most states listed in the summary tables of the Review of Particle Physics (PDG) [22] were 'discovered' in this reaction. Only in the last update of the PDG [23] a few states also appear that were first reported from photon-induced reactions. This situation will change drastically in the near future when the large body of data from photon-induced reactions become available, not only for the $N\pi$ channel, but also for many other final states.

Photoproduction of η and η' mesons is complementary to the $N\pi$ final state in several aspects. The isoscalar η, η' are only emitted in the decay of isospin $I = 1/2$ $N^\star$ resonances. Furthermore, due to their large mass, the number of contributing partial waves at a given incident photon energy is more limited than for pions. This not only simplifies the model analyses, but it makes these mesons particularly promising tools for the study of low-spin $N^\star$ states at reasonably high excitation energies. Such states are at the core of the 'missing resonance' problem: many more states have been predicted by nucleon models than have been so far observed experimentally [22]. For most quantum numbers only the lowest lying state has so far been observed in experiment though models predict many higher lying states.

The photoproduction of $\pi\eta$ pairs, like double pion production, aims at the study of excited nucleon states that have only a small branching ratio for direct decay to the nucleon ground state but decay in a cascade via an intermediate excited state. In such a cascade decay, isospin conservation allows η

emission for $N^\star \to N^{(\star)}$ and $\Delta^\star \to \Delta^{(\star)}$ transitions, while all combinations are possible for the pion emission. As discussed later, this reaction offers interesting possibilities for the search for η-mesic states for nuclei for which coherent production of single η mesons is forbidden or suppressed.

Photoproduction reactions off protons can be studied with hydrogen targets (typically liquid H_2). However, since the electromagnetic interaction is charge dependent, measurements off the neutron are also required. The isospin decomposition for photoproduction of isoscalar mesons like the η and η' is simple; the amplitudes for the reactions off protons and neutrons are:

$$\begin{aligned} A(\gamma p \to \eta p) &= (A^{IS} + A^{AV}) \\ A(\gamma n \to \eta n) &= (A^{IS} - A^{AV}) \end{aligned} \tag{2.1}$$

with the (photon) isoscalar and isovector amplitudes A^{IS} and A^{IV}. The data base for reactions with neutrons in the initial state is so far much more limited than for the corresponding reactions off protons. Since free neutrons are not available, it is unavoidable to extract the information about the elementary $\gamma n \to Nx$ reactions (N: nucleon, x: any meson or mesons) from experiments using nuclear targets. Such measurements are technically more challenging and, for the interpretation of the results, several complications must be taken into account.

The experimental issues arise from the necessary coincident detection of the recoil nucleons. Experiments based on magnetic momentum analysis of the produced particles are therefore limited to final states with charged mesons (e.g. $\gamma n \to p\pi^-$). Electromagnetic calorimeters that cover large solid angles are much better suited for this purpose. However, even in this case, neutron detection (with typical efficiencies on the order of 10-30%) reduces the statistical precision of the results compared to the corresponding measurements off proton targets. The neutron detection efficiency, and the possible contamination of the neutron sample with misidentified protons, introduce additional systematic uncertainties. The statistical quality of the data achievable has been much enhanced over the last few years, mainly due to the ever increasing speed of the data acquisition systems (this is in particularly true for experiments such as Crystal Ball/TAPS at MAMI, where the primary beam intensity can be increased to whatever values the detection system can cope with). Even measurements of double polarization observables off neutrons are thus feasible.

Systematic effects from the detection of the recoil neutrons are most important for cross section measurements (they cancel at least partially in asymmetries). Although the Monte Carlo codes (mostly Geant4 [24]) used for the simulation of detection efficiencies include special program packages for neutrons, these are not as precise as for protons and by no means as precise as for electromagnetic showers. Precision can be increased by comparing the simulated detection efficiencies to measurements using, for example, reactions like $\gamma p \to p\pi^0$, $\gamma p \to p\eta$ (for recoil protons) or $\gamma p \to n\pi^+$, $\gamma p \to n\pi^0\pi^+$ (for recoil neutrons) with free protons targets, where the detection efficiency as function of the nucleon momentum and polar angle can be directly determined from the ratios of events with and without coincident nucleons.

Most experiments with light nuclear targets (deuterons, ^{3}He) discussed below used, in addition, the internal consistency of the data. For this purpose the cross sections of the two exclusive reactions $\gamma d \to xp(n)$ (σ_p) and $\gamma d \to xn(p)$ (σ_n) (x: any meson or system of mesons, p,n detected participant nucleons, (n),(p) non-detected spectator nucleons) are compared to the cross section $\sigma_{\rm incl}$ of the inclusive reaction $\gamma d \to xX$ (X: candidate for recoil proton or recoil neutron or not present). The inclusive cross section accepts all events, independent of whether a candidate for a recoil nucleon was detected or not. It thus includes, for example, the roughly 70 - 90% of events with recoil neutrons that escape detection. For most reactions discussed below the cross section of the coherent process $\gamma d \to dx$ is negligible (or can be determined and included in the comparison) so that $\sigma_{\rm incl} = \sigma_p + \sigma_n$ must hold. Since $\sigma_{\rm incl}$ is independent of recoil nucleon detection efficiencies this comparison provides a powerful cross check.

The interpretation of the results obtained in quasi-free kinematics is complicated by two factors. All

results depend on the momentum distribution assumed for the bound nucleons and final state interaction (FSI) processes may obscure the properties of the elementary reactions off free nucleons.

The importance of Fermi motion effects can vary significantly. For example, cross section measurements at energies away from the production threshold of the investigated process will be only somewhat smeared out with respect to the free reactions. In regions where the cross section does not show sharp variations or narrow structures, such effects can easily be accounted for by folding model results with the assumed nucleon momentum distributions. On the other hand, fast variations of the cross sections can be strongly suppressed and asymmetries can be significantly modified by the Fermi motion.

For differential cross sections and asymmetries it is important to extract the meson polar and azimuthal angles in the true photon-nucleon centre-of-momentum (c.m.) frame, taking into account the incident nucleon momenta, so that the z-axis is no longer along the photon beam axis. Fortunately, most experiments allow a complete kinematic reconstruction of the Fermi momenta. For a typical $\gamma d \to xN_1(N_2)$ reaction the kinematics of the initial state (photon with energy E_γ moving along beam axis and hitting a deuteron at rest) is completely determined. In the final state the three-momentum $\vec{p}_x$ and the mass m_x of the meson (or system of mesons) x are known. For the detected participant nucleon N_1 all angles and its mass are known. This means that the direction $\vec{p}_{N_1}/|\vec{p}_{N_1}|$ of its momentum is measured. In the case of recoil protons, their kinetic energy can often also be extracted from the energy deposition in the calorimeter, but this is not true for recoil neutrons. Finally, for the undetected spectator nucleon (N_2) only its mass is known. This means that four kinematic quantities in the final state - the kinetic energy of the participant nucleon and the three-momentum of the spectator - are missing. These four quantities can be extracted from the four equations that follow from energy-momentum conservation. The four-momenta of all three final state particles can thus be reconstructed and used to determine the effective c.m. system and the effective total energy W in that system in plane-wave approximation. The only disadvantage of this method is that the extraction of W depends on the experimental resolution (angles, deposited energies) of the production detector while, for tagged photon measurements off free protons, it depends only on the momentum resolution for the scattered electrons in the tagging device, which is usually much better (for example for Crystal Ball/TAPS at MAMI a few MeV from tagging compared to a few 10 MeV from kinematic reconstruction).

Final state interactions between the two recoil nucleons, a nucleon and a meson, or even three-particle effects, show two completely different faces for the research reviewed in this paper. For the measurement of elementary reactions off neutrons discussed in this section, they present difficulties that must be understood and corrected for as far as possible. On the other hand, FSI effects offer the only access to the interaction of short lived mesons (which cannot be prepared as secondary beams) with nucleons. The experiments aiming at meson-nucleus bound states discussed later in this review are entirely based on meson-nucleon (meson-nucleus) FSI.

The influence of FSI on the elementary reactions is so far not very well understood. It depends strongly for example on the reaction channels and its effects are also probably rather different for different observables for the same reaction channel. Experimentally one can, of course, get some information about FSI effects from a comparison of the results for a quasi-free $\gamma d \to xp(n)$ reaction with free $\gamma p \to xp$ data. It might even be tempting to use the deviations between these two reactions as a correction to approximate the observables of the $\gamma n \to xn$ reaction by the results measured for the quasi-free $\gamma d \to xn(p)$ meson production, but this approximation is certainly not always valid.

Examples for strong FSI effects reported in the literature are, for example, those for pion photoproduction off quasi-free nucleons [25, 26, 27, 28]. However, for the same reactions (e.g., $\gamma d \to (n)p\pi^0$) effects for polarization observables seem to be less important [29]. As it turns out (see results discussed below) for single η and η' meson photoproduction FSI effects are not even important for cross sections but play a substantial role for the photoproduction of $\eta\pi$ pairs.

2.1.1 *Photoproduction of η-mesons off nucleons*

The photoproduction of η-mesons off free protons was studied at all the major tagged photon facilities, sometimes even with repeated and improved experiments. Quasi-free η production off neutrons has also recently attracted much interest. We first summarize the available data base. The total cross section data are shown in Fig. 1. For publications that quoted only values for the differential cross sections (as long as they covered a reasonable range in the polar angle) the total cross section was extracted from fits to the angular distributions (see below).

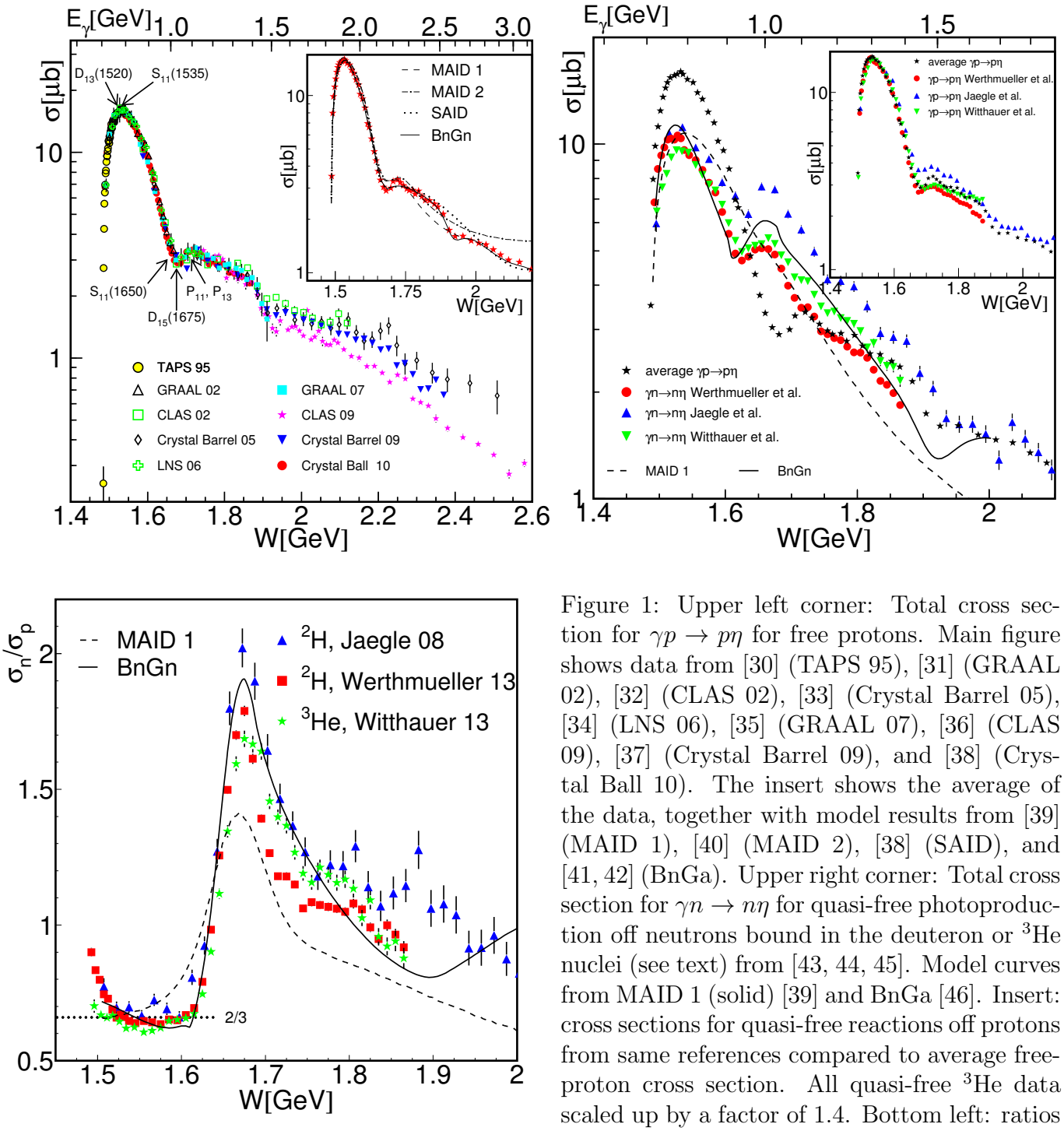

Figure 1: Upper left corner: Total cross section for $\gamma p \to p\eta$ for free protons. Main figure shows data from [30] (TAPS 95), [31] (GRAAL 02), [32] (CLAS 02), [33] (Crystal Barrel 05), [34] (LNS 06), [35] (GRAAL 07), [36] (CLAS 09), [37] (Crystal Barrel 09), and [38] (Crystal Ball 10). The insert shows the average of the data, together with model results from [39] (MAID 1), [40] (MAID 2), [38] (SAID), and [41, 42] (BnGa). Upper right corner: Total cross section for $\gamma n \to n\eta$ for quasi-free photoproduction off neutrons bound in the deuteron or ^{3}He nuclei (see text) from [43, 44, 45]. Model curves from MAID 1 (solid) [39] and BnGa [46]. Insert: cross sections for quasi-free reactions off protons from same references compared to average free-proton cross section. All quasi-free ^{3}He data scaled up by a factor of 1.4. Bottom left: ratios of quasi-free neutron and proton cross sections for data and models shown in the earlier panels.

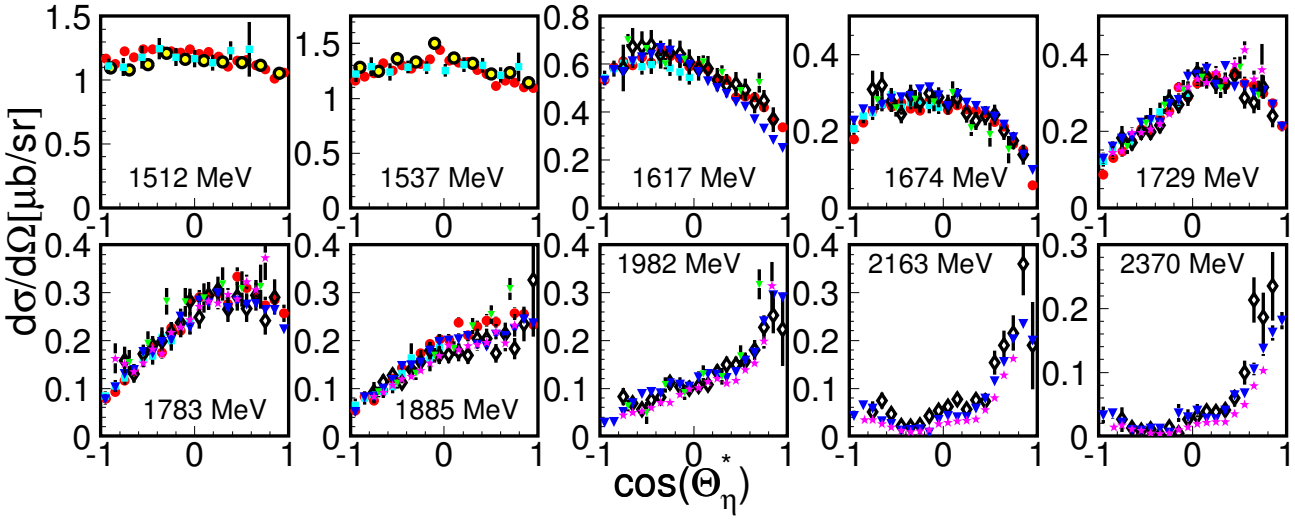

Figure 2: Comparison of angular distributions from different measurements for some typical c.m. energies W for $\gamma p \to p\eta$. Symbols are as in Fig. 1.

Angular distributions for the $\gamma p \to p\eta$ reaction have been reported in [30, 31, 32, 33, 34, 35, 47, 37, 36, 48, 38] (we have omitted some older references that can be found in [49]). Typical examples that demonstrate the level of agreement between the experiments are shown in Fig. 2. Several different experimental approaches have been used so that the sources of systematic error are different. The first CLAS experiment [32] identified the η mesons through a missing-mass analysis of the recoil protons and determined the absolute normalization of the cross sections by comparing the data for single π^0 production (analyzed in the same way) with the results of the SAID partial wave analysis. This CLAS experiment included all the η decay channels. The second CLAS experiment [36] used the $\eta \to \pi^+\pi^-\pi^0$ decay channel, detected the two charged pions and the recoil proton, reconstructed the π^0 in a kinematic fit, and then studied the invariant mass of the three pions. The cross sections were absolutely normalized.

The first Crystal Barrel experiment [33, 47] used the $\eta \to 2\gamma$ and $\eta \to 3\pi^0 \to 6\gamma$ decay channels of the η meson (analyzed by invariant mass after kinematic fitting) but triggered on the recoil proton. This experiment also used the SAID π^0 results for absolute normalization. The second experiment [37] was similar, but used an absolute measurement of the photon flux and target density for normalization. Also in the GRAAL experiment [35] the two- and six-photon decay channels of the η-meson were analyzed and an absolute normalization was made. All the experiments discussed above detected the coincident recoil protons (which is useful to ensure overdetermined kinematics but also introduces a further source of systematic uncertainty). The two MAMI experiments used the two-photon decay of the η [30] or the six-photon decay [38] and did not require detection of the recoil proton. Both experiments were absolutely normalized.

The angular distributions were fitted in a series of Legendre polynomials up to fourth order:

$$\frac{d\sigma}{d\Omega}(W, \cos\theta^*_\eta) = \frac{q^*_\eta(W)}{k^*_\gamma(W)} \sum_{i=0}^{N} A_i(W) P_i(\cos\theta^*_\eta)\,, \tag{2.2}$$

where the coefficient A_0 is related to the total cross section $\sigma(W)$ by $A_0(W) = 4\pi(k^*_\gamma(W)/q^*_\eta(W))\sigma(W)$. Here q^*_η and k^*_γ are c.m. momenta of the η and γ, respectively. The coefficients for fits with N=4 normalized to A_0 are summarized in Figs. 4 and 5.

The measurement of angular distributions and total cross sections for the quasi-free $\gamma n \to n\eta$ reaction has recently made much progress. Early experiments measured only the inclusive reaction $\gamma d \to \eta(np)$

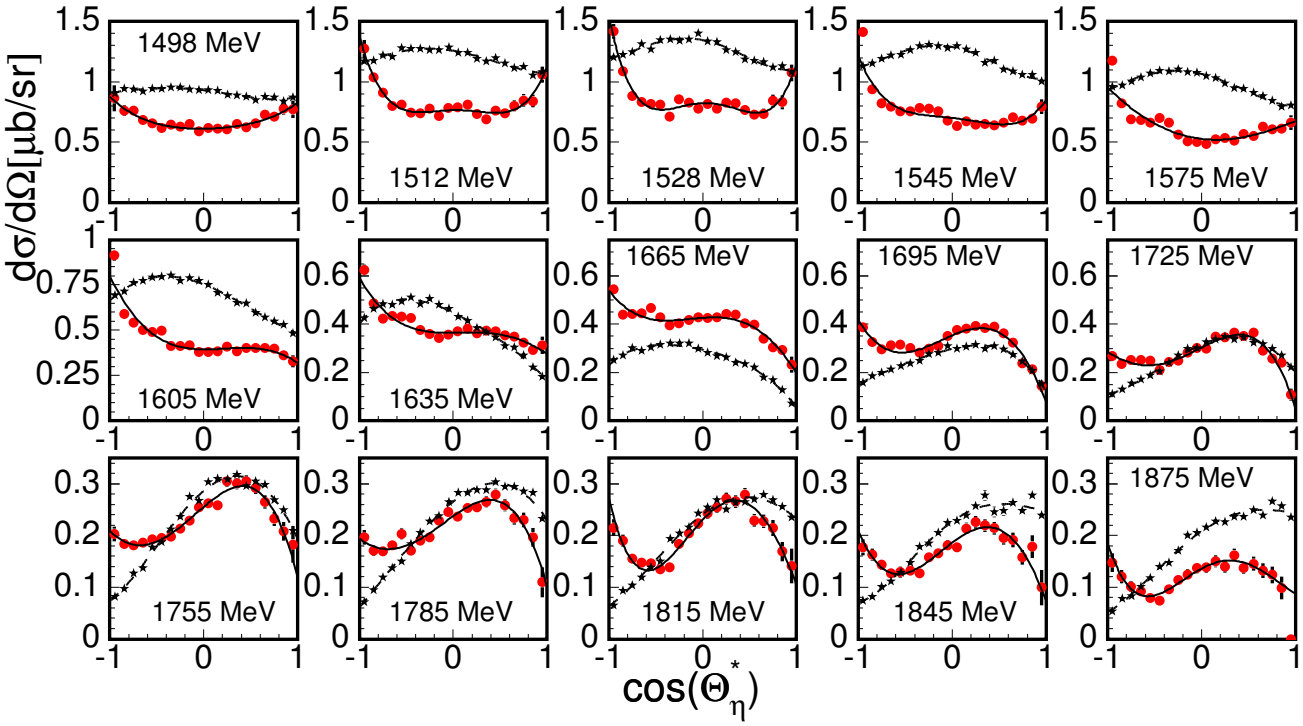

Figure 3: Angular distributions for $\gamma n \to n\eta$ [44] (red dots) compared to the results for $\gamma p \to p\eta$ from [38] (black stars). Solid and dashed curves are fits to the data with Eq. (2.2).

(without the detection of recoil nucleons) [51] or detected only the recoil nucleons using missing-mass analysis [52]. The first fully exclusive measurement, which already used a complete reconstruction of the final state kinematics to remove the Fermi motion effects, was done in the threshold region [53]. This reaction generated a lot of interest when the first exclusive measurements [54] at higher incident photon energies carried out at the GRAAL facility revealed a pronounced, narrow structure at incident photon energies around 1 GeV, which is absent for the $\gamma p \to p\eta$ reaction. Subsequently, the quasi-free production of η mesons off neutrons was studied in detail with deuteron targets at LNS in Tohoku [55], at ELSA in Bonn [56, 43], and at MAMI in Mainz [44, 50]. At MAMI it was also studied for neutrons bound in ^{3}He nuclei [45]. The experimental strategies were also different. The Tohoku experiment measured the inclusive quasi-free reaction $\gamma d \to \eta(np)$ and subtracted the cross section of the $\gamma p \to p\eta$ reaction, after folding the latter with the momentum distribution of the bound nucleons. The experiments at GRAAL, ELSA, and MAMI measured the η-mesons in coincidence with the recoil neutrons and extracted the cross sections as function of the incident photon energy (obtaining Fermi-smeared results) and as function of kinematically reconstructed total c.m. energy W, thus eliminating Fermi motion effects. Results for the latter type of analysis are summarized in Figs. 1, 3, and 5.

Before we discuss the experimental results, we first give a short summary of existing modelling approaches, which are quite diverse. For the reaction off free protons, they include the SAID partial wave analysis [38] (and references therein), effective Lagrangian models of different types such as the MAID isobar model (MAID 1) [39] and the Reggeized MAID isobar model (MAID 2) [40], different coupled channel models such as the Giessen model [57], the Bonn-Gatchina (BnGa) model [41, 42], and even an approach based on the constituent quark model [58]. The $\gamma n \to n\eta$ reaction was also analyzed in the framework of the MAID models [39, 40] and with the BnGa coupled-channel analysis [46].

The experimental results for differential cross sections off free protons are in good overall agreement. The largest systematic discrepancy occurs in the fits of the angular distributions for the A_4 coefficient

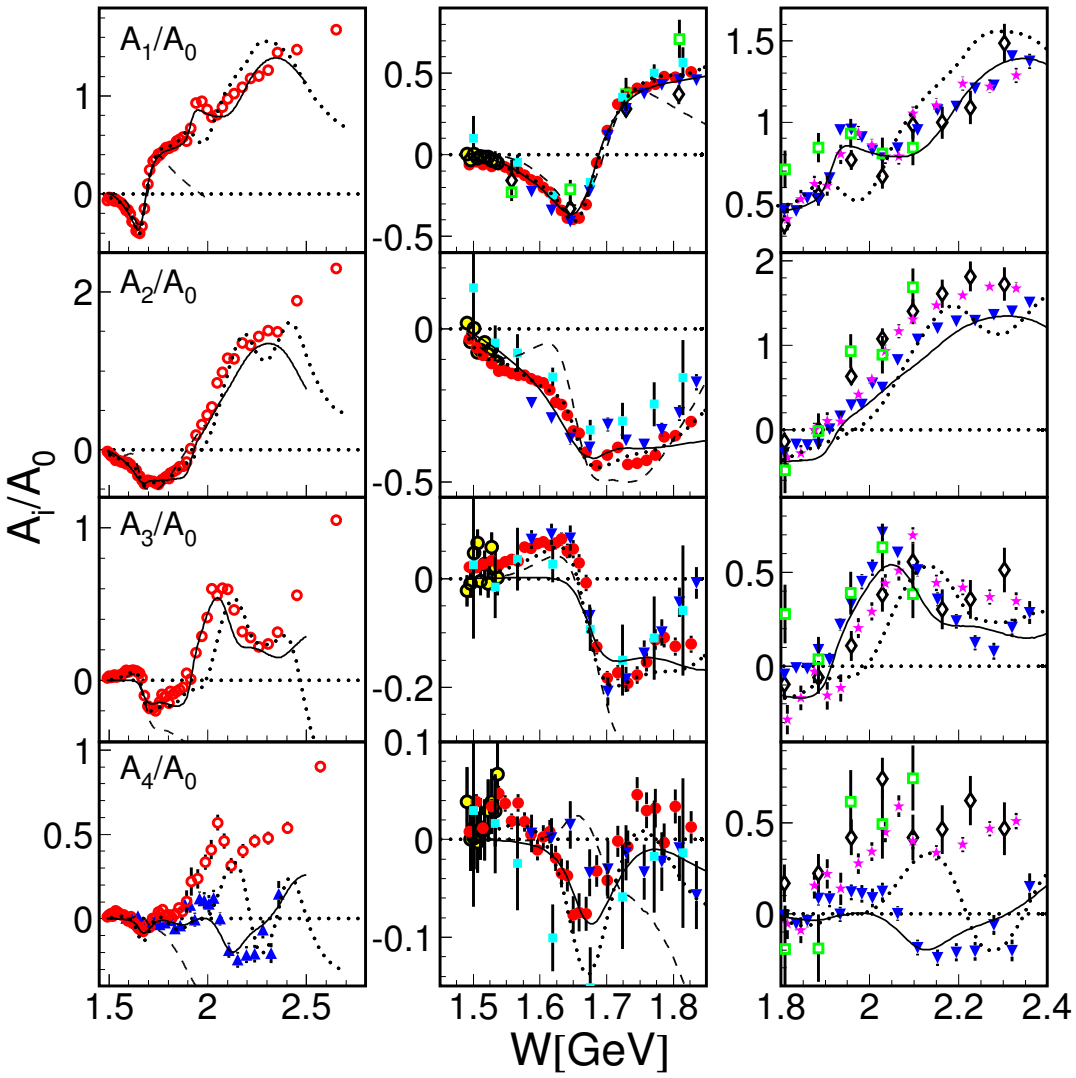

Figure 4: Legendre coefficients obtained from fits to the $\gamma p \to p\eta$ angular distributions using Eq. (2.2). Left column: average of all experimental data compared to MAID 1 [39], SAID [38], and BnGa [41, 42] (notation as in Fig. 1). The A_4/A_0 data from Ref. [37] is not included in the average but shown separately. Central column: individual data sets for low energy data (symbols as in Fig. 1). Right column: same for high energy data.

(see Fig. 4) where above $W \approx 1.8$ GeV the results from Ref. [37] disagree with all other measurements. Here one should note, however, that this measurement is the only one that reports results for extreme forward angles with small statistical uncertainties. The A_4 coefficient is very sensitive to these extreme angles, so that the deviation could also be a reflection of the other measurements not having sufficient coverage in this region.

The agreement between the measurements of the quasi-free production off nucleons bound in light nuclei is in part less good. The Fermi-smeared cross sections as function of the incident photon energy from the ELSA [43] and the MAMI [44, 50] experiments are in good (for participant protons) and in reasonable (for neutrons) agreement (see Fig. 45, left hand side in Appendix A). However, the cross sections extracted with the reconstructed kinematics from the ELSA and the MAMI experiments agree only in the range of the S_{11} resonance peak, for quasi-free protons as well as for neutrons, but they deviate at higher energies, where the ELSA cross sections are larger. The effect is similar for protons and neutrons. The σ_n/σ_p cross section ratios, also shown in Fig. 1, are not much different and certainly agree

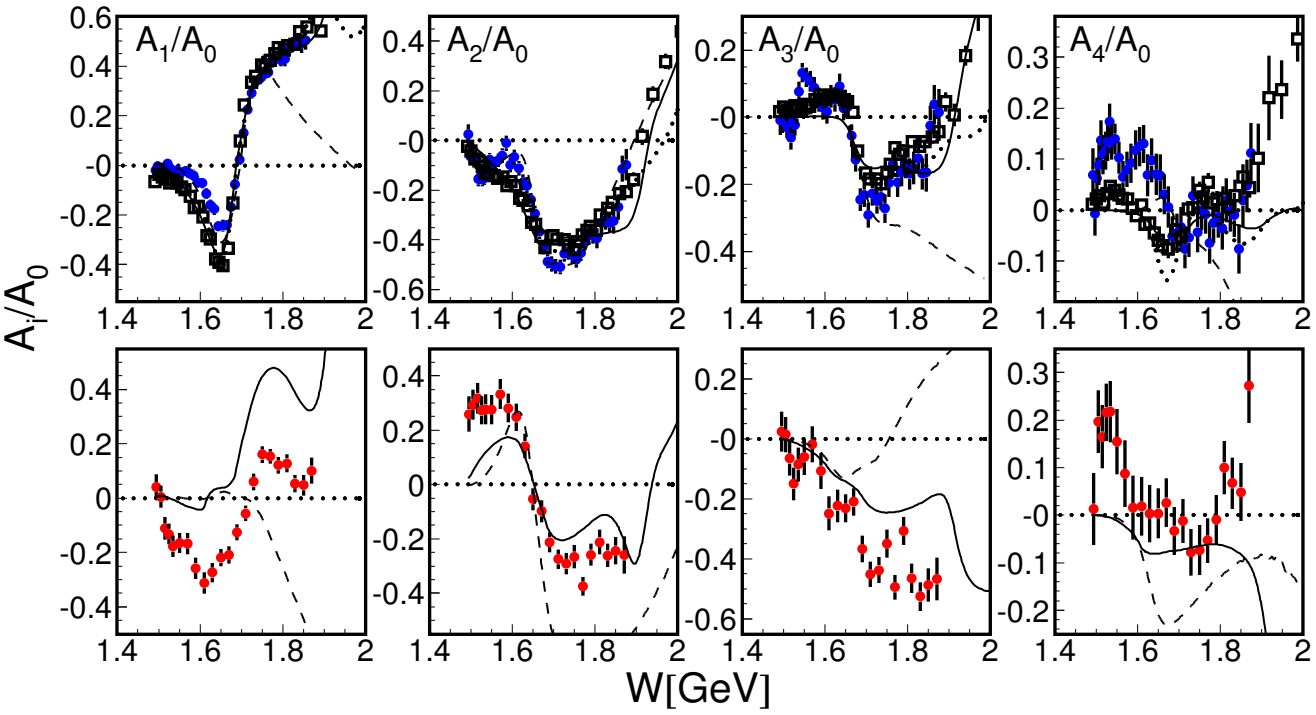

Figure 5: Upper row: Coefficients of the Legendre series of Eq. (2.2) for $\gamma p \to p\eta$ for a free proton target (averaged over all experimental data, as in the left column of Fig. 4, black open squares) compared to the results for quasi-free $\gamma d \to \eta p(n)$ [44, 50] (blue dots). Model curves are from MAID 1 [39] (dashed), BnGa [41, 42] (solid), and SAID [38] (dotted). Lower row: coefficients for quasi-free $\gamma d \to \eta p(n)$ [44, 50] compared to model results for MAID 1 [39] (dashed) and BnGa [46] (solid).

within experimental systematic uncertainties. The problem seems to be related to an energy-dependent normalization issue for the kinematically reconstructed ELSA data [43] (see Appendix A for a detailed discussion). Here one should note that these data included only four points per angular distribution compared to the 20 points for [44, 50]. Detailed angular distributions for the ELSA experiment [43] were only given for the Fermi-smeared E_γ data, which agree with the MAMI data within systematic uncertainties.

No significant FSI effects have been noted, within experimental uncertainties, from the comparison of free and quasi-free $\gamma p \to p\eta$ data measured with a deuterium target. The quasi-free total cross section from [44] is close to the free proton results and also the Legendre coefficients from the fits of the angular distributions shown in Fig. 5 are very similar. Deviations occur only for the high order A_4 coefficient at low energies, where systematic uncertainties due to the detection of the recoil protons are difficult to control for certain angular regions, as discussed in [50]. Also for the ELSA deuterium measurement [43] there is agreement between the measured quasi-free proton cross section and free proton data after these have been folded with the deuteron Fermi motion. This is not the case for the ^{3}He target for which quasi-free cross sections for protons as well as for neutrons are suppressed by roughly a factor of 1.4 compared to free proton data (or quasi-free proton and neutron data from the deuteron target). Some possible reasons for this are discussed in [45]. Fermi motion effects are much stronger for the ^{3}He target and a kinematic reconstruction is only possible under the assumption that there is no relative momentum between the two spectator nucleons. FSI effects may be significantly larger than for the deuteron but there are so far no model calculations for such effects. These data have only been used to demonstrate that the general behaviour of the quasi-free neutron cross section, in particular the narrow

structure around incident photon energies of 1 GeV, does not depend much on the target nucleus. The ^{3}He results have been scaled up by a factor of 1.4 in Fig. 1.

We discuss the experimental results for three different ranges of incident photon energy, i.e., for different total c.m. energies W. These are the threshold region that extends through the $S_{11}(1535)$ peak, the following region up to $W \approx 2$ GeV, and higher energies. For the proton, as well as for the neutron target, the threshold region up to incident photon energies of 0.9 GeV ($W \approx 1.6$ GeV) is quite well understood. The reaction is dominated by the excitation of the $S_{11}(1535)$ resonance [59] via the E_{0+} amplitude, leading to the strong peak at ≈ 1.53 GeV. This resonance overlaps with the η-production threshold at $W = 1486$ MeV ($E_\gamma^{\rm thr} = 707.8$ MeV) and has an unusually large branching ratio of around 50% for the emission of η mesons. It is responsible for the strong η - nucleon interaction in the threshold region (on which the discussion about possible η - nucleus bound states is based). The properties of the E_{0+} amplitude are reflected in the energy dependence of the total cross section (almost perfectly $\propto (E_\gamma - E_\gamma^{\rm thr})^{1/2}$ in the threshold region [60, 61]) and in the shape of the angular distributions (almost isotropic). The dominance of this state has also allowed a detailed investigation of the dependence of its electromagnetic coupling $A_{1/2}$ on the four momentum transfer Q^2 in electroproduction, which shows a surprisingly slow falloff [62]. This feature is important for understanding the quark model structure of this isobar. The deviation from isotropy in the angular distributions close to threshold is due to an interference between the leading E_{0+} multipole and the E_{2-} and M_{2-} multipoles related to the excitation of the nearby $D_{13}(1520)$ resonance. The interference term is proportional to $\mathrm{Re}[E_{0+}^\star(E_{2-}-3M_{2-})]\cos^2\theta_\eta^\star$ [30] and is thus reflected in the A_2 coefficient of the Legendre series of Eq. (2.2). The branching ratio for the $D_{13}(1520) \to N\eta$ decay is very small; the Particle Data Group quotes (0.23±0.04)% [23] and this is mainly determined by the beam asymmetries of the $\gamma p \to p\eta$ reaction (see below).

The measured ratio of neutron σ_n and proton σ_p cross sections in this energy range is $\sigma_n/\sigma_p \approx 2/3$ (see Fig. 1). The ratio increases towards threshold but this is an artefact of the plane-wave impulse approximation interpretation. Very close to threshold, energy and momentum conservation force the 'participant' and 'spectator' nucleons to have almost identical momenta and the kinematics become similar to the coherent reaction. This means that the simple participant - spectator picture breaks down and the measured cross section ratio will approach unity.

The σ_n/σ_p ratio can be translated into one for the magnitudes of the electromagnetic couplings of the S_{11} state to protons and neutrons (see [49] for details): $|A_{1/2}^n|/|A_{1/2}^p| \approx 0.8$. This means, according to Eq. (2.1), that either the isoscalar or the isovector part of the coupling must be small. The relative sign of the electromagnetic helicity couplings can be fixed in two ways. The cross section for the coherent reaction $\gamma d \to d\eta$ will be much larger when the coupling is dominantly isoscalar. The experimental results [52, 63] clearly favour a dominant isovector coupling and thus a negative relative sign. An alternative access to the sign comes from the interference term between the S_{11} and D_{13} states. It was shown in Ref. [53] that, with a few simple approximations, the interference term is proportional for protons and neutrons to the products of their helicity couplings $A_{1/2}^N(S_{11})$ and $A_{1/2}^N(D_{13})$. Since the helicity couplings of the D_{13} state are well known from pion photoproduction and have the same sign for protons and neutrons, a negative relative sign for the S_{11} state will result in angular distributions for η production with opposite curvature for protons and neutrons. The precise angular distributions shown in Fig. 3 have this behaviour; the corresponding A_2 coefficients in Fig. 5 have opposite sign in the relevant energy region. The interference effect is larger for the neutron because the D_{13} neutron coupling is a factor of ≈ 2.5 larger than its proton coupling [23].

The same arguments can be made for the beam asymmetry Σ discussed below. The interference effect is even more pronounced in this observable [64], but the relevant term here is $\propto \mathrm{Re}[E_{0+}^\star(E_{2-}+M_{2-})]$, which involves the product of the $A_{1/2}$ coupling of the S_{11} with the $A_{3/2}$ coupling of the D_{13}. Since both couplings have a relative negative sign between protons and neutrons, this interference term has the same sign for the proton and the neutron. All the more advanced analyses (e.g. MAID [39], BnGa [46]) come to the same conclusions and indicate also that contributions from the non-resonant background

are small in this energy range. There is only one experimental result that does not fit into this picture. This is the target asymmetry measured by the PHOENICS experiment at ELSA at the end of the nineties [65]. As discussed, e.g., in Ref. [49], none of the existing models could reproduce the observed nodal structure of this observable for incident photon energies below 800 MeV. Tiator and collaborators [66] showed, with a truncated multipole analysis, that the measured target asymmetry forces a large and strongly varying phase between the s-wave E_{0+} multipole and the d-wave E_{2-}, M_{2-} multipoles. Since the first is dominated by the $S_{11}(1535)$ excitation and the latter by the $D_{13}(1520)$ state, this would indicate a strongly varying phase between two resonances with almost identical excitation energies and thus mean that at least one of them would show an unusual behaviour. This problem persisted until very recently when new and statistically much more precise data for the target asymmetry were obtained at MAMI and ELSA. The results from MAMI have been published in the meantime [67] (see discussion at the end of this chapter) and did not confirm the critical nodal structure. The ELSA results are sill under analysis, but preliminary results seem to support this finding.

In view of the experiments to search for η - nucleus bound states, which are discussed later, one should note that η photoproduction in the threshold region is completely dominated by the isovector component of the E_{0+} multipole. This has strong consequences for coherent production processes of the $\gamma A \to A\eta$ type, which are the most natural entrance channel for the formation of bound states. Since E_{0+} is a spin-flip multipole the final state s-wave is forbidden for $J = 0$ and, because it is dominantly isovector, it is strongly suppressed for $I = 0$.

The energy region above the S_{11} peak up to W values around 2 GeV is complicated and far from being understood in terms of nucleon resonance physics. Above $W \approx 1.65$ GeV ($E_\gamma \approx$1 GeV) the results from model analyses differ already for the total cross section of the $\gamma p \to p\eta$ reaction (see Fig. 1). The measured angular distributions change rapidly in this energy range. The Legendre coefficients $A_1, ..., A_4$ (see Fig. 4, central column) show a strong energy dependence around W= 1.65 GeV. The large and fast varying values of the A_1 coefficient point to an interference between the strong S_{11} contribution and p-wave states (S_{11} - P_{11} interference is $\propto \cos\theta^\star_\eta$). This effect was also observed in η electroproduction [68] and found to be almost independent of the four momentum transfer Q^2, which would mean that the relevant multipoles - E_{0+} and M_{1-} - have a similar Q^2-dependence. At these energies contributions can be expected from the $S_{11}(1650)$, $D_{15}(1675)$, $D_{13}(1700)$, $P_{11}(1710)$, and $P_{13}(1720)$ resonances. Branching ratio estimates given by PDG [23] are 5 - 15% for the $S_{11}(1650)$, 10–30% for the P_{11}, (4±1)% for the P_{13}, and (0±1)% for the two d-wave states. The values extracted from different analyses have a significant spread for some resonances and have recently changed, due to the results from the analysis of the new photoproduction data in the framework of the BnGa model [41, 42].

The picture becomes more complicated by the results for the $\gamma n \to n\eta$ reaction. The most striking feature is the extremely steep rise of the σ_n/σ_p cross section ratio above $W = 1.6$ GeV. All experiments that measured total cross sections reported this effect; the results from [43, 44, 45] are compared in Fig. 1. Interestingly, a strong rise of this ratio was predicted by the MAID model [39], though not as prominent and steep as was later observed. This prediction was even among the motivations for the experimental activities but, as it turns out now, it was made for the wrong reasons. The MAID fit of the proton data produced an $N\eta$ decay branching ratio of the $D_{15}(1675)$ resonance ($\approx$ 17%) much larger than any other analysis; PDG [23] has it compatible with zero. Since this state is Moorhouse-suppressed [69] in the electromagnetic excitation off the proton, it couples more strongly to the neutron. This state thus made a large contribution to the $\gamma n \to n\eta$ reaction in MAID. However, a comparison (see Fig. 1) of the total cross section predicted by MAID already shows that the model misses completely the peak-like structure in the neutron excitation function. The peak in the cross section ratio results entirely from the 'dip' in the proton excitation function at the same energy. The 'dip' is reproduced because the model was fitted to the proton data, but it is then of course questionable whether it reflects the correct physics. The description of the angular distributions (see, e.g., Fig. 5) and the beam asymmetries discussed below (see Fig. 8) by the MAID fit, in particular for the neutron, is also not good above

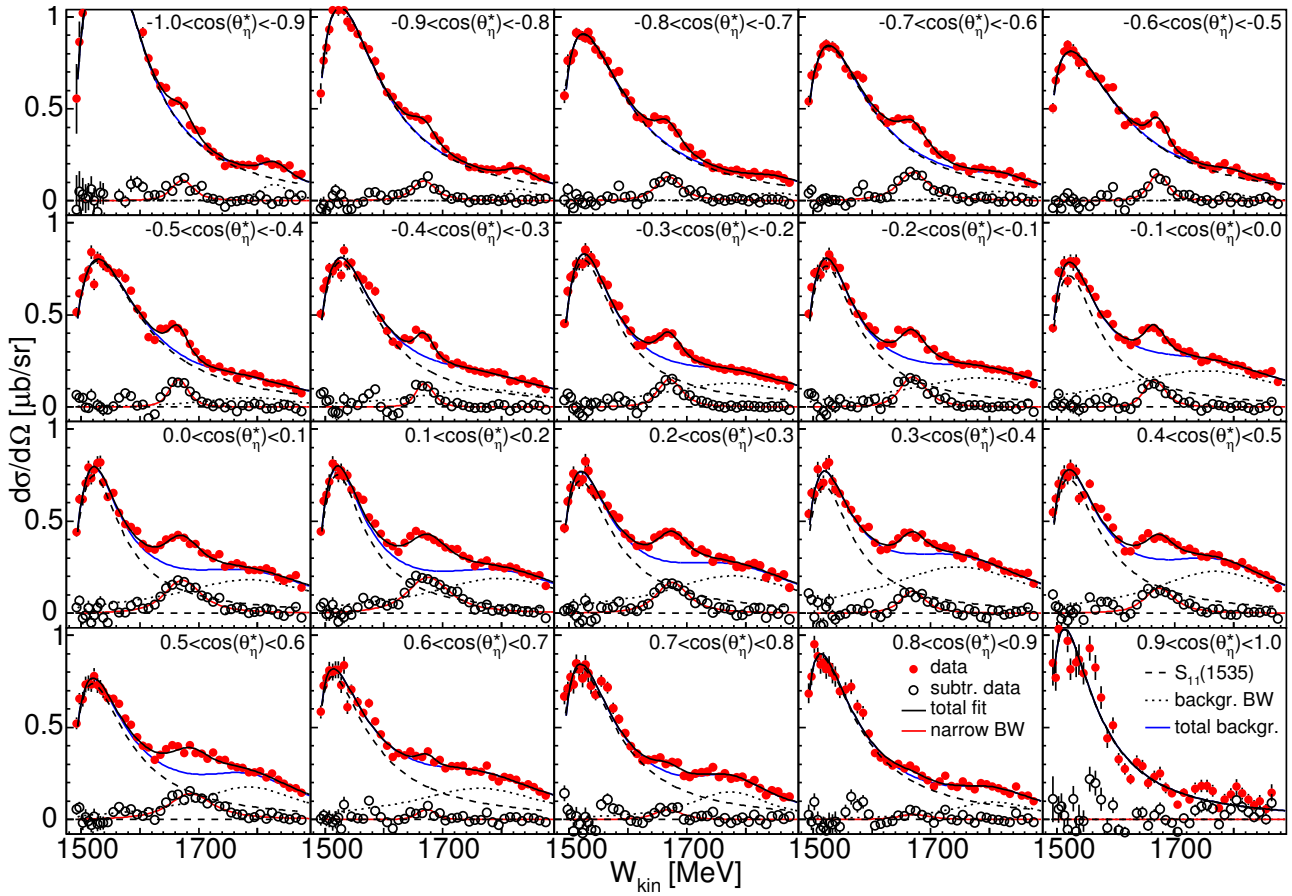

Figure 6: Differential cross sections for the $\gamma n \to n\eta$ reaction [44] for different bins of polar angle as function of the $n\eta$ c.m. energy W. The curves are a phenomenological fit with a Breit-Wigner resonance for the S_{11} state, a second BW for the narrow structure, and a third BW for the broad background underneath the narrow structure (see text). The open symbols represent data with S_{11} and background fit contributions subtracted.

W=1.6 GeV so that the extraction of resonance contributions in this energy range is almost certainly not realistic. A refit of the model to the data now available would be desirable.

The agreement between data and the BnGa fit is better for all observables, but this model was also fitted to all the available results. For the $\gamma n \to n\eta$ reaction, the BnGa fit included the Fermi-smeared cross section data from [56] and the beam asymmetries from GRAAL [64]. This explains why the total cross section without Fermi smearing as function of W is closer to the new MAMI data from [44] (which were not yet included in the fit) than to the older ELSA data from [43]. The fit to the neutron data might be improved by a refit of the new differential cross section data (this is already under way). Typical examples for the evolution of the fit results, due to the continuing improvements of the experimental data base, are the $P_{11}(1710)$ and $P_{13}(1720)$ states. The MAID model [39], and also the Giessen coupled-channel model [70], found a significant contribution to $\gamma p \to p\eta$ from the P_{11} and almost none from the P_{13} resonance. The early fits with the BnGa coupled-channel model, on the other hand, found no signature for the P_{11} but a large branching ratio of 30% [33] for the P_{13}. In the meantime, the situation in the BnGa fit has reversed; in the most recent version [41] the branching ratio for the P_{11} has risen to (17±10)% and the one for the P_{13} has dropped to (3±2)%.

Some comments should be made about the pronounced narrow structure in the excitation functions around $E_\gamma \approx 1$ GeV. More than ten years ago there were predictions for such a structure related to the

conjectured baryon anti-decuplet [71] of pentaquarks. Taking together, the results from [71, 72, 73, 74] suggested that the non-strange P_{11}-like member of the anti-decuplet should be electromagnetically excited more strongly on the neutron, should have a large decay branching ratio to Nη, an invariant mass around 1.7 GeV/c^2, a width of a few tens of MeV/c^2, and a radiative coupling to the neutron corresponding to $A^n_{1/2} = 15 \times 10^{-3}$ GeV$^{-1/2}$. The structure that was subsequently observed in the $\gamma n \to n\eta$ reaction fitted exactly to these properties. It was seen in *all* experiments that looked for it (even using the in-principle unfavourable ^{3}He target nucleus) and the statistical significance, in particular in the most recent data [44], is beyond any doubt. In this sense it is very different from the experimental claims for the observation of the exotic pentaquark, which could not be reproduced by subsequent experiments. Although the existence of this structure is unambiguous, its nature is not yet understood. Phenomenological analyses of the excitation function found for the position and widths of the structure values of (we cite the most recent results from [44, 50]; other experiments found comparable values) $W = (1670 \pm 5)$ MeV with an intrinsic width of $\Gamma \approx 30$ MeV. This would be a very unusual value for a nucleon resonance (which in this energy range rather have widths above 150 MeV), but a bump in an excitation function need not necessarily correspond to a nucleon resonance.

It was already argued in [43] that the 'bump' in $\gamma n \to n\eta$ and the 'dip' (although less prominent) in $\gamma p \to p\eta$ are probably related structures. The structure in the proton excitation function has been recently investigated in detail with the BnGa coupled channel analysis [75]. The main result was that the narrow 'dip' cannot be reasonably well explained by broad resonances and standard background amplitudes. The fit could be improved by either introducing a narrow P_{11} state or by a threshold effect resulting from a strong coupling of the $\gamma p \to \omega p$ reaction to the S_{11} partial wave (however, most recent analyses by the Bonn-Gatchina group including experimental data for ω production do not favour a strong coupling). Various scenarios have been suggested in the literature for the narrow structure in the neutron excitation function. They range from different coupled-channel effects of known nucleon resonances [70, 76], interference effects in the S_{11} partial wave [77, 46], effects from the opening of strangeness thresholds [78], to intrinsically narrow states [73, 77, 79, 80, 81]. The available data are still insufficient for an unambiguous analysis. However, the precise angular distributions shown in Fig. 6 have added some new clues. They do not favour a scenario where a narrow P_{11} resonance interferes with the broad S_{11} structures. An interference term between the M_{1-} multipole from a P_{11} excitation and the E_{0+} multipole from S_{11} excitations has an angular dependence $\propto \cos\theta^\star_\eta$. This means that the narrow structure should have a maximum contribution either at extreme forward or at extreme backward angles, a linear dependence across the angular distribution, and then a minimum at the opposite extreme angle. Depending on the sign, one would then expect a maximum bump at forward angle and a dip at backward angle (or vice versa). But the excitation functions for different bins of polar angle (see Fig. 6) show the most pronounced bump-like structure at intermediate angles and almost no effect at forward and backward angles.

A fit of the BnGa model to the previous ELSA data [56] gave comparable quality for a scenario with a narrow P_{11} state or interference effects in the S_{11} channel [77]. A refit [84] to the more precise angular distributions from the new MAMI data [44] preferred the solution without a narrow P_{11} state, for which the 'bump' in the total cross section arises entirely from subtle interference effects in the S_{11} channel. This solution requires, however, a change of sign of the electromagnetic coupling of the $S_{11}(1650)$ resonance for the neutron. Most analyses (MAID, SAID) previously found a negative sign for the $A^n_{1/2}$ (in the following all values are in units of 10^{-3} GeV$^{-1/2}$) neutron helicity coupling of this four star state (PDG: -15 ± 21) and thus a destructive interference between the two S_{11} states for the neutron (as for the proton). A negative sign was also preferred by quark models (e.g., Capstick [85]: -35; Burkert et al. [86]: -31 ± 3). However, the most recent analyses of the Bonn-Gatchina group [46] (25 ± 20) and Shresta and Manley [81] (11 ± 2) find positive values corresponding to a constructive interference. This solution might be appealing, in so far as it could explain the structures in the proton and neutron excitation function with the same mechanism. However, it requires significant fine-tuning

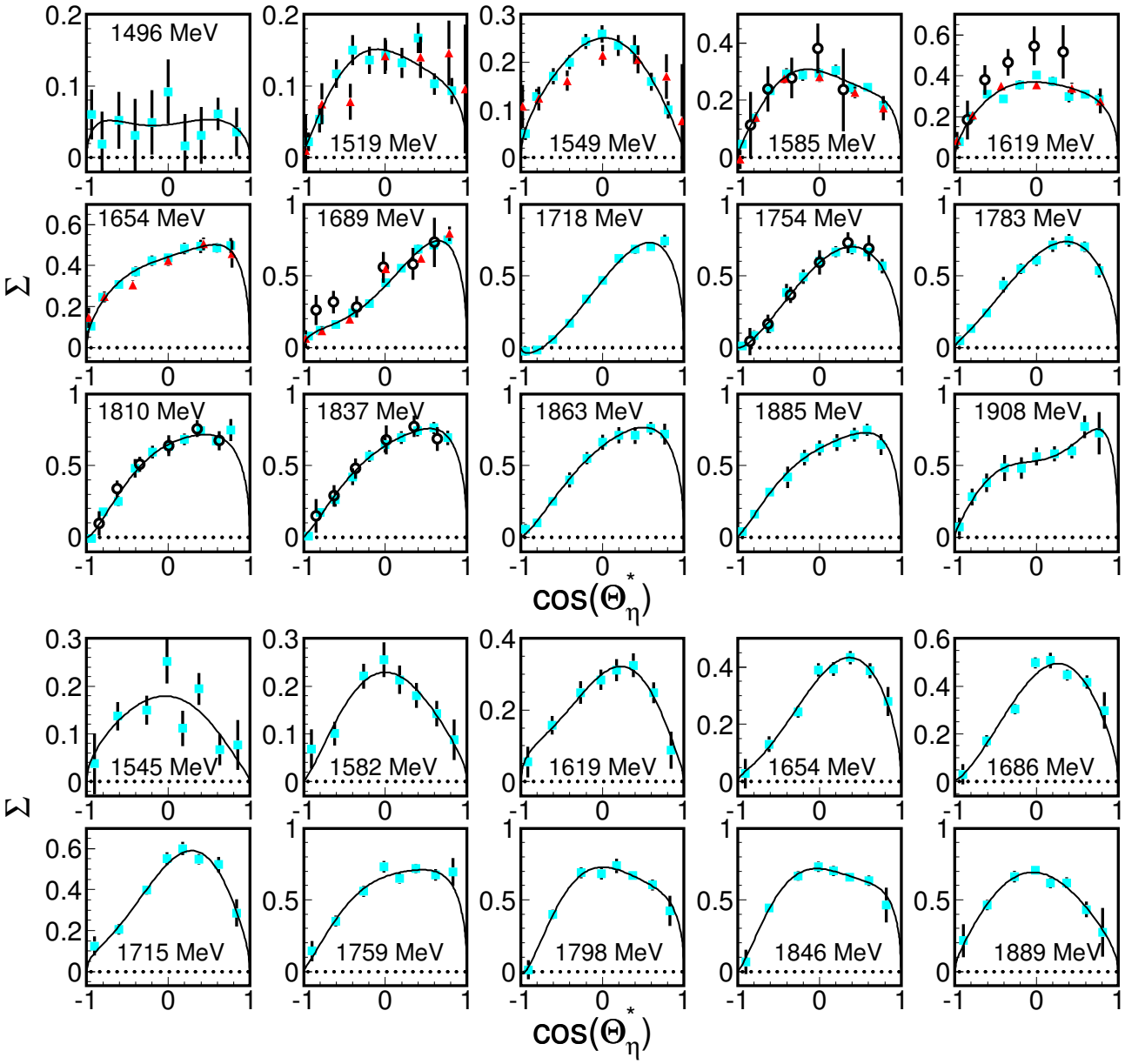

Figure 7: Top row: Beam asymmetries Σ for the free $\gamma p \to p\eta$ reaction. Light blue dots [35] and red triangles [82] from GRAAL experiment, open circles [83] from CBELSA/TAPS. Solid lines: fits with Eq. (2.3) to data from [35]. Results are given for the different values of W indicated in the panels. Bottom: Beam asymmetries Σ for the quasi-free $\gamma n \to n\eta$ reaction from the GRAAL experiment [64]; the solid lines are fits with Eq. (2.3).

in the S_{11} sector and it remains to be seen whether the results for polarization observables, which will soon be available, fit this interpretation.

For $W \gtrsim 2$ GeV, t-channel contributions from vector mesons exchange become important and the angular distributions start to peak at forward angles. These contributions have been analyzed for the proton target in Ref. [47]. Data for the neutron target in this energy range have only been reported from the ELSA experiment for the Fermi-smeared data [56, 43] up to incident photon energies of 2.5 GeV (corresponding to $W \approx 2.36$ GeV). They also show the pronounced peaking at forward angles. The large diffractive contributions could obscure the small signals from the nucleon resonances that have

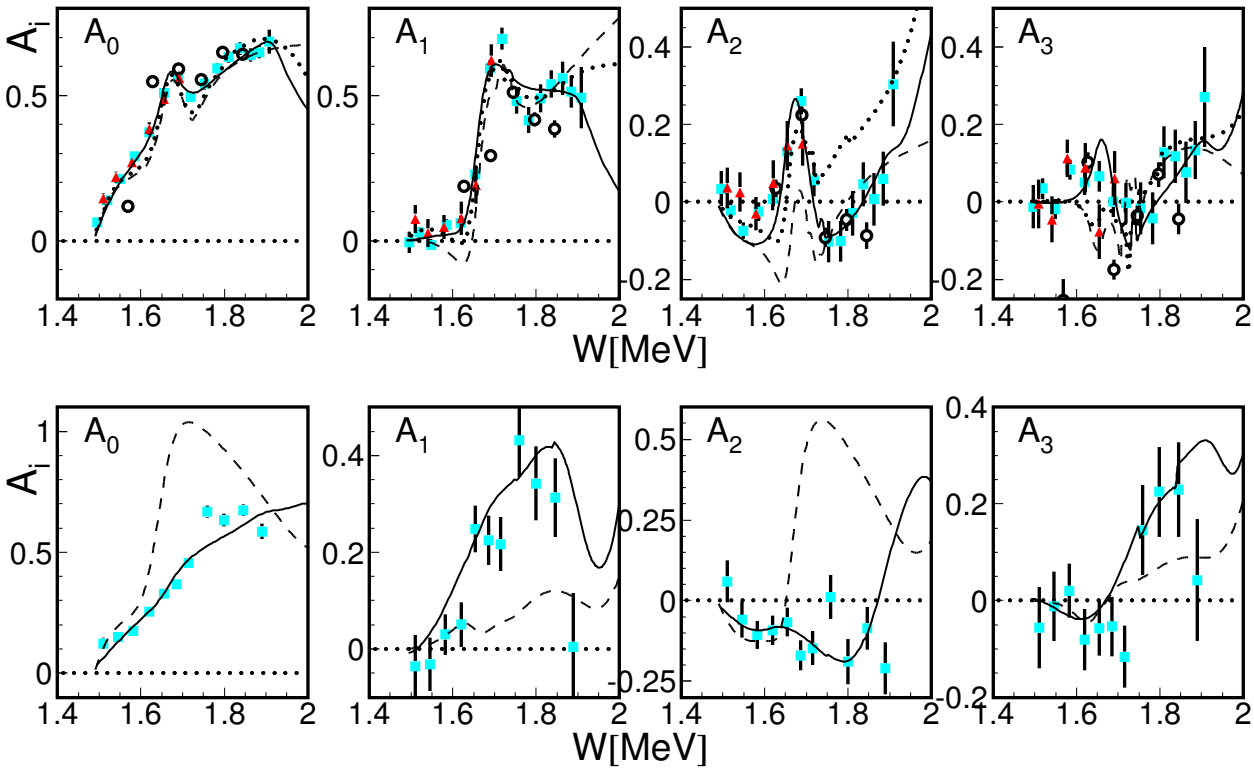

Figure 8: Coefficients of the Legendre series (2.3) fitted to the beam asymmetries $\Sigma(W, \cos\theta^*_\eta)$ as function of W. Upper part: $\gamma p \to p\eta$, Bottom: $\gamma n \to n\eta$. Symbols for data are as in Fig. 7. Solid curves: results of BnGa fit [42, 41] for proton and [46] for neutron target, dashed: MAID model [39], dotted: SAID partial wave analysis [38] (only for proton target).

been suggested by the model fits. However, the interpretation of the data is even more tentative than at lower photon energies. The first analysis of the ELSA data for $\gamma p \to p\eta$ in the framework of the BnGa model [33] claimed, for example, contributions from $F_{15}(2000)$, $D_{15}(2070)$, $D_{13}(2080)$, and $P_{13}(2200)$ states. In particular, the contribution of the $D_{15}(2070)$ (which was introduced by this analysis as a previously unknown nucleon resonance) was strong. In the more recent BnGa fit [41, 42], only two states with significant coupling to $N\eta$ are reported above 2 GeV, viz. the $F_{15}(2000)$ and the $D_{15}(2060)$, the latter now with a branching ratio of (4±2)%.

It is clear that there are still many open questions about the resonance contributions to $\gamma N \to N\eta$ above the $S_{11}(1535)$ region. Cross section data alone, even with improved precision, can certainly not solve this problem since a unique description of photoproduction of a single pseudoscalar meson off nucleons requires the measurement of at least eight carefully selected observables [87].

Apart from angular distributions the only other reasonably precise results that are available so far (very recent new polarization data [67] are shortly discussed at the end of this chapter) are for the photon beam asymmetry Σ (linearly polarized photon beam, unpolarized target) for free protons and quasi-free neutrons. These data have gone into the model analyses discussed above. They have been measured mainly at the GRAAL facility [35, 64, 82] and at ELSA [83]. The primary results are summarized in Fig. 7 and have been fitted with the Legendre series

$$\Sigma(W, \cos\theta^*_\eta) = \sin^2\theta^*_\eta \sum_{i=0}^{3} A_i(W) P_i(\cos\theta^*_\eta)\,, \tag{2.3}$$

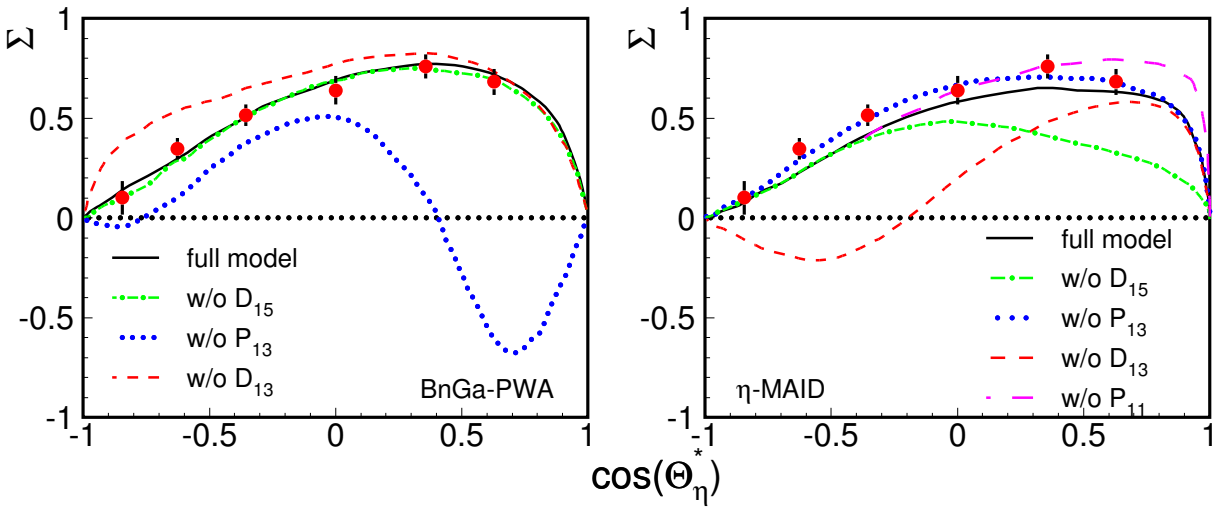

Figure 9: Beam asymmetry data from [83] for $\gamma p \to p\eta$ for incident photon energies around 1.25 GeV ($W \approx 1.8$ GeV) compared to results from the MAID model [39] (right hand side) and the BnGa fit [88] (left hand side). Solid (black) curves: full fits, dotted (blue): without the $P_{13}(1720)$ state, dashed (red): without $D_{13}(1520)$, long dashed (magenta): without $P_{11}(1710)$ (no difference to full model for BnGa model), dash-dotted (green): without $D_{15}(1675)$.

with the fitted coefficients being shown in Fig. 8. All the experimental results for the $\gamma p \to p\eta$ reaction [35, 82, 83] are in reasonable agreement; for $\gamma n \to n\eta$ only results from the GRAAL experiment [64] are so far available. We have already discussed above the strong contribution of the $S_{11}(1535)$ - $D_{13}(1520)$ interference to the beam asymmetry, which is responsible for the fast rise of the A_0 coefficient from threshold. In a similar behaviour to that seen for the angular $\gamma p \to p\eta$ distributions, the corresponding beam asymmetry Σ also shows a strong energy dependence for W between 1.6 and 1.8 GeV. The A_1 coefficient rises sharply and A_2 (and perhaps also A_3) shows a narrow structure around 1.65 GeV. The MAID [39], SAID [38], and BnGa [42, 41] analyses reproduce this behaviour reasonably well. However, a word of caution is needed here. The fact that the fits (with many free parameters) can describe the data does not of course guarantee that the right physics is included in the models. An instructive example of this is given in [83].

The measured beam asymmetries around $W \approx 1.8$ GeV are compared in Fig. 9 to results from the MAID [39] and BnGa models [88] (note that these are not the most recent results from BnGa [42, 41]). Both models described the beam asymmetry comparably well (see figure) and were also in reasonable agreement with the angular distributions. Nevertheless, as the figure shows, the physics contents of the fits were quite different, which is demonstrated by 'switching-off' certain resonance contributions. While for the BnGa model the P_{13} state was very important, it played almost no role in the MAID model which, on the other hand, included large contributions from the D_{13} and D_{15} d-wave states. The model results start to diverge quickly above the region where experimental Σ values are available (see Fig. 8, top row).

Little structure is observed for the $\gamma n \to n\eta$ reaction around $W \approx$1.7 GeV, although also in this case the A_0 coefficient shows an abrupt rise around this energy. However, resolution effects might play a role here. Although the c.m. angles were reconstructed from the final state kinematics taking into account Fermi motion, the results are given in terms of the incident photon energy without correction for Fermi-smearing effects. Nevertheless, the effects do not seem to be very large since the quasi-free proton results are close to those of the free proton data. The BnGa model agrees reasonably well with

these data (because it has been fitted to them). The MAID model largely overestimates the asymmetries between 1.6 - 1.8 GeV, mainly because of the large contribution of the $D_{15}(1675)$ state, which is clearly not realistic. Agreement with the Reggeized version of MAID [40] is better [64] because a smaller $N\eta$ branching ratio for the D_{15} is used.

Apart from the beam asymmetries, until very recently only the previously mentioned results for the target asymmetry in the S_{11} peak [65], and a few low statistics values for the separation of the total cross section into $\sigma_{1/2}$ and $\sigma_{3/2}$ components (longitudinally polarized target, photon beam circularly polarized parallel ($\sigma_{3/2}$) or antiparallel ($\sigma_{1/2}$)) right in the maximum of the S_{11} peak, have been reported [89]. The latter only confirm the expectation that $\sigma_{1/2}$ is very dominant in the S_{11} peak ($\sigma_{3/2}$ is compatible with zero, within large statistical uncertainties). However, this situation has now changed dramatically. The CLAS experiment and the experiments at MAMI and ELSA have acquired data for the $\gamma p \to p\eta$ reaction for the single polarization observables Σ, T, P (P measured not by analysis of the recoil nucleon polarization but as double polarization observable with linearly polarized beam and transversely polarized target), and the double polarization observables E, F, G, and H (not all experiments measure all observables, but all observables are measured in at least one, most in two, and some even in three experiments). These data are presently under analysis (preliminary results from CLAS for the E observable have, e.g., been shown at the NSTAR 2011 workshop [90]). Data on E, T, and F for the $\gamma n \to n\eta$ reaction have been measured at MAMI and further measurements of observables with linearly polarized photon beams for the neutron target are planned at ELSA. Therefore, at present it would be completely premature to draw final conclusions on nucleon resonance contributions to η-photoproduction, in particular at higher incident photon energies. The large body of new data will have a strong impact on all partial wave analyses.

The first data from the new measurements of $\gamma p \to p\eta$ with polarized beams and polarized targets have just been published [67]. They come from a measurement with Crystal Ball/TAPS at MAMI with transversally polarized target (solid buthanol) and circularly polarized photon beam, giving access to the target asymmetry T and the double polarization observable F defined by [91]

$$\frac{d\sigma}{d\Omega} = \frac{d\sigma_o}{d\Omega}\left(1 + Tp_T \sin\phi + Fp_T p_\odot \cos\phi\right) \tag{2.4}$$

where $d\sigma_o$ is the unpolarized cross section, p_T is the degree of transverse target polarization in the y-direction, $p_\odot$ the degree of right circular beam polarization, and ϕ the azimuthal angle of the meson.

The much more precise new results for the threshold behaviour of the target asymmetry clearly refute the sign change between forward and backward polar angles reported from the only previously available data [65] and thus settle the issue of the unnatural phase between the $S_{11}(1535)$ and $D_{13}(1520)$ multipoles discussed above. The comparison of the experimental results to different predictions from reaction models/partial-wave analysis in Fig. 10 demonstrates the selective power of these new observables. None of the models that describe differential cross sections and beam asymmetries quite well agrees with the new data for the asymmetries. We mention only one example; predictions for the target asymmetries in the range between 950 - 1050 MeV, where the peculiar structures in the $\gamma N \to N\eta$ excitation functions were observed, disagree strongly with data for all models. Consequently, conclusions like the one drawn by the latest Bonn-Gatchina analysis [84], that the bump-like structure in the neutron excitation function can be explained by S_{11} interferences alone, will have to be cross checked against the new data (in this case upcoming polarization data for the neutron target will be even more important).

In summary, all reaction models will have to be refitted against the new polarization data (results for E, P, H, G... are still to come) and then one will have to check whether different approaches converge in terms of nucleon resonance contributions (which seems to happen for single π^0 production, where more observables are already available).

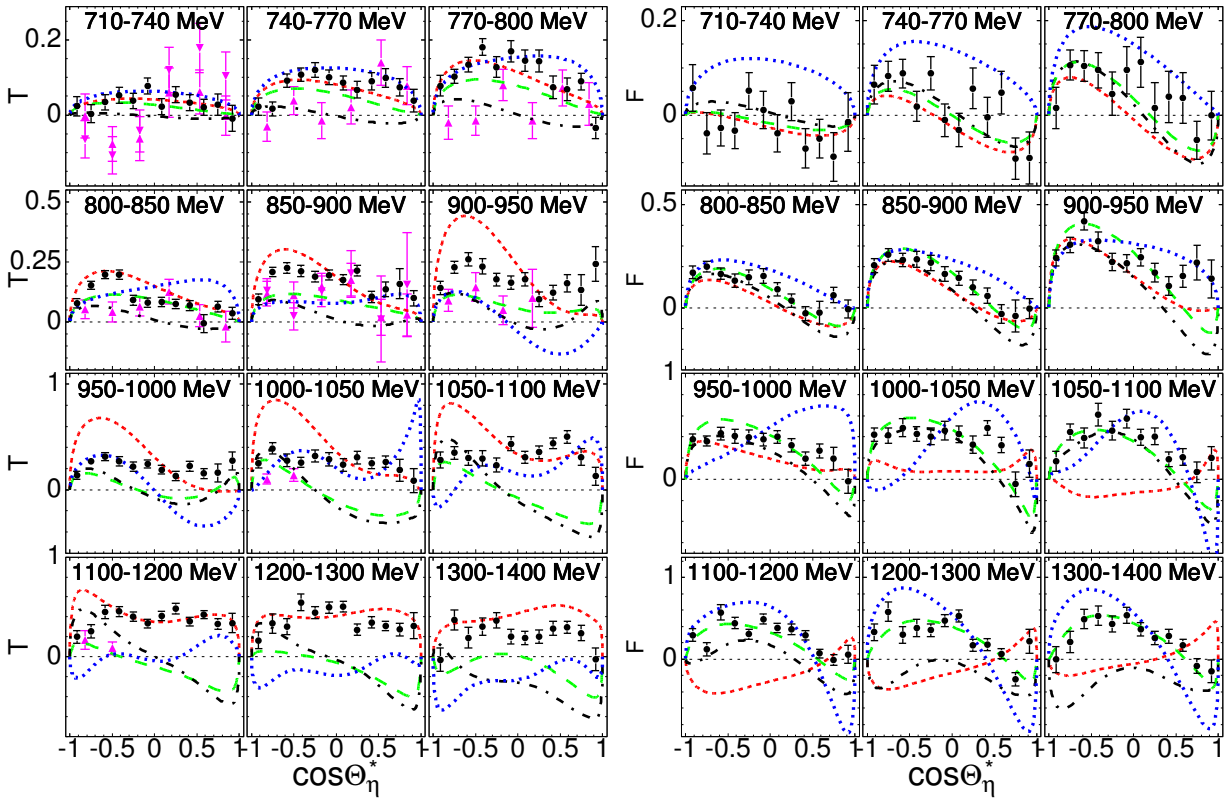

Figure 10: Left hand side: target asymmetry T for the $\gamma p \to p\eta$ reaction. Right hand side: double polarization observable F for the same reaction. Ranges of incident photon energies quoted in the figure. Experimental results (black dots) are from Crystal Ball/TAPS at MAMI [67]. For T also previous results (magenta triangles) from PHOENICS at ELSA [65] are shown (for these data the energy bins do not correspond exactly to the present results, see [67] for details). The curves are predictions from the following models: dashed (red): η-MAID [39], long-dashed (green): Giessen model [57], dash-dotted (black): BnGa [42], dotted (blue) SAID [38].

2.1.2 *Photoproduction of η'-mesons off nucleons*

In the context of nucleon resonance physics, the η' meson can be regarded as the heavy twin of the η, where the isoscalar nature ensures that only $N^\star$ resonances contribute. The much larger mass shifts the interesting W range upwards. The production threshold at $W = 1.896$ GeV corresponds to an incident photon energy of 1.447 GeV for a free proton target. This means that one can still expect in an energy range above $W \approx 1.9$ GeV, where η production shows already a complicated behaviour, a situation where only a few low-order partial waves contribute. This is the W range where most of the predicted, but so far unobserved, $N^\star$ states should be located.

However, the available data base for η' photoproduction is much more scarce than for the η meson and, as a consequence, resonance contributions are not yet well determined. The reason is twofold. The total cross section of η' production reaches at most the 1 μb level (η production falls below this level only above $W \approx 2.3$ GeV). Secondly, the decay modes of the η' are much less accessible for most experiments. For electromagnetic calorimeters that cover large solid angles, both the $\eta \to 2\gamma$ (branching ratio $\approx 39\%$) and the $\eta \to 3\pi^0 \to 6\gamma$ (branching ratio $\approx 31\%$) [23] decay are favourable. The two-photon decay of the η' meson has only a probability of $\approx 2.2\%$ and the largest decay branching ratio for photon final states is only $\approx 8.3\%$ for the $\eta' \to \eta\pi^0\pi^0 \to 6\gamma$ decay [23]. Finally, few experiments reach the necessary incident photon energies so that there are statistically relevant results for total cross section and angular distributions only from the CLAS and ELSA facilities.

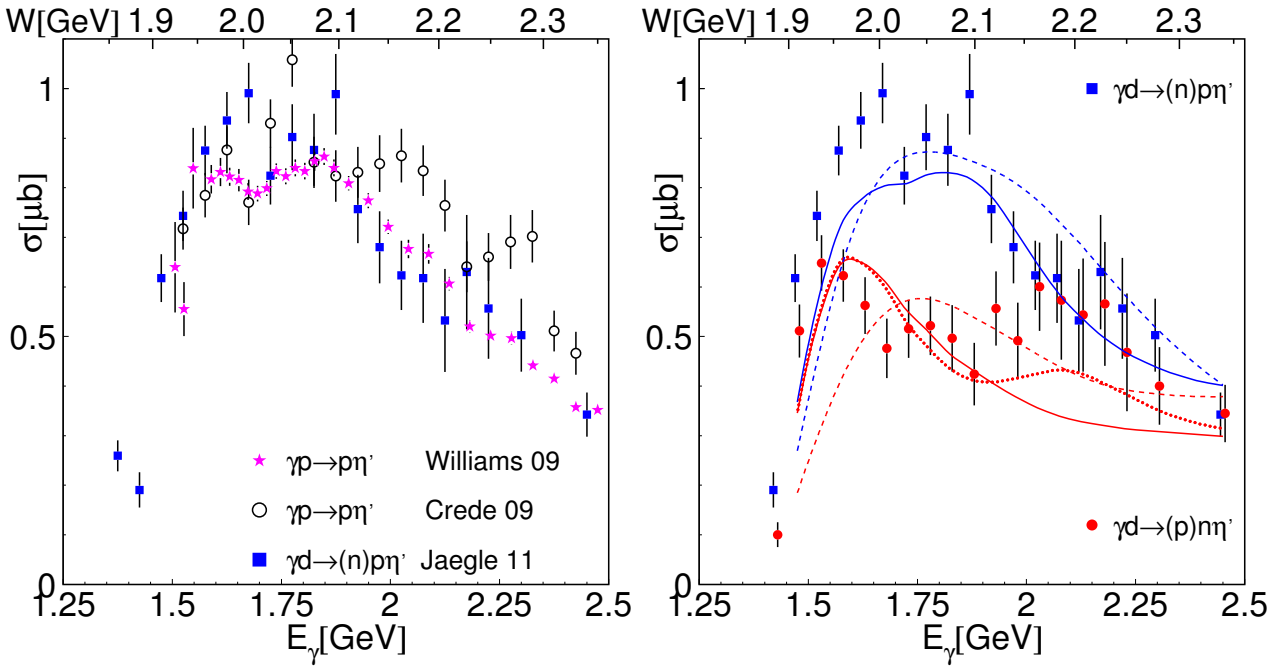

Figure 11: Total cross section for the $\gamma N \to N\eta'$ reactions. Left hand side: data for $\gamma p \to p\eta'$ from [37] (Credé 09, open black circles), [36] (Williams 09, magenta stars) and the quasi-free $\gamma d \to (n)p\eta'$ [43] (Jaegle 11, blue squares) reactions. Right hand side: quasi-free data for $\gamma d \to (n)p\eta'$ (participant proton) and $\gamma d \to (p)n\eta'$ (participant neutron) from [43]. Curves: model results from ETA′-MAID [40] (dashed blue proton target, dashed red neutron target), solid blue NH-model [92] for proton target, solid and dotted red different solutions from NH model for neutron target (see discussion in [43]).

Until the end of the 1990s the only data came from old bubble chamber measurements [93, 94] at DESY. They were analyzed in 1995 by Zhang, Mukhopadhyay, and Benmerouche [95], preparing the ground for the analysis of the expected results from the modern tagged photon experiments, in the framework of an effective Lagrangian model. They reported strong contributions from vector meson exchange (ω, ρ mesons) and a leading nucleon resonance contribution from a $D_{13}(2080)$ two-star state. This, however, did not come from the multipoles (E_{2-}, M_{2-}), where this state is resonant, but from a *background* contribution of this state to the E_{0+} multipole. In the meantime, due to the results of more recent coupled-channel analyses, this resonance has been split into two states, the three-star $D_{13}(1875)$ and the two-star $D_{13}(2120)$ [23].

The first *modern* measurement with a tagged photon beam came from the SAPHIR experiment at ELSA [96], which used the $\gamma p \to p\eta' \to p\pi^+\pi^-\eta \to p\pi^+\pi^-\pi^+\pi^-\pi^0$ reaction chain. However, it was based on only 250 events so that the statistical quality was not significantly better than the earlier bubble chamber results. The total cross section and angular distributions from this measurement have been interpreted in completely different ways. In the SAPHIR paper [96], the main emphasis was on the rapid rise of the total cross section from threshold and the linear behaviour of the angular distributions (i.e., $\propto \cos\theta^*$) between the backward and forward directions. The authors argued that the minimal model to describe such a behaviour has to include two resonances of opposite parity and the most natural choice is an S_{11} and a P_{11} state. A simple fit gave excitation energies and widths of $W \approx 1.897$ GeV, $\Gamma \approx 0.4$ GeV for the S_{11} and $W \approx 1.986$ GeV, $\Gamma \approx 0.3$ GeV for the P_{11} state.

The same data were analyzed in the framework of a Reggeized effective Lagrangian model (ETA′-MAID) [40]. There was also some evidence in this approach for contributions from an S_{11} state in the

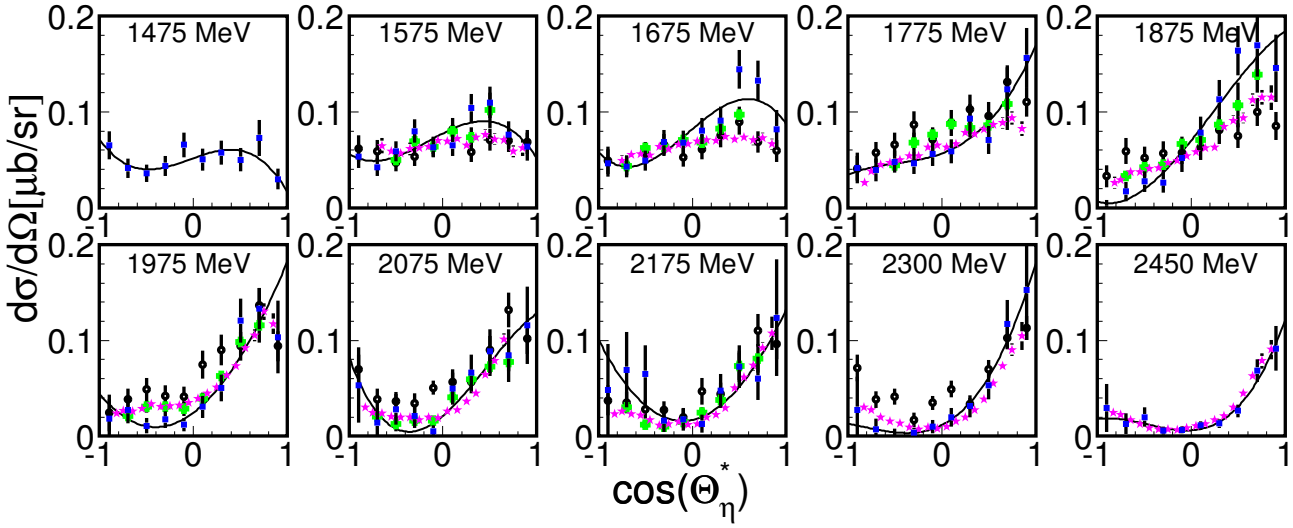

Figure 12: Selected angular distributions (mean incident photon energies quoted in the figure) for the reaction $\gamma p \to p\eta'$ off free protons (magenta stars: [36], black open circles: [37], green stars: [97]) and off quasi-free protons (blue squares: [98] bound in the deuteron). Black solid lines: fit of the quasi-free proton data with Eq. (2.2) (N=3).

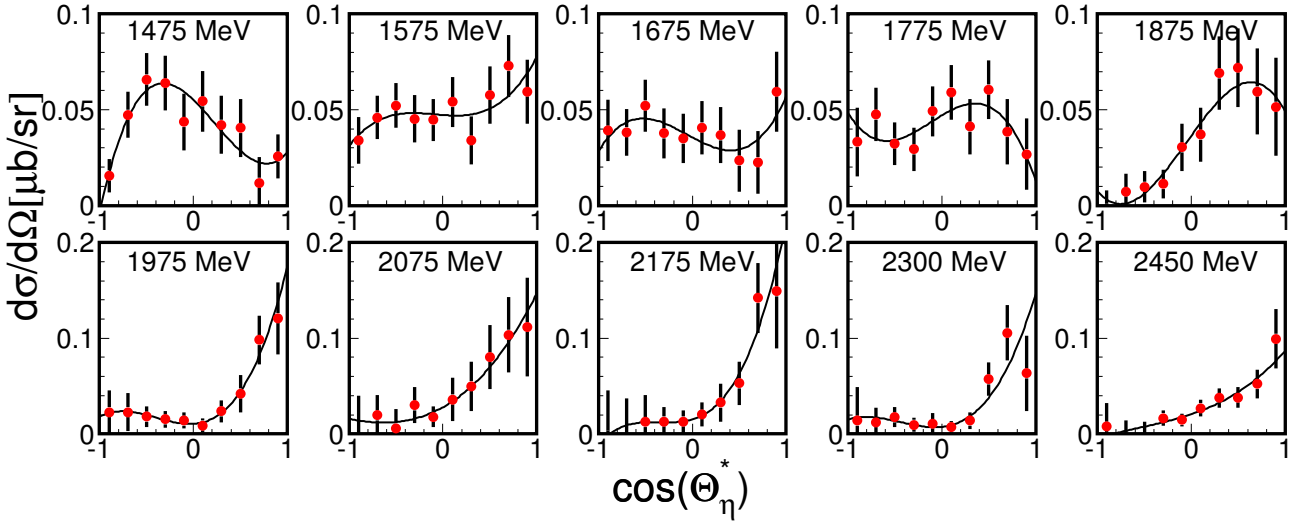

Figure 13: Selected angular distributions for different values of E_γ for the reaction $\gamma n \to n\eta'$ off quasi-free neutrons bound in the deuteron. Solid lines: fits with Eq. (2.2) (N=3).

mass range 1.932 - 1.959 GeV, but a P_{11} state was not absolutely necessary. The shape of the angular distributions could be reproduced by an interference of the E_{0+} multipole from the S_{11} resonance with the (in this case large) contributions from the Reggeized ρ and ω t-channel exchange. Elster and coworkers [99] also found large contributions from vector meson exchange and even argued that such contributions plus the tail of the well-known $S_{11}(1535)$ resonance could explain the data. More refined analyses were excluded by the low statistical quality of the cross section data and the lack of any results for polarization observables.

In the meantime the situation for the angular distributions has improved somewhat. The reaction $\gamma p \to p\eta'$ has been measured twice by the CLAS experiment at Jlab [97, 36] and by the CBELSA/TAPS experiment [37]. The quasi-free $\gamma d \to (n)p\eta'$ and $\gamma d \to (p)n\eta'$ reactions (spectator nucleons in brackets) have also been measured at CBELSA/TAPS [98]. Total cross sections from these measurements are

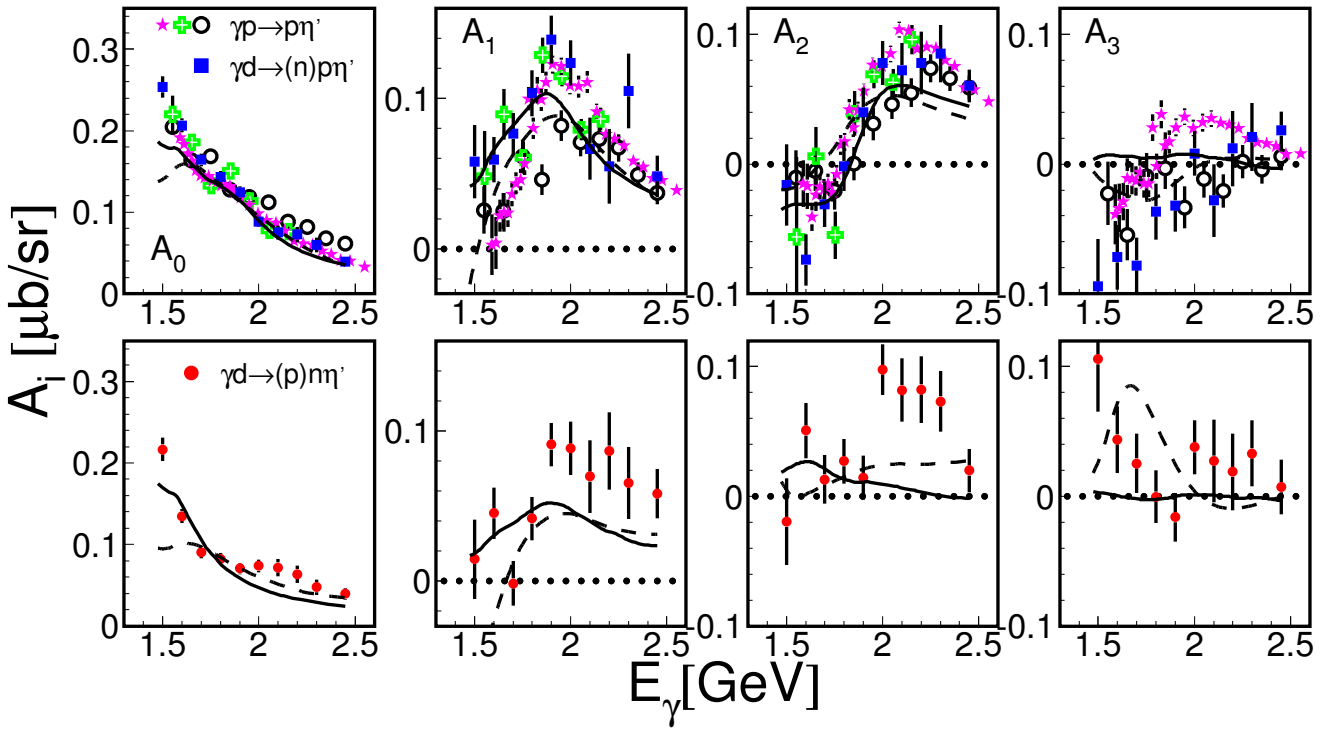

Figure 14: Coefficients of the Legendre series of Eq. (2.2) for η' photoproduction from fits with $N = 3$ ($N = 2$ for the data from [97]). Top row: free proton data from [97, 36, 37] and quasi-free proton data from [98]. Symbols as in Fig. 12. Bottom row: quasi-free neutron data from [98]. Curves: model results. Solid: NH model (solution (I), see [92],[98]), dashed: ETA′-MAID [40].

compared in Fig. 11. The two CLAS experiments published only angular distributions and the total cross sections have been extracted from fits of the distributions of [36] using Eq. (2.2) and taking the leading Legendre polynomial coefficient. The fits of the data from [97] are less stable, due to the smaller angular range, but the comparison of the A_0 coefficients of all data sets in Fig. 14 shows that the earlier CLAS data are also compatible with the other measurements.

As was the case for η-production, these experiments used different approaches to measure the reaction. The first CLAS measurement was based purely on the detection and momentum analysis of the recoil protons; the η' meson was then identified in a missing-mass analysis. This technique included all the decay channels of the meson but the background underneath the missing-mass peak was large. The proton detection efficiency was determined empirically using the $\gamma p \to p\pi^+\pi^-$ reaction. The photon flux was measured absolutely and the method for its extraction was tested with photoproduction of π^0 mesons, for which precise cross section data are known (although not in the photon energy range of interest). The second CLAS experiment [36] used the $\eta' \to \pi^+\pi^-\eta$ decay channel (branching ratio $\approx 43\%$ [23]), reconstructed the η meson as a missing particle and then analyzed the invariant mass of the $\pi^+\pi^-\eta$ system, which resulted in a much lower background level. This experiment also had absolute normalization.

The two measurements at ELSA [37, 98] used the $\eta' \to \pi^0\pi^0\eta \to 6\gamma$ decay (effective branching ratio 8.3%). Both were absolutely normalized; the free-proton measurement used kinematic fitting while the quasi-free reactions from the deuteron target were studied with a combined invariant- and missing-mass analysis. The quasi-free measurement off the deuteron was not analyzed with full kinematic reconstruction (which it was for the η data), which would be needed to eliminate the effects from Fermi

motion, because the statistical quality was not sufficient. The quasi-free $\gamma n \to n\eta'$ reaction was analyzed in two different ways, once with the coincident detection of the recoil neutron and once as the difference between the simultaneously measured inclusive cross section (without condition for recoil nucleons) and the quasi-free proton cross section, measured in coincidence with recoil protons. Both results agreed within statistical uncertainties and were averaged. The comparison of the total cross sections for the reactions off protons (see Fig. 11) show reasonable agreement (but see discussion below). Within the level of precision reached there are no systematic deviations between the free and quasi-free proton data, at least not more significant than between the different data sets for the free proton (although effects arising from Fermi motion were not reconstructed for the quasi-free data). All data sets deviate much more strongly in absolute scale from the earlier SAPHIR measurement (which had a maximum cross section of almost 2 μb, although with large uncertainties) and also in the shape of the angular distributions, where the more recent data show a slower rise to forward angles in the near-threshold region. We therefore ignore the SAPHIR data in the further discussion.

Typical angular distributions for the proton and neutron target are shown in Figs. 12 and 13. In the near-threshold region they are rather flat, which would be consistent with a substantial contribution from an s-wave. At the highest incident photon energies the angular distributions for protons and neutrons peak at forward angles, as expected for non-resonant t-channel contributions. However, they seem to rise also for extreme backward angles, which might be an indication for significant u-channel nucleonic contributions, but could also arise from the excitation of nucleon resonances (see discussion in [92]). The coefficients of the Legendre fits Eq. (2.2) are summarized in Fig. 14. They do not show such rapid variations as observed for η production.

The experimental results have been analyzed with different model approaches [40, 92, 100, 101], in particular in the context of nucleon resonance physics, but the results are not yet conclusive. A reaction model based on a relativistic meson-exchange model of hadronic interactions developed by Nakayama and Haberzettl (NH-model) [92] was first employed to describe the earlier CLAS data [97]. The authors claimed significant contributions from t-channel exchange, for which descriptions in terms of ordinary vector-meson exchange or Regge trajectories gave comparable results (with a slight advantage for the standard ρ, ω exchange). Contributions from u-channel nucleonic currents were found to be small but not well determined, due to the ambiguities in the s-channel resonance contributions. Different sets of $N^\star$ states were tested, in particular for the S_{11}, P_{11}, P_{13}, and D_{13} partial waves. Some evidence was found that such states do contribute, but the solutions were far from unique. It was pointed out that polarization observables, especially beam and target asymmetries, would be much more sensitive to discriminate between the different fits.

The results from the ETA′-MAID model [40] and the NH model were later updated to include also the quasi-free neutron data (see the discussion in [98]). Both models found contributions from the S_{11}, P_{11}, P_{13}, and D_{13} partial waves (in the NH model the latter two were below threshold). However, the resonance parameters, including also the neutron/proton electromagnetic coupling ratios, differed significantly between the two approaches. Total cross sections and Legendre coefficients of these models are compared to the measured values in Fig. 11 and 14.

In a different approach, Zhong and Zhao [100] analyzed the free and quasi-free nucleon data within a chiral quark model. They included only s- and u-channel contributions and omitted completely the t-channel terms in order to avoid double counting. In this model the leading contributions came from the u-channel and the $S_{11}(1535)$ resonance, actually a constructive interference between these two terms was held responsible for the strong rise of the total cross section from threshold. The $S_{11}(1650)$ also had a significant effect. Contributions from the higher lying $S_{11}(1920)$ were only small and the most significant resonant term above threshold was associated with a $D_{15}(2080)$ state.

Most recently, Huang, Haberzettl, and Nakayama [101] have updated the NH model to include all the available $\gamma N \to N\eta'$ data together with the results from the $NN \to NN\eta'$ and $\pi N \to N\eta'$ hadronic reactions. Apart from t-channel exchange, they find now mainly contributions from $P_{13}(1720)$,

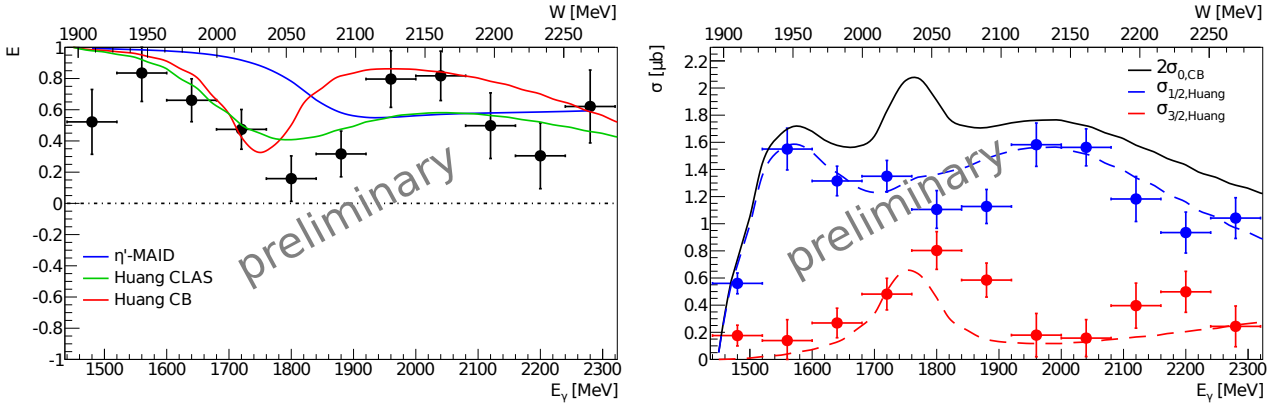

Figure 15: Preliminary $\gamma p \to p\eta'$ results for the double polarization observable E (left hand side) and the split of the total cross section (right hand side) into the $\sigma_{1/2}$ and $\sigma_{3/2}$ helicity components from the CBELSA/TAPS experiment [102]. Curves on the left are model predictions from ETA′-MAID (blue) [40] and the NH model [101] (green: NH fit to CLAS data, red: NH fit to CBELSA data). Curves on the right: NH fit to CBELSA data, black: total cross section, blue: $\sigma_{1/2}$, red: $\sigma_{3/2}$.

$P_{13}(2050)$, $S_{11}(1925)$, and $P_{11}(2130)$ states for the photon-induced reactions. However, the parameters of these resonances depend strongly on the different data sets used. In particular, the systematic differences between the most recent free-proton data from CLAS [36] and CBELSA/TAPS [37] have a significant effect (compare the total cross sections in Fig. 11, left hand side). The fit to the CBELSA data produces a relatively narrow peak structure around an invariant mass of 2.05 GeV. This peak hinges, however, on only one data point which, at the level of statistical uncertainties, could well be a simple fluctuation. The fit of the CBELSA data thus produces a relatively narrow $P_{13}(2050)$ state (widths $\Gamma \approx 50$ MeV), while for the CLAS data the width of the same state is around $\Gamma \approx 140$ MeV. The contribution of the $P_{11}(2130)$ state is also quite different for the two fits. Finally, one should note that the structure ascribed in the NH model to the $P_{13}(2050)$ state is assigned in the chiral quark model to a $D_{15}(2080)$ resonance [100].

In spite of the recent efforts in modelling the reaction, many ambiguities still exist in the interpretation of the $\gamma N \to N\eta'$ data in terms of nucleon resonance contributions. Up to now there are not even total cross sections and angular distributions that are sufficiently well determined experimentally and polarization observables are not yet avaiable. This situation will change in the near future. The total cross section and angular distributions right at threshold have been already precisely measured at MAMI (data under analysis). Polarization observables have been measured with CLAS at Jlab and with CBELSA/TAPS. These data sets are also still under analysis.

As one example of the data to come, we show in Fig. 15 preliminary results for a measurement with a circularly polarized photon beam and a longitudinally polarized target. These allow the extraction of the double polarization observable E and the division of the total cross section into its helicity components $\sigma_{1/2}$ and $\sigma_{3/2}$. The E asymmetry is positive over the entire range of photon energies measured, which means that $\sigma_{1/2}$ is always dominant. This is apparent in the separation of the helicity components shown on the right hand side of the figure. Here one should note, however, that only the values for the E asymmetry were extracted directly from data; the points for the two helicity components were then obtained by applying this asymmetry to the model fit for the total cross section. Nevertheless, the $\sigma_{3/2}$ component seems to show a local maximum around $W = 2050$ MeV where the NH-model [101] predicts the contribution from the P_{13} state and the chiral quark model the D_{15} state. Both these states could

have significant $\sigma_{3/2}$ couplings so that the E asymmetry cannot distinguish between them. However, the upcoming results for observables such as beam and target asymmetries will be more selective between different spin configurations.

First experimental data for the beam asymmetry Σ for the $\gamma p \to p\eta'$ reaction at threshold measured with a linearly polarized photon beam have very recently been reported by the GRAAL collaboration [103]. The results are very surprising. The asymmetry shows a strong polar-angle dependence (positive for forward angles, negative for backward angles with a zero crossing around 90°.), the closer to threshold the stronger. Such a behaviour is not in agreement with dominant contributions from $S-$ and $P-$wave states in the threshold region, which were favoured by all previous model analyses. The authors discuss possible P - D or S - F interferences. It is obvious that data for Σ with finer energy binning and also measurements of further polarization observables will be needed to finally identify the dominant contributions to η' threshold production. In this sense, this reaction even in the immediate threshold region is still much less understood then η-production or the production of $\eta\pi$-pairs discussed in the next section.

2.1.3 *Photoproduction of $\eta\pi$ pairs off nucleons*

The photoproduction of meson pairs plays an increasingly important role in the investigation of nucleon resonances. High lying states have an appreciable phase-space available for sequential decay modes involving an intermediate excited state. Furthermore, sometimes such decays might be preferred for nucleon structure reasons. In some higher lying multiplets in the quark model, both oscillators may be excited. It is then plausible that such states will de-excite first one oscillator in a decay to an appropriate excited nucleon state, which subsequently decays to the nucleon ground state. It is thus possible that direct decays to the nucleon ground state could be strongly suppressed for an entire multiplet of states which must therefore be searched for and studied through cascade decays. The problem is similar to ones in nuclear physics. If only direct decays to the ground state of nuclei had been looked for, many excitation degrees of freedom, such as collective rotations or vibrations, would have been missed.

The many degrees of freedom associated with the photoproduction of pseudoscalar meson pairs complicate, of course, the interpretation of the results. Such transitions involve eight complex amplitudes [104] that are functions of five kinematic variables (for example, two Lorentz invariants and three angles). The measurement of eight independent observables would be needed just to extract the magnitudes of all the amplitudes in a unique way (not even considering ambiguities arising from finite statistical precision of the data). Fixing in addition the phases would require the measurement of 15 observables. It is therefore clear that the analysis of differential cross section data alone cannot solve the problem. A complete measurement appears totally unrealistic but the measurement of at least a few polarization observables will be indispensable.

It is mostly the production of pion pairs that was so far studied (see e.g., [105, 106, 107] and references therein), but over the last few years $\eta\pi$-pairs have also moved into the frame. Their production is more selective since the isoscalar η can be only emitted in $N^\star \to N^{(\star)}$ and $\Delta^\star \to \Delta^{(\star)}$ decays. One may therefore expect that two classes of nucleon resonances may play important roles for $\eta\pi$ production, viz. excited $\Delta^\star$-states with significant η-decays to the $\Delta(1232)$ and $N^\star$ and $\Delta^\star$ resonances decaying to $S_{11}(1535)$ via pion emission. Both types of decays select in a unique way sub-classes of nucleon states with special properties. At higher incident photon energies there should also be contributions from the decay of the $a_0(980)$ meson, which decays dominantly to $\eta\pi$ [23]. Particularly interesting for nucleon resonance physics is the neutral $\eta\pi^0$ decay where the non-resonant background is suppressed. Most recent results were obtained for this channel.

Total cross sections, invariant mass distributions, and also some polarization observables for the $\gamma p \to p\pi^0\eta$ reaction have been measured at LNS [34], GRAAL [109], ELSA [111, 112, 113, 114, 115], and at MAMI [110, 116]. The three-body final state cannot be identified through a missing-mass analysis of

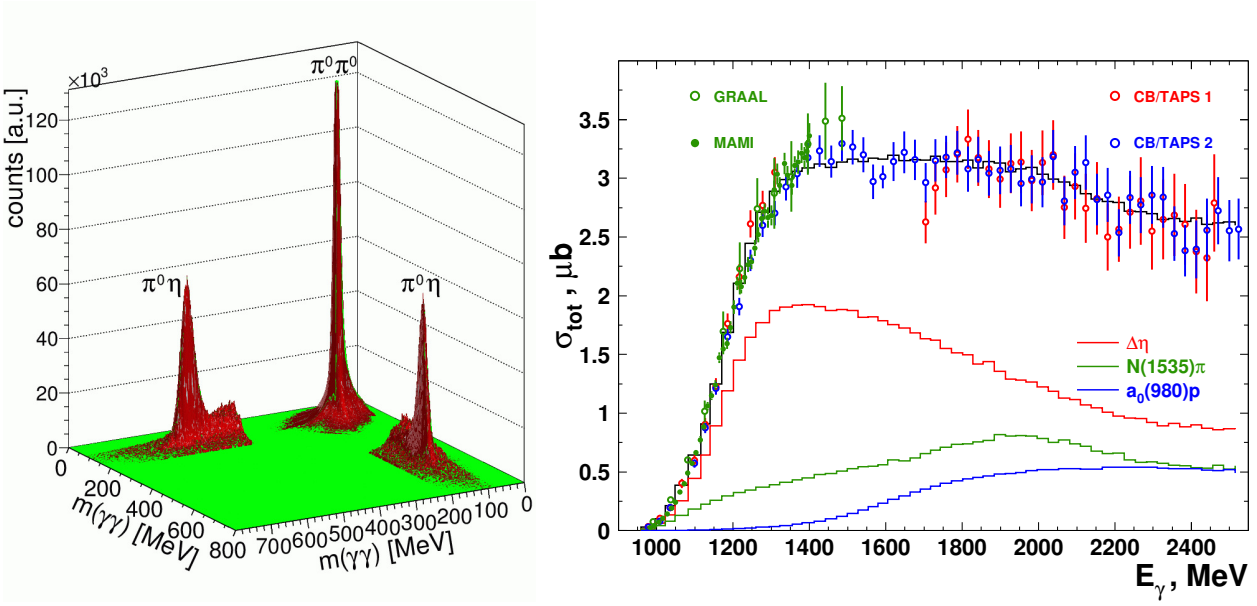

Figure 16: Left hand side: typical two-dimensional invariant mass spectrum for four-photon events from $\gamma p \to pX$ with $X = 2\pi^0$ and $\eta\pi^0$ peaks (data from Crystal Ball/TAPS at MAMI [108], the region around the $\eta\pi$ peak is scaled up). Right hand side: Total cross section for $\gamma p \to p\pi^0\eta$ from [109] (GRAAL, green open circles), Crystal Ball/TAPS at MAMI [110] (filled green circles) and two data sets from CBELSA/TAPS [111] (CBTAPS 1, CBTAPS 2, open red and blue circles). The red, green, and blue histograms show the results of the BnGa analysis for the $\Delta\eta$, $S_{11}(1535)\pi^0$, and $a_0(980)p$ final states; the black histogram represents the full fit.

the recoil proton and all decay modes of the $\eta\pi^0$ pair with reasonably large branching ratios involve four or more photons (from the π^0 decay and the $\eta \to 2\gamma$, $\eta \to 3\pi^0 \to 6\gamma$, or $\eta \to \pi^0\pi^+\pi^- \to 2\gamma\pi^+\pi^-$ decays). Only experiments equipped with electromagnetic calorimeters that cover almost 4π can successfully investigate this reaction. All the recent measurements used the $\eta\pi^0 \to 4\gamma$ decay channel (branching ratio ≈38.9%) and identified the reaction by combining invariant- and missing-mass analyses, with or without kinematic fitting.

A typical two-dimensional invariant-mass spectrum for the reaction is shown on the left-hand side of Fig. 16. The results for the total cross section are summarized on the right of the same figure. The overall shape of the excitation function, with the rapid rise from the threshold at $E_\gamma^{\rm thr} = 930$ MeV and the flattening out up to $E_\gamma = 2.5$ GeV is well established, but there are still discrepancies between different measurements in the absolute normalization. The data from the earlier Crystal Barrel experiment [112, 113] (not shown in the figure) reach a maximum cross section of almost $4\mu b$ (but have systematic uncertainties on the 20% level); the recent CBELSA/TAPS data [111] shown in the figure have been normalized in the absolute scale to the low energy GRAAL and MAMI data (renormalization factors on the order of 20%).

For the unpolarized data angular distributions (in different frames) and invariant mass distributions of the meson pairs and the nucleon - meson pairs (Dalitz plots) have been measured. Typical results for the invariant mass distributions from the most recent CBELSA/TAPS measurement are summarized in Fig. 17. Already without a detailed model it is obvious from these results that the three reaction types discussed above make significant contributions: $\Delta^* \to P_{33}(1232)\eta$ decays produce a pronounced peak in the $p\pi^0$ invariant mass around 1232 MeV/c^2, $(N^\star, \Delta^\star) \to S_{11}(1535)\pi^0$ decays lead to an accumulation of strength in the $p\eta$ spectra at the lower limit of possible invariant masses (the sum of the proton and

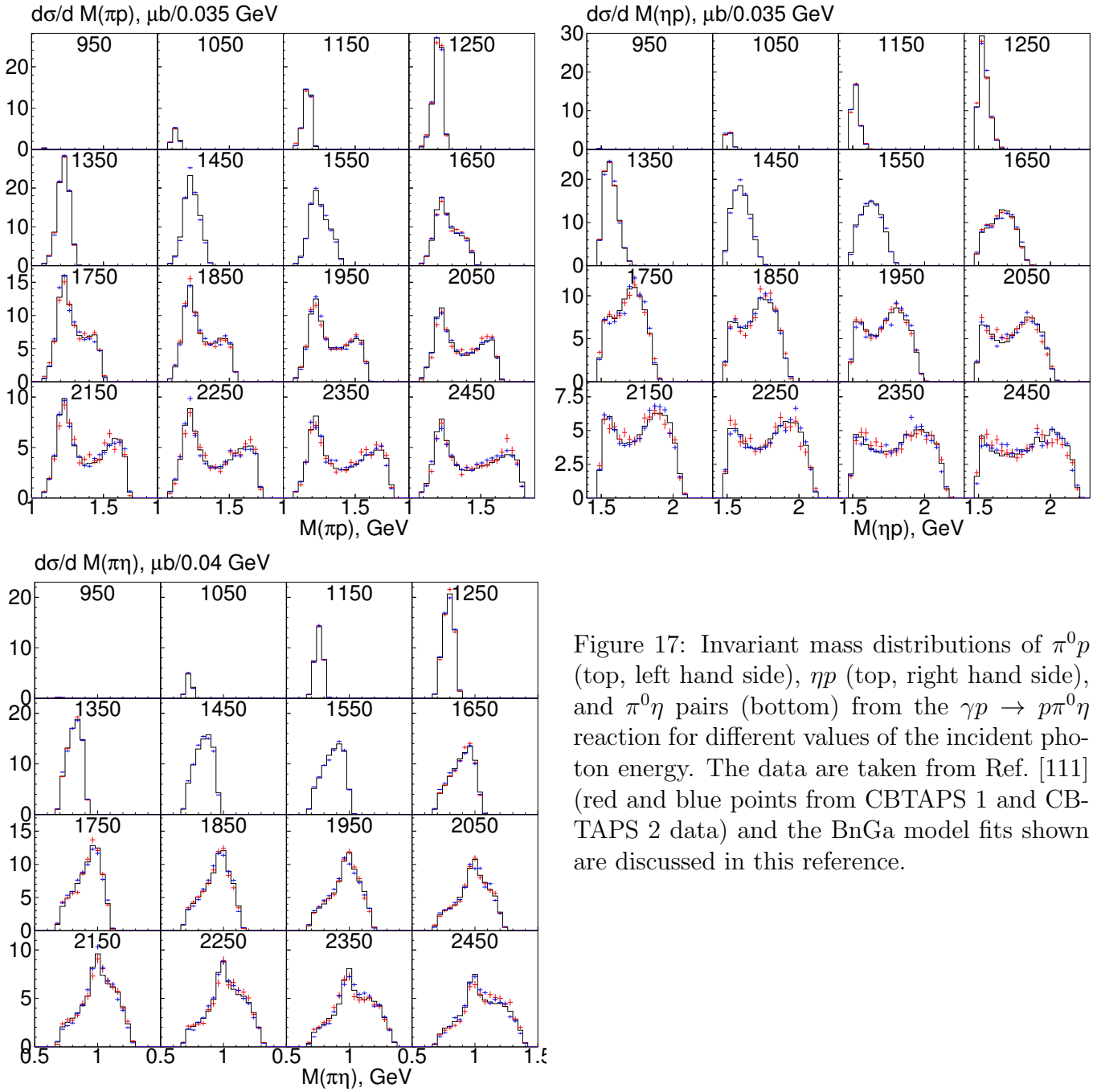

Figure 17: Invariant mass distributions of $\pi^0 p$ (top, left hand side), ηp (top, right hand side), and $\pi^0\eta$ pairs (bottom) from the $\gamma p \to p\pi^0\eta$ reaction for different values of the incident photon energy. The data are taken from Ref. [111] (red and blue points from CBTAPS 1 and CBTAPS 2 data) and the BnGa model fits shown are discussed in this reference.

η mass of 1485 MeV/c^2 is not much below the resonance position), and the $a_0(980)$ meson shows up as a peak in the $\eta\pi^0$ invariant masses.

Polarization observables have so far only been explored with polarized photon beams (linearly polarized at GRAAL and ELSA [109, 111, 115] and circularly polarized at MAMI [116]). Such observables for a final state with a nucleon and a pair of pseudoscalar mesons can be analyzed in different ways (see Refs. [104, 117] for a general discussion). For the results from the GRAAL [109] and CBELSA/TAPS [111] experiments, beam asymmetries were analyzed in quasi-two-body kinematics assuming $\gamma p \to \eta X$, $\gamma p \to \pi^0 Y$, and $\gamma p \to pZ$, where $X \to p\pi^0$, $Y \to p\eta$, and $Z \to \eta\pi^0$ were considered as intermediate state particles. One can, however, also use a full three-body approach, which involves additional degrees of freedom. The kinematics are depicted in the left-hand side of Fig. 18. In contrast to single meson production, two independent planes can be defined, for example the reaction plane spanned by the inci-

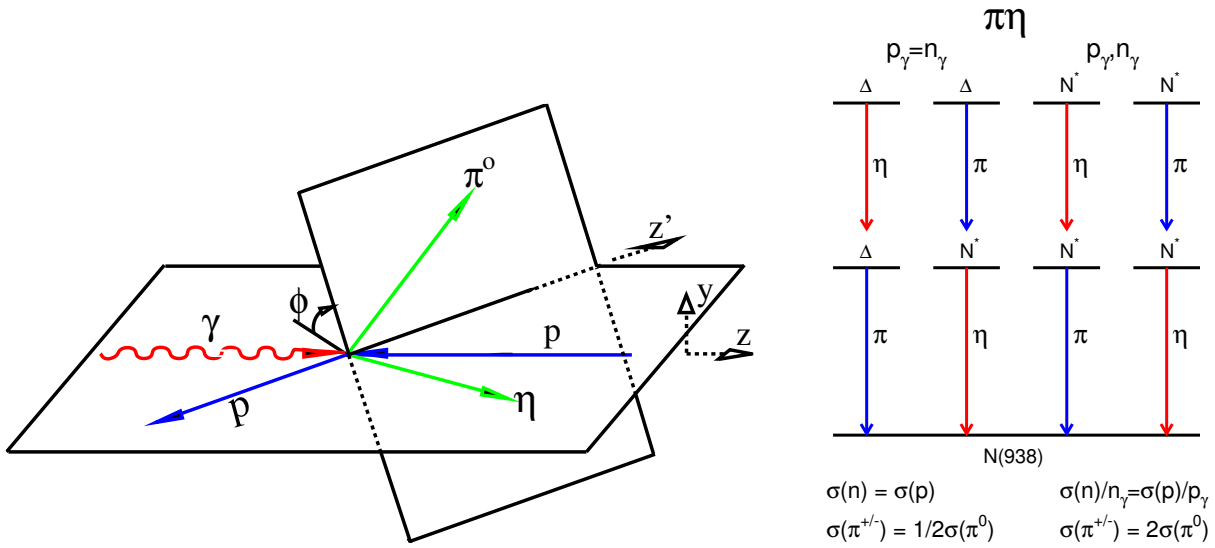

Figure 18: Left hand side: Vector and angle definitions in the c.m. system. ϕ is the angle between the reaction plane (defined by $\vec{k}$ and $\vec{p}_p$) and the production plane of the two mesons (defined by $\vec{p}_{\pi^0}$ and $\vec{p}_\eta$). Right hand side: possible decay chains and their cross section relations for production off protons and neutrons, and for neutral and charged pions.

dent photon and the recoil nucleon and the production plane spanned by the two mesons. Modulations of the differential cross section can then be observed as function of the angle ϕ between the two planes.

For a linearly polarized beam the differential cross section is then given by

$$\frac{d\sigma}{d\Omega} = \left(\frac{d\sigma}{d\Omega}\right)_0 \left[1 + p_l(I^c(\phi)\cos 2\phi + I^s(\phi)\sin 2\phi)\right], \tag{2.5}$$

where p_l is the degree of linear polarization and I^s and I^c are polarization observables with

$$I^s(\phi) = -I^s(2\pi - \phi) \;\; = \;\; \sum_{n=1}^{\infty} a_n \sin n\phi\,, \tag{2.6}$$

$$I^c(\phi) = \;\; I^c(2\pi - \phi) \;\; = \;\; \sum_{n=0}^{\infty} b_n \cos n\phi\,. \tag{2.7}$$

The constant ($n = 0$) term in the expansion of I^c corresponds to the two-body beam asymmetry Σ.

For a circularly polarized photon beam (which due to parity invariance does not produce asymmetries for two-body final states) one gets

$$\frac{d\sigma}{d\Omega} = \left(\frac{d\sigma}{d\Omega}\right)_0 \left[1 + p_\odot I^\odot(\phi)\right]\,, \tag{2.8}$$

where $p_\odot$ is the degree of circular polarization and $I^\odot(\phi)$ can be also expanded in the form of Eq. (2.7).

The polarization observables are very sensitive to small reaction amplitudes that enter only via interference terms. The asymmetry $I^\odot$, e.g., has been recently much explored for the photoproduction of pion pairs [118, 119, 120, 121], where it uncovered many deficiencies in the existing model analyses of these reactions. The asymmetries for the $\eta\pi^0$ final state are substantial; experimental results for I^s and I^c are discussed in [111, 115] and results for $I^\odot$ in [116].

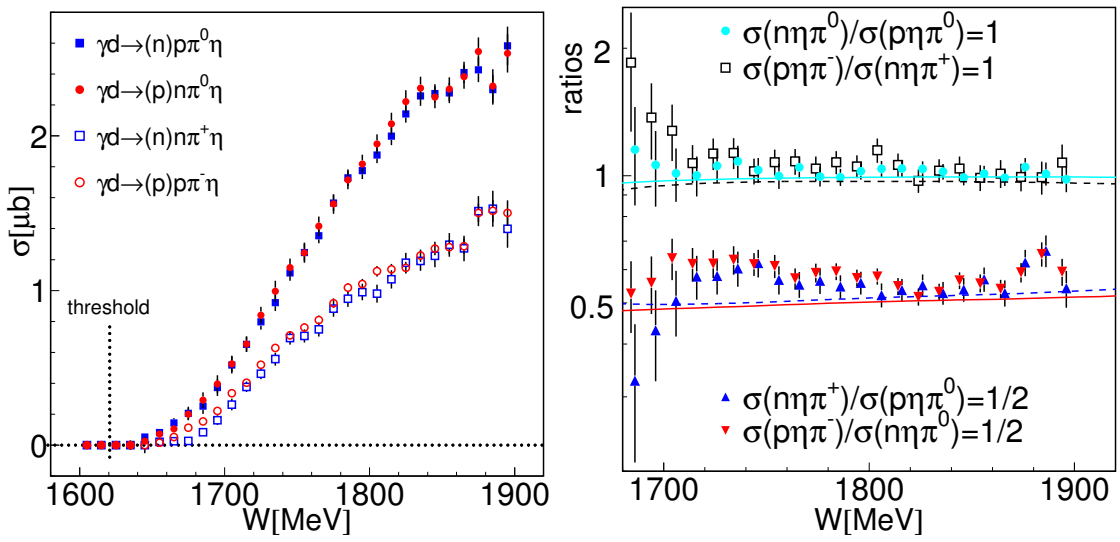

Figure 19: Quasi-free excitation functions for $\gamma N \to N\eta\pi$ measured with a deuteron target. Left hand side: total cross sections, right hand side: cross section ratios. All data are preliminary. The model results are from [110, 125].

The experimental results have been studied within the BnGa coupled-channel analysis (see [111, 112, 113, 115]), an isobar model developed by Fix and collaborators (see [110, 116, 122]), and were also compared to the results from a chiral unitary approach (see [109, 123, 124]). Although there are differences between the details of the results from the models, the main features seem to be quite stable. All models agree that close to threshold the reaction is dominated by the excitation of the $D_{33}(1700)$ resonance and its decay to $\eta P_{33}(1232)$. Contributions from non-resonant backgrounds, such as nucleon Born or t-channel exchanges, appear to be small.

The division of the total cross section into the $\eta P_{33}(1232)$, $S_{11}(1535)\pi^0$, and $a_0(980)p$ final states in the BnGa model analysis is shown in Fig. 16. The dominance of the $\Delta\eta$ final state in the threshold region is obvious. Apart from the $D_{33}(1700)$, the BnGa analysis finds contributions from several other Δ-resonances $S_{31}(1900)$, $F_{35}(1905)$ (both weak), and from $P_{31}(1910)$, $P_{33}(1920)$, and $D_{33}(1940)$ with decays into $\Delta\eta$ and $S_{11}(1535)\pi^0$ (the $\Delta\eta$ decays are always stronger) and contributions from $N^\star \to S_{11}(1535)\pi$ decays for $P_{11}(1710)$, $P_{11}(1880)$, $P_{13}(1900)$, $P_{11}(2100)$, and $D_{13}(2120)$. The analysis by Fix and coworkers [110, 122] does not extend over the same energy range (it used mainly the MAMI and GRAAL data up to an incident photon energy of 1.5 GeV) and did not clearly identify contributions from the $S_{11}(1535)\pi$ final state. For the $\Delta\eta$ final state, contributions from $D_{33}(1700)$, $P_{33}(1600)$ (weak), $P_{31}(1750)$, $F_{35}(1905)$, $P_{33}(1920)$, and $D_{33}(1940)$ are quoted. The two states $P_{33}(1920)$, and $D_{33}(1940)$ were seen in both analyses. These two states were first reported from the $\gamma p \to p\eta\pi^0$ reaction by Horn and coworkers [112] and are very interesting for nucleon structure because they form a parity doublet.

The $\gamma p \to p\pi^0\eta$ reaction is obviously an excellent tool for the study of the $D_{33}(1700)$ state. Döring, Oset, and Strottman [123, 124] have made predictions within a coupled-channel chiral unitary theory for meson-baryon scattering in which this state is dynamically generated. They predict a strong decay to the $S_{11}(1535)\pi$ final state and this is clearly reflected in the invariant mass distributions within their model. However, it does not agree well with experiment; invariant mass distributions with a dominant decay to $\Delta\eta$ fit much better [109].

Further information about the reaction mechanism comes from the isospin degree of freedom. The possible sequential resonance decays are summarized on the right-hand side of Fig. 18. The $\gamma N \to \Delta^\star \to \eta\Delta(1232) \to \eta\pi N$ reaction chain is characterized by the equal electromagnetic $\gamma N\Delta$ couplings

for the excitation of $I = 3/2$ states on neutrons and protons, the isoscalar nature of the η, and the isovector nature of the pion. It then follows immediately that the above reaction chain must have the same isospin pattern as photoproduction of single pions through the Δ-resonance:

$$\sigma(\gamma p \to \eta\pi^0 p) = \sigma(\gamma n \to \eta\pi^0 n) = 2\sigma(\gamma p \to \eta\pi^+ n) = 2\sigma(\gamma n \to \eta\pi^- p) \ . \tag{2.9}$$

Preliminary results from a measurement of all four possible final states at MAMI in quasi-free kinematics from a deuteron target shown in Fig. 19 [126] demonstrate that, up to invariant masses of 1.9 GeV this relation holds almost perfectly. This means that significant contributions from $N^\star$ excitations are ruled out for this energy range. The isospin argument does not help to distinguish between the $\Delta^\star \to P_{33}(1232)\eta \to N\eta\pi$ and $\Delta^\star \to S_{11}(1532)\pi \to N\eta\pi$ decay chains. Their contributions can be probed, e.g., by the energy distributions of the mesons discussed in Sec. 3.2.

It should be noted that important FSI effects have been observed for $\eta\pi$ photoproduction on the deuteron. The cross sections for the $\eta\pi^0$ final state are suppressed for quasi-free protons by the order of 25% with respect to free proton targets, although one should bear in mind that there are still issues concerning the absolute normalization of the free proton data sets.

2.2 η production in πN collisions

In contrast to the photoproduction case, most of the measurements of the near-threshold $\pi^- p \to \eta n$ differential cross section were carried out many years ago and some inconsistencies are apparent in the data base [127, 128, 129, 130, 131, 132, 133, 134]. There are, however, two more recent experiments where the η meson was reliably identified through its 2γ or 6γ decay mode [135, 136].

At threshold the production cross section is dominated by the $S_{11}(1535)$ isobar but, at a little higher energy, the differential cross section develops an anisotropy, as illustrated by the data [135, 136] shown in Fig. 20a at a c.m. momentum $p_\eta \approx 140$ MeV/c, i.e., an invariant mass of $W \approx 1515$ MeV/c^2. Because the distribution is fairly symmetric, it was suggested that the main deviations from isotropy could arise from the interference between s- and d-waves, where the d-wave amplitude could be quite small [135, 136]. However, the partial wave analysis curve that is also shown involves significant p-wave contributions [42].

In addition to the binning in the incident pion momentum, a more serious problem in interpreting the data is the uncertainty in the knowledge of the absolute pion momentum, which is quoted as being $\approx \pm 2.5$ MeV/c [135] or $\approx \pm 1.5$ MeV/c [136] in the two more recent experiments. Such uncertainty is particularly significant close to threshold, as can be seen in the evaluation of the average amplitude-squared:

$$\overline{|f(\pi^- p \to \eta n)|^2} = (p_\pi/p_\eta)\sigma_{\rm tot}(\pi^- p \to \eta n)/4\pi, \tag{2.10}$$

where p_π and p_η are c.m. momenta. Thus the biggest contribution to the error bars in Fig. 20b near threshold comes from the uncertainty in the absolute value of the incident beam momentum, which is a systematic effect. In all cases the s-d interference drops out in the evaluation of $\overline{|f|^2}$. The agreement with the selected older data [127, 128, 130, 133] is reasonable.

Also shown in Fig. 20b is the original scattering-length fit [137] to the older results. This clearly fails to reproduce the new data close to threshold but, on the other hand, a parameterization of the $S_{11}(1535)$ resonance [81] describes well the forward dip in $\overline{|f|^2}$. However, other masses and widths for the S_{11} resonance give an equally good description so that these data are not precise enough to tie down the resonance parameters accurately. It is important to note that the scattering lengths for both the solid and dashed lines in Fig. 20b are rather similar. The major difference lies in the neglect of the effective range term in the early work [137] and the consequent scaling to fit the data in the high p_η region.

The data on η' production in pion-nucleon collisions are even rarer. Apart from early bubble chamber work [138, 139], there were counter measurements of the $\pi^- p \to n\eta'$ cross sections near threshold [130].

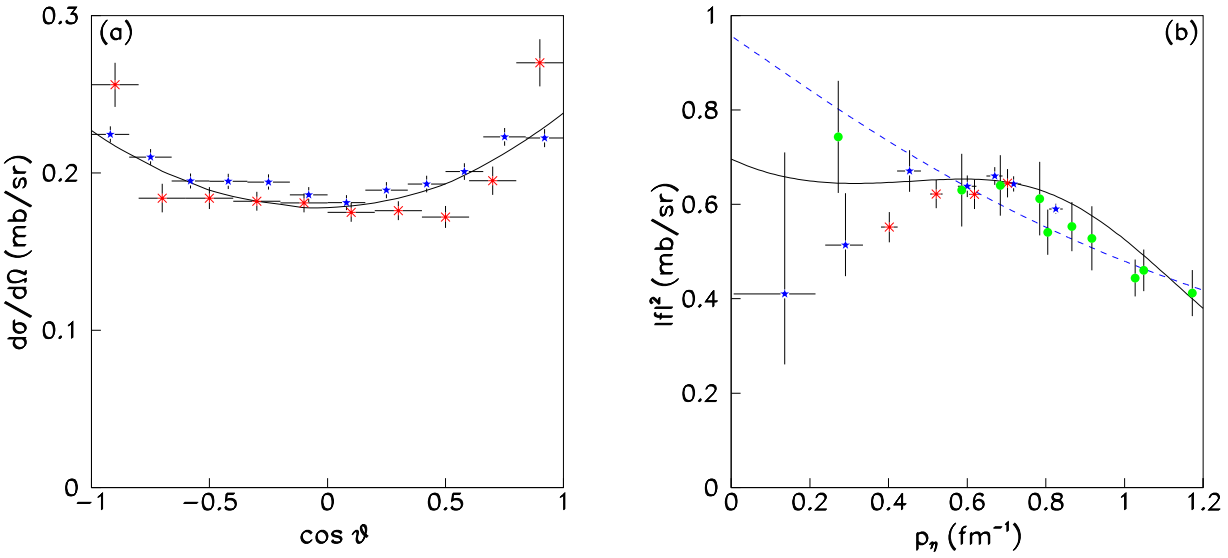

Figure 20: (a) The $\pi^- p \to \eta n$ differential cross section measured at a pion laboratory momentum of 732 MeV/c (blue stars) [135] and 730 MeV/c (red crosses) [136]. The systematic uncertainties were $\approx 6\%$ for the Brookhaven experiment [135] and rather more at Gatchina [136], mainly due to the evaluation of the acceptance. The curve represents the results of the Bonn-Gatchina partial wave analysis [42]. (b) Average amplitude-squared of the $\pi^- p \to \eta n$ reaction showing the results of Ref. [135] (blue stars) and [136] (red crosses) as well as a selection of older data [127, 128, 130, 133] (green circles). The solid (black) line represents the contribution from the $N^*(1535)$ isobar with parameters taken from Ref. [81]. The (blue) dashed line is an effective-range fit [137] to the older data.

2.3 Partial wave analysis

The only $\pi^- p \to \eta n$ results available are unpolarized differential cross sections so that the use of these data alone would necessarily involve significant ambiguities. In addition, as remarked in the previous section, the data are not very precise and their main use seems to be to determine well the branching ratios of different nucleon resonances into the ηn channel. However, the ηn system is very strongly coupled to the $\pi^- p$, as is seen in the energy dependence of the pion charge-exchange reaction $\pi^- p \to \pi^0 n$ in the backward direction, which has a clear cusp at the ηn threshold [140].

Several coupled-channel partial wave analyses have been carried out in recent years [42, 57, 81, 141], generally using also information gained from η photoproduction from the proton. Although the main resonance findings are qualitatively similar, there are significant differences in the details that were discussed in the photoproduction section.

3 Production in γA reactions

In section 2 we already discussed photoproduction of mesons off light nuclei where the aim was the study of quasi-free production on the neutron. However, the photoproduction of mesons off medium and heavy nuclei is mostly used as a tool for the investigation of meson - nucleon (meson - nucleus) interactions and in-medium properties of hadrons. The experiments can be grouped into three different types of final states (although this characterization is not always unique and intermediate situations exist), where different physics topics are explored.

- In breakup reactions, at least one nucleon is removed from the nucleus and this includes the so-called quasi-free processes. In the simplest picture of such a reaction, the incident photon interacts with one individual nucleon, the 'participant' off which the meson is produced, while the rest of the nucleons in the nucleus act only as spectators. This is the approach used for the extraction of elementary cross sections off neutrons bound in light nuclei but, for heavier nuclei, FSI processes involving the 'spectator' nucleons will always be important. Reactions of this type are explored for the study of meson - nucleus interactions and for the investigation of hadron in-medium properties. A recent review of the in-medium properties of scalar and vector mesons derived from photoproduction and other reactions is given by Leupold, Mosel, and Metag [142]; results for the in-medium properties of nucleon resonances are summarized, e.g., in [143].

- Coherent meson photoproduction is characterized by a final system where the target nucleus remains in its ground state. By exploiting the spin and isospin quantum numbers of the nucleus one can in principle project out specific parts of the elementary reaction amplitudes. This was, for example, used (as discussed in section 3.2) to unravel the isospin decomposition of the electromagnetic $S_{11}(1535)$ excitation using the photoproduction of η-mesons on the deuteron. The coherent reaction is also used as a doorway for the search of meson-nucleus bound states, such as the η or η' mesic nuclei. However, with few exceptions, the typical cross sections are small and the experiments are demanding (in most cases coherent reactions are difficult to identify in the presence of much larger contributions from breakup reactions). Detailed studies are so far only available for π^0 mesons to investigate the in-medium behaviour of the $\Delta(1232)$ resonance (see e.g., [144, 145]) and, in a completely different context, for the extraction of nuclear mass form factors [146, 147, 148].

- In incoherent production the final-state nucleus is excited (but otherwise identical with the initial state nucleus) and de-excites typically by the emission of γ-radiation. Such processes provide additional selection possibilities as spin- and isospin filters or may be used to study transition form factors. However, they are still almost unexplored, due to the small reaction cross sections. For π^0 photoproduction there is a recent measurement for the 4.4 MeV excited state of ^{12}C [149].

3.1 Inclusive production

In this section we will summarize the results for reactions where only the produced meson is used to characterize the final state. Since the cross sections for coherent production of η and η' mesons are very small (see section 3.2), the inclusive reactions are completely dominated by the breakup contributions. The interaction of mesons with nuclei has contributed greatly to our knowledge of the strong interaction. Many properties of meson - nucleon potentials have been studied with elastic or inelastic reactions induced by pion or kaon beams. However, such beams are only available for long-lived, charged mesons. The interaction of short-lived neutral mesons, such as the η, η', and ω, can only be studied in indirect ways when they are produced by some initial reaction in a nucleus and then interact within the same nucleus. Such measurements provide data for the extraction of meson - nucleus potentials, of meson in-medium properties like modified masses and/or lifetimes, and may also test the in-medium properties of nucleon resonances.

Photoproduction is advantageous because there are almost (apart from small shadowing corrections [155]) no complications from initial state interactions. Due to the small cross section of the electromagnetic reaction, photons interact also with nucleons bound deeply in heavy nuclei, while hadron-induced reactions explore mostly the nuclear surface. A comparison of the cross sections for photoproduction of mesons off nuclei with different mass numbers therefore gives an easy tool to study the absorption properties of nuclear matter for a particular meson. Within some modelling approaches - for example

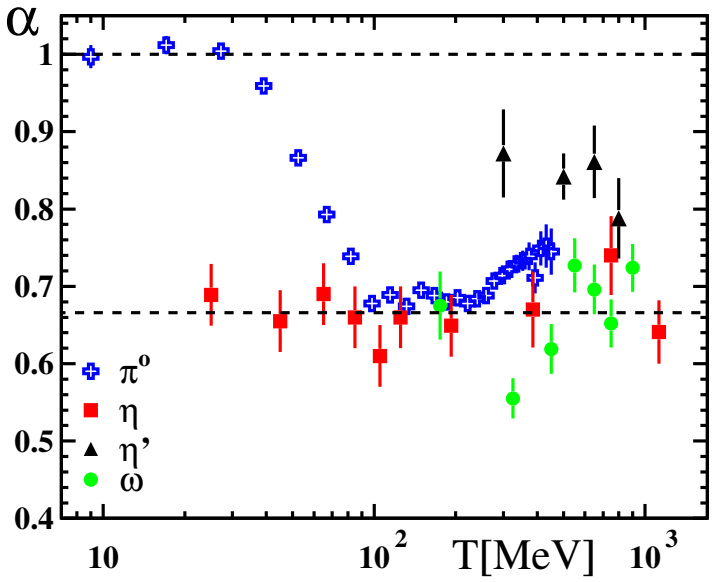

Figure 21: Scaling parameter α as a function of meson kinetic energy T for π^o [150], η [151, 152], η' [153], and ω mesons [154].

the Glauber-type approximations as in [151] - these can be converted into a meson - nucleon absorption cross section.

A convenient technique is the study of the scaling of the meson production cross sections with nuclear mass number A. This typically exhibits a power-law behaviour

$$\frac{d\sigma}{dT}(T) \propto A^{\alpha(T)}, \tag{3.1}$$

where T is the kinetic energy of the mesons. Qualitatively, small absorption cross sections (*transparent nucleus*) correspond to a scaling of nuclear meson production with the volume of the nuclei, i.e., with their mass number A ($\alpha \approx 1$), while large absorption cross sections (*black nucleus*) result in a scaling corresponding to the nuclear surface, i.e., with $\alpha \approx 2/3$. Typical results are summarized in Fig. 21 for π^0, η, η', and ω mesons (details for η and η' are discussed below). The absorption properties for these mesons are quite different. Pions are strongly absorbed when their kinetic energy is high enough (> 100 MeV) to excite the $\Delta(1232)$ resonance, but nuclei are transparent for low-energy pions [150].

The pion - nucleon interaction is weak at low momenta so that pions cannot be bound in nuclei (though negative pions can be bound with the help of the Coulomb force [156]). The situation is completely different for η mesons. Almost independent of their kinetic energy, over a wide range from a few 10 MeV to 1 GeV, the scaling coefficient is close to 2/3 [151, 152]. The absorption is large, which means that the meson - nucleon interaction is strong. The difference in the low-energy behaviour for pions and η mesons is due to the properties of the $S_{11}(1535)$ nucleon resonance. An s-wave resonance with strong coupling to $N\eta$ located very close to (and overlapping with) the η production threshold generates a very efficient absorption channel for low-energy η mesons. The η - nucleon interaction at low relative momenta is strong, which is the basis for the investigation of possible η-mesic states to be discussed later. The absorption of ω mesons is also strong [154] but η' mesons show an intermediate behaviour, with scaling coefficients around 0.8 - 0.9 [153].

Inelastic meson - nucleon cross sections have been estimated from the scaling of the cross sections, either from the scaling coefficients in Glauber-type analyses or from an analysis of the so-called transparency ratios, discussed below in the framework of different models. The η-nucleon absorption cross

section $\sigma_{\eta N}$ in nuclear matter was determined from such data [151] to be around 30 mb, corresponding to a typical mean free path of $\lambda \approx 2$ fm. For the ω meson an absorption cross section of 70 mb was deduced [154], which is roughly a factor of three larger than the accepted $\sigma_{\omega N}$ cross section for free nucleons. A similar result had been previously reported from the LEPS collaboration for the ϕ meson [157]. In this case an absorption cross section of ≈ 30 mb was deduced, which has to be compared to the free nucleon absorption cross section of 7.7 - 8.7 mb. Both experiments have produced strong evidence for the much discussed in-medium modification of vector mesons. The inelastic $\eta' N$ cross section, on the other hand, was estimated in the range of 3 - 10 mb from similar analyses [153]. The absorption cross sections are responsible for an increase of the widths of the mesons in nuclear matter (due to the absorption-related decrease of their lifetimes), which is connected to the imaginary part of the meson - nucleus optical potential. The real part of the potential is reflected in a modification of the meson masses. For ω mesons a very strong broadening from ≈ 8.5 MeV in vacuum to 130 - 150 MeV in nuclear matter has been reported [154] while, for the η', in-medium widths on the order of 15 - 25 MeV have been extracted [153] (compared to ≈ 0.2 MeV in vacuum).

In the low-density approximation the absorption cross section and in-medium width are related by [153, 154]

$$\Gamma = \rho_o \, \sigma_{\text{inel}} \, \beta \, , \tag{3.2}$$

where Γ is the meson width in normal nuclear matter density ρ_o, σ_{inel} is the inelastic cross section, and $\beta = p_m/E_m$ the meson velocity. If the same relation is assumed for η mesons, the absorption cross section of ≈ 30 mb corresponds to an in-medium width of 70 - 95 MeV (vacuum width 1.3 keV) for η mesons with kinetic energies between 200 and 1000 MeV. For mesons with lifetimes as long as those of the η and η', a measurement of the absorption cross sections is the only way to access the in-medium width. A direct measurement of the width is not possible since the mesons are either absorbed by nucleons or escape from the nucleus and subsequently decay in vacuum.

We now discuss in greater detail the results for η and η' production. Inclusive photoproduction of η mesons from nuclei has been measured for the deuteron [43, 51, 52, 53, 55], for ^{3}He [45], and for heavier nuclei such as ^{12}C, ^{40}Ca, ^{63}Cu, ^{93}Nb, $^{\text{nat}}$Pb [151, 152, 158, 159] at MAMI, at KEK, in Tohoku, and at ELSA. In general, the agreement between the different measurements is good (see comparisons in [152]). Typical results for total inclusive cross sections for heavy nuclei from the most recent measurement [152], covering the widest energy range, are summarized in Fig. 22 (angular and energy-dependent differential cross sections are also given in [152]). The experimental results are compared to calculations in the framework of the Giessen version (see [160] for a recent review) of the Boltzmann-Uehling-Uhlenbeck (BUU) transport model, which incorporates all relevant elementary production cross sections and then traces the space-time evolution of an ensemble of interacting particles $N, N^\star, \Delta, \pi, \eta, ...$ in nuclear matter from the moment of their creation to their absorption or their escape through the outer boundaries of the nucleus. Effects like Fermi motion and Pauli-blocking of final states are of course included. In short, the model incorporates all *trivial* in-medium effects (such as, e.g., collision broadening of hadrons in nuclear matter due to the additional decay channels) and, as long as all reaction cross sections are known precisely enough, can be used as a kind of *null* hypothesis for non-trivial quantum mechanical in-medium effects (such as, e.g., chiral restoration effects).

The production of η-mesons from nuclei is complicated by two factors. At incident photon energies above 930 MeV the cross section for the production of $\eta\pi$ pairs (see Sec. 2.1.3) rises rapidly and reaches values comparable to single η production. But these two reactions are not easily distinguishable. Experimental difficulties arise in particular in the case of charged pions, which might escape detection when they are too low in energy or emitted along the beam-pipe. Furthermore, the pions may be lost due to FSI in the production nucleus. However, one could argue that, for the measurement of the absorption properties of η mesons in nuclear matter, such effects do not matter much because the absorption probability of an η depends only on its kinetic energy and not on its initial production

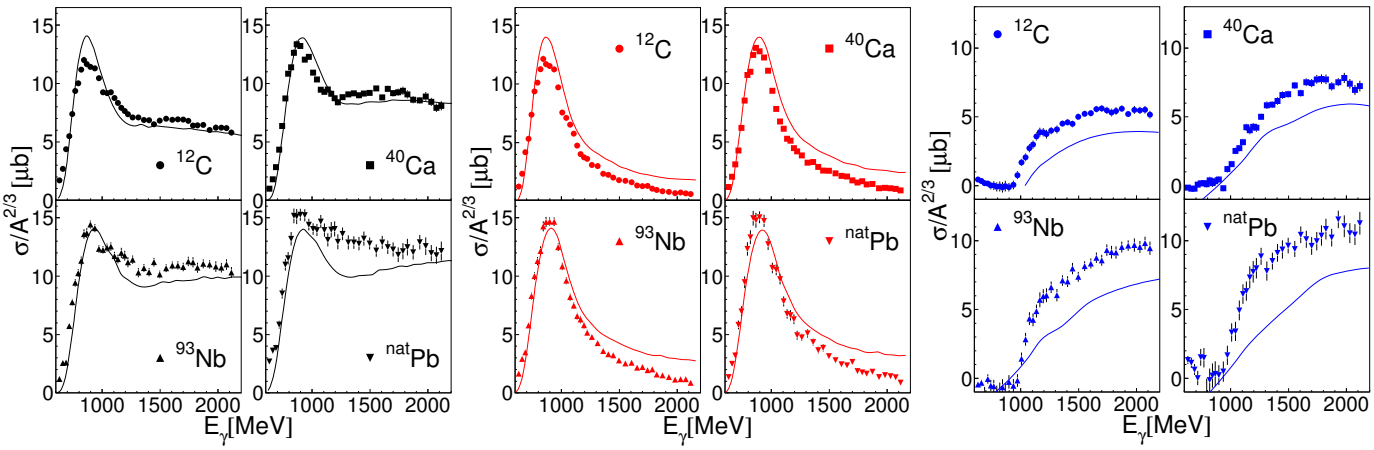

Figure 22: Total cross sections for η photoproduction off heavy nuclei from [152]. Left hand side: fully inclusive η production ($\gamma A \to X\eta$, no restriction on X, which can be a multi-particle final state, possibly also including further mesons such as pions). Centre: exclusive quasi-free η-production $\gamma A \to (A-1)N\eta$ (identified by cuts on the reaction kinematics). Right hand side: difference between the inclusive and exclusive cross section, which arise mainly from $\gamma A \to (A-1)N\eta\pi$. Data from [152], theory curves from GiBUU model [161, 162, 163, 164] taken from [152].

reaction. More problematic are the η that are produced in secondary reactions where, in the first step for example a pion is produced, which is then reabsorbed by a nucleon to produce an η. This reaction chain contributes significantly since the production cross section for pions is large and the $S_{11}(1535)$ resonance, which has an almost 50:50 branching ratio to $N\pi$ and $N\eta$, offers a very efficient conversion mechanism. In contrast to the direct processes, secondary production will not scale linearly with the mass number so that the scaling behaviour of the final and initial states will be mixed.

The left hand side of Fig. 22 shows the total inclusive reaction cross section $\gamma A \to \eta X$ (no condition on X) for different nuclei. The agreement with the BUU calculation is quite good for carbon, calcium, and niobium, but somewhat poorer for lead. The central part of the figure shows the best possible approximation for single, quasi-free production of η mesons, which has been selected by a cut on the missing mass of the reaction (cut at $\Delta m > 140$ MeV/c^2, see the missing-mass spectra in Fig. 23). This cut removes the production of $\eta\pi$ pairs but not all the contributions from secondary reactions. Nevertheless, the comparison of data and BUU predictions shows that the $S_{11}(1535)$ resonance does not show any unexpected in-medium modifications. The peak shape agrees reasonably well with the BUU predictions and the cross sections scales with $A^{2/3}$. The right hand side of the figure shows the difference of the inclusive and exclusive reactions. This cross section rises strongly at the $\eta\pi$ production threshold (for free nucleons at 930 MeV) and has an energy dependence similar to the photoproduction of $\eta\pi$ pairs. The peak cross sections are in the range of 2.2μb/A for ^{12}C and 1.7μb/A for Pb, which are in reasonable agreement with the $\approx 2\mu$b/A cross section average for the $\pi^0\eta$ and $\pi^\pm\eta$ final states measured for the deuteron target (see Sec. 2.1.3). In this sense one may regard the data as an indirect measurement of $\eta\pi$ production off nuclei. These data include, of course, contributions from secondary processes. The BUU model results suggest that this contribution is at the same level or even larger than $\eta\pi$ production. However, the results of this model are not in good agreement with data. They underestimate the difference cross section (see Fig. 22, right hand side) and do not reproduce the shape of the missing-mass spectra. A comparison of the data and model results demonstrates that the excess of the measured cross section compared to the BUU results is related to large missing masses in the region where both $\pi\eta$ and secondary production peak, while single η production seems to be much better described by the model (see Fig. 23, right hand side).

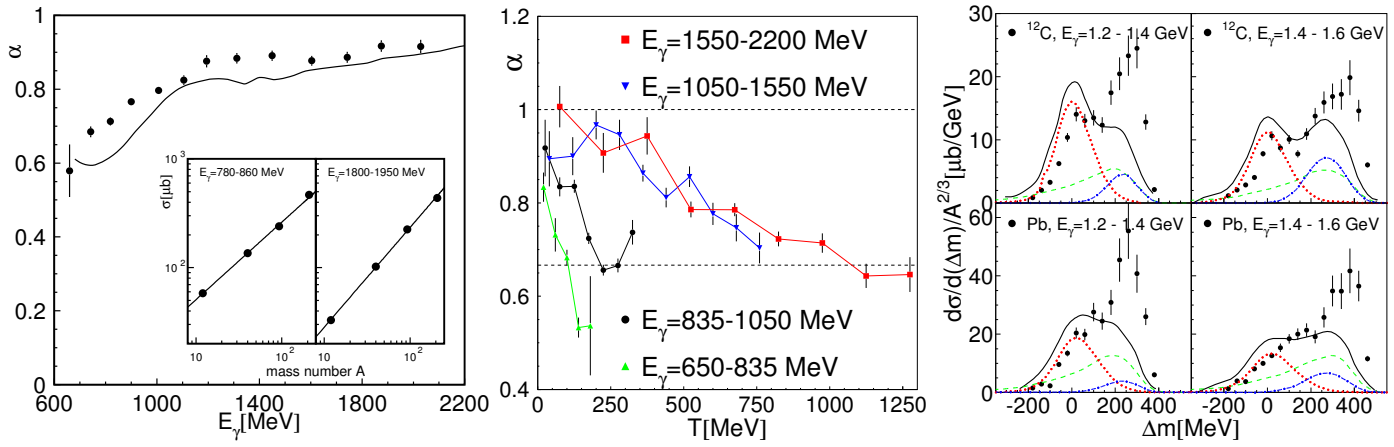

Figure 23: Left hand side: scaling parameter α as function of E_γ for fully inclusive η production. Insert: two examples of individual fits. Centre: scaling parameter α as a function of the η kinetic energy for different ranges of incident photon energy. Right hand side: missing-mass distributions. All data from [152]. Results from the GiBUU model for the missing mass [152], solid (black) curves: full model, dotted (red): single, quasi-free η production, dash-dotted (blue) $\eta\pi$ production, dashed (green) η production from secondary processes. All cross sections normalized to $A^{2/3}$, figures from Ref. [152].

The analysis of the scaling behaviour for η mesons is summarized in Fig. 23. The left hand side shows the scaling coefficient for the total cross section. It rises from $\approx 2/3$ at threshold to almost unity at the highest incident photon energies. It might be tempting to interpret this as showing that close to threshold nuclear matter is black for η mesons, due to absorption into the $S_{11}(1535)$ state, but then becomes more transparent at higher incident photon energies, where no strong coupling to resonances exists. However, the central part of the figure shows that this is not the case. Plotted are the scaling coefficients as functions of the meson kinetic energy for different ranges of incident photon energy. The expectation is that the absorption properties of the nucleus, and thus the scaling, should depend mainly on the kinetic energy of the mesons, regardless of the initial photon energy, but the opposite is the case. For all the incident photon energies investigated, the scaling coefficients drop for constant E_γ from almost unity at small T_η to $\approx 2/3$ at maximum T_η; for a given kinetic energy they are very dependent on E_γ. Such a behaviour can arise if the initial production cross sections (before FSI) do not scale with the mass number, which would be the case if there were significant contributions from secondary production processes. The *true* dependence of α on T_η can thus be tested best with the scaling at kinetic energies close to the maximum values of T_η for a given incident photon energy (because secondary production processes are then strongly suppressed by the kinematics). For this a compromise has to be made between the suppression of the secondary processes and the statistical precision. The results from [152], which are included in Fig. 21, were analyzed under the condition that

$$T_\eta > (E_\gamma - m_\eta)/2, \tag{3.3}$$

where E_γ is the incident photon energy and m_η the mass of the η meson. The results indicate strong absorption for all the η kinetic energies investigated.

The photoproduction of η' mesons was analyzed in the same way (actually for the only experimental results available so far, the data from the Crystal Barrel/TAPS experiment analyzed in [152] for η production were used). The η' mesons were identified via an invariant-mass analysis of their $\eta' \to \eta\pi^0\pi^0 \to 6\gamma$ decay [153]. The analysis of the nuclear absorption properties used the so-called transparency ratio T, which compares the total production cross section $\sigma_{\gamma A\to mX}$ from a nucleus with

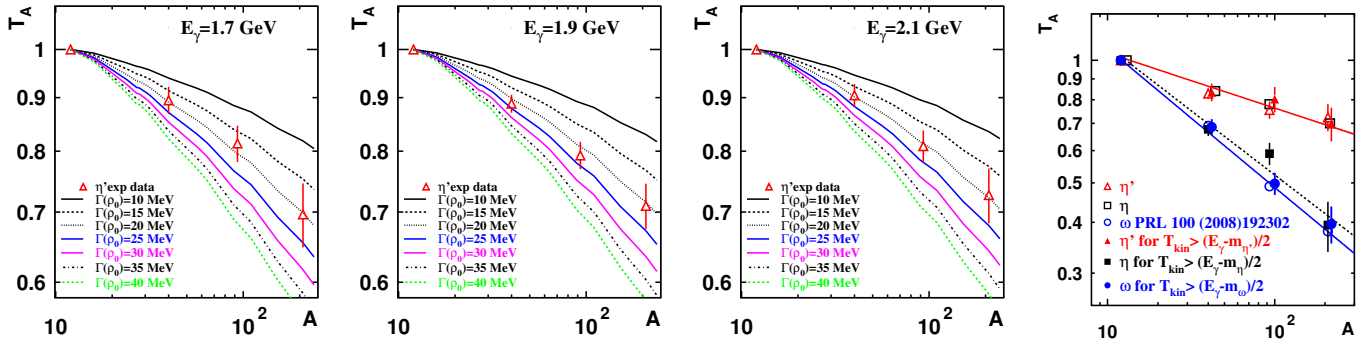

Figure 24: First three figures from left to right: transparency ratios as functions of the nuclear mass number for three ranges of incident photon energy. Data (red triangles) compared to model predictions for different values of the η' in-medium width. Right hand side: transparency ratios for η, η', and ω production with (closed symbols) and without (open symbols) cut on $T_{kin} > (E_\gamma - m_{\rm meson})/2$. Figures from [153].

mass number A to A-times the elementary production cross section $\sigma_{\gamma N\to mX}$ on the nucleon:

$$T_A = \frac{12\,\sigma_{\gamma A\to mX}}{A\,\sigma_{\gamma^{12}{\rm C}\to mX}} \tag{3.4}$$

where m denotes any meson. In order to account for the cross section difference between the proton and neutron, and also possible secondary production processes, it is better to normalize to an average nucleon cross section measured for a light target nucleus with equal numbers of protons and neutrons. Generally this is taken to be carbon, which leads to the T_A defined in Eq. (3.4). This type of analysis is equivalent to the evaluation of the scaling coefficients α, which were also extracted from the data.

The deviations of the cross sections from the scaling with the mass number A can be related to the in-medium width of the produced meson (the basic idea is simple; the smaller the scaling coefficient the larger the absorption probability, the larger the reduction of lifetime of the meson and the larger its effective in-medium width). The formalism, which does not require a particular model for the elementary production process, is given in [165, 166, 167]; details such as corrections for photon shadowing effects [155] and two-body absorption processes are discussed in [153]. Results for T_A for η' production off nuclei are summarized in Fig. 24 and compared to predictions assuming different values for the η' in-medium width [153]. The comparison reveals an in-medium width of 15 - 25 MeV at normal nuclear matter density $\rho = \rho_o$, which corresponds to an imaginary part of the η - nucleus optical potential of $-(10\pm2.5)$ MeV [168].

The absorption probability and the imaginary part of the optical potential for η' mesons are significantly smaller than for other mesons for which similar analyses have been performed. This is shown at the right hand side of Fig. 24, where the transparency ratios for η, ω, and η' mesons are compared. The slope for the η' meson is much less steep. The analysis demonstrates also that the complications from secondary production mechanisms is only important for η mesons. The η, ω, and η' data have been analyzed with and without a cut of Eq. (3.3) on the meson kinetic energy. The effect of the cut, which selects mesons with large kinetic energy that are unlikely to be produced by secondary processes, is almost negligible for η' and ω but is strong for the η, due to the efficient $\pi N \to S_{11}(1535) \to N\eta$ conversion chain. Such a conversion mechanism is absent for the η' and the $\pi N \to N\eta'$ cross section of only ≈ 0.1 mb is unusually small [138, 139].

The measurement of the absorption cross section gives practically the only access to the imaginary part of the nucleus - meson optical potentials for mesons that live long enough in vacuum to escape

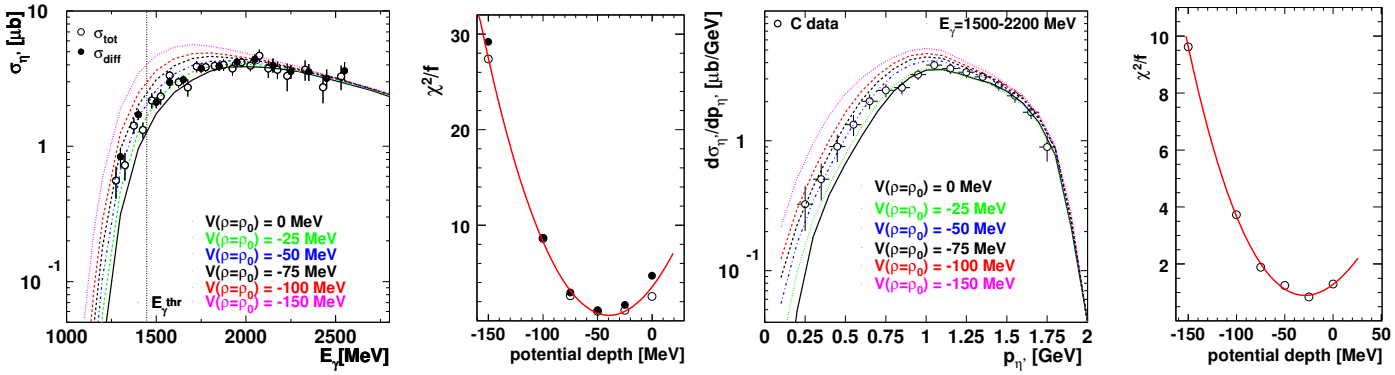

Figure 25: Left hand side: the threshold behaviour of $\gamma A \to X\eta'$ [168]. The vertical line indicates the threshold for free nucleons. Open and closed symbols represent two different analyses of the data, which should be equivalent (see [168] for details). The curves represent model predictions for different assumptions on the depths of the real potential [169]. The reduced χ^2 for the fit of the theory curves to the data is shown as function of the potential depth. Right hand side: comparison of data [168] and model calculations [169] for the momentum distributions of the η' mesons for incident photon energies between 1500 - 2200 MeV and reduced χ^2/f for the fit of model results to the data. All model results are normalized by a common factor (0.75) to the total cross section of the data for $E_\gamma > 2.2$ GeV. Figures are taken from [168].

from nuclei unless they are absorbed by a nucleon. The situation is different for very short-lived mesons decaying inside the nucleus, which have been explored by direct measurements. One example is the ρ in-medium width, which was studied by the CLAS collaboration [170, 171] using the $\rho \to e^+e^-$ Dalitz decay. However, already for ω mesons with much shorter lifetimes than the η and η', line-shape measurements are challenging [172].

A similar restriction applies to the η and η' measurements of the real part of the optical potential where a direct measurement of a mass shift of the mesons in nuclear matter is also excluded. One may, however, explore two indirect consequences of a meson mass shift in nuclear matter and this has been done for the η' produced off ^{12}C nuclei by Nanova and coworkers [168] with data taken at the CBELSA/TAPS experiment. The first method is based on the energy dependence of the total cross section close to the production threshold. Due to the nuclear Fermi motion, the production threshold for $\gamma A \to mX$ (m any meson) is pushed far below the production threshold for free nucleons. Such reactions can, in principle, occur almost down to the threshold of the coherent reaction $\gamma A \to mA$ (only shifted slightly upward due to the nucleon binding energy). The production threshold for η' mesons off the free nucleon is at ≈ 1.447 GeV, while the threshold energy for the coherent reaction is only ≈ 1 GeV. The absolute value and the energy dependence of the cross section around and below the free production threshold depend on the in-medium mass of the meson.

The use of the threshold effect, is of course, quite model dependent. One needs predictions of the nuclear cross section based on the elementary production cross sections for protons and neutrons, the nuclear spectral function taking into account the bound-nucleon momentum distribution, and the influence of FSI processes. The analysis in [168] used model predictions by Paryev [169] which had, as input, the elementary production cross sections off protons and neutrons from [37] and [98] and, for final state absorption, an inelastic in-medium $\eta' N$ cross section of $\sigma_{\rm inel}$ that is similar to the values extracted from the nuclear transparency measurements discussed above ($\sigma_{\rm inel}$= 3 - 10 mb). Model predictions for nuclear potential depths of $V = 0$, -25, -50, -75, -100, -150 MeV and normal nuclear density ρ_o are

compared to the data on the right hand side of Fig. 25. It should, however, be noted that the model does not reproduce the absolute magnitude of the measured cross sections. Part of the difference may be related to the photon shadowing effect [155], which was not included into the model. It accounts, however, only for a 10% correction while the mismatch is on the 25% level. All model results have therefore been renormalized to the measured cross section for incident photon energies above 2.2 GeV. This is the energy range where the model does not show any sensitivity to the nuclear potential (the same renormalization factor was used for all model curves). After this renormalization, the reduced χ^2 for fits of the data to the model curves were determined (see Fig. 25). As a result a potential depth of $-(40\pm6)$ MeV was extracted. There are also, of course, systematic uncertainties in this procedure, but strongly attractive potentials on the order of -100 MeV or deeper appear improbable.

Another means to access the in-medium mass shift comes from the momentum distribution of the observed mesons. Mesons that are produced inside the nucleus with a reduced mass must somehow restore their on-shell value when they emerge into free space. As a consequence of energy conservation, this will happen at the expense of their kinetic energy. Therefore, the kinetic energy spectra (or the momentum distributions) also carry, of course in a model-dependent way, information about the in-medium mass. This was demonstrated with GiBUU calculations [173] and is also included in the model predictions from Paryev [169]. The measured cross sections and the model predictions for the momentum distributions are compared on the right hand side of Fig. 25. The model results were renormalized to the data with the same common normalization constant as for the total cross sections. The reduced χ^2 of the fit to the data results in a potential depth of $-(32\pm11)$ MeV. The systematic uncertainty is somewhat larger than for the analysis of the threshold behaviour of the cross section because the experimental resolution for the $p_{\eta'}$ (between 25 and 50 MeV) must also be considered while resolution effects for the incident photon energy (≈ 4 MeV) are negligible. The final result for the real part of the potential is [168]

$$V_o(\rho = \rho_o) = -(37 \pm 10_{\mathrm{stat}} \pm 10_{\mathrm{sys}})\ \mathrm{MeV}. \tag{3.5}$$

Taken together with the results for the imaginary part (-10 ± 2.5 MeV) from the transparency measurements [153], this leads to an optical potential for η' mesons in a carbon nucleus of:

$$U_{\eta'}(r) = V(r) + iW(r) = (V_o + iW_o)\,\rho(r)/\rho_o = -(37 + i10)\,\mathrm{MeV}\,\rho(r)/\rho_o, \tag{3.6}$$

where r is the distance of the meson from the centre of the nucleus and the uncertainties in the numerical values of the potential parameters are given above.

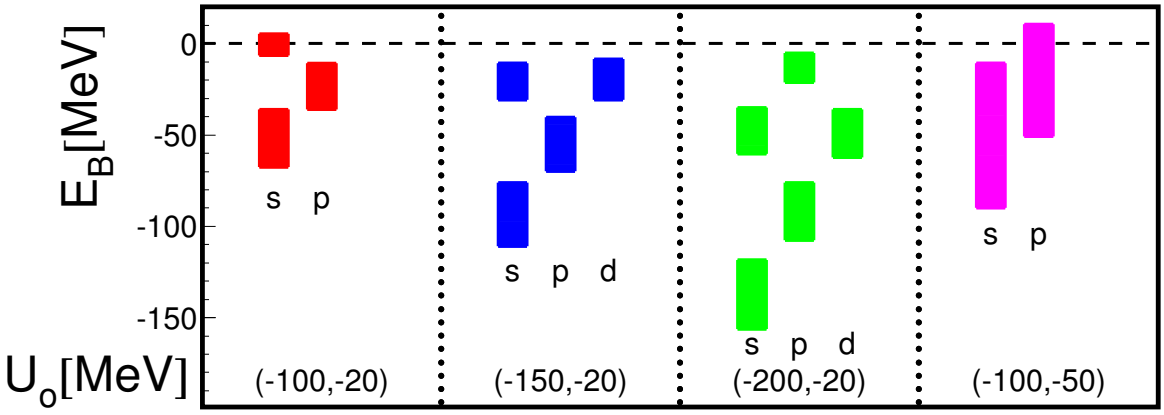

Figure 26: Predicted positions and widths of quasi-bound η' states states in ^{12}C for different optical potential parameters [174].

The potential parameters are important input for the question whether quasi-bound states exist for the η' meson in nuclei. Figure 26 summarizes the predictions of the positions and widths of quasi-bound η' states in ^{12}C nuclei for different potential depths made by Jido and co-workers [174]. For sufficiently large real parts of the potential, several states with widths much smaller than the binding energy are predicted. However, one should note that all predictions refer to depth of the real potential of 100 MeV or larger, while the experimental results suggest a more shallow potential with a depth not larger than 50 MeV. A large imaginary part of the potential results in very broad states, which would probably escape detection. The combined results from [153, 168] suggest that the potential is attractive ($V_o < 0$), although only moderately strong. However, since $|V_o| >> |W_o|$, it is not impossible that reasonably narrow states might be formed.

Photon-induced searches for quasi-bound η' states are planned for the BGO-OD experiment at ELSA, where two types of measurements are envisaged [20]. Both of them are based on reactions where the η' is produced in quasi-free kinematics off a proton, which is kicked out of the target nucleus (^{12}C) at very forward angles so that it takes away most of the momentum of the incident photon, leaving the η' almost at rest in the residual nucleus. In an inclusive measurement, only the momentum of the fast proton will be measured (the magnetic spectrometer of BGO-OD will have a momentum resolution of 1 - 2%). The reaction identification will then be based on the missing-mass spectrometry of the proton. Characteristic spectra from the formation of quasi-bound states have been predicted, e.g., by Nagahiro and coworkers [175]. In a semi-inclusive mode the decay of the η'-mesic state should be detected in coincidence with the fast forward proton. States below threshold cannot, of course, decay via η' emission; they will emit lighter mesons or nucleons. Model results from Oset and Ramos [176] indicate that the dominant decay mode should be $\eta' N \to \eta N$, so the planned experiment will detect η mesons in coincidence with fast forward protons.

However, one should keep in mind that the cross sections for these reactions are small (predictions for the inclusive experiment are on the order of a few nb/sr MeV [175] for potential parameters (V_o, W_o)=$(-100, -5)$ MeV). The background from competing processes may be substantial and so these proposed measurements appear quite challenging. Furthermore, not only the nuclear ground state but also excited nuclear states may couple so that the structures may be additionally washed out.

3.2 Coherent production

3.2.1 Single η-production off ^{3}He and ^{7}Li nuclei

The coherent photoproduction of mesons can give valuable information on the isospin decomposition of the production amplitudes. This has been exploited for η production, where measurements of the breakup reaction [51, 52, 53] revealed a neutron/proton cross section ratio of 2/3. According to Eq. (2.1), this indicated that either the isoscalar or the isovector photons dominate the reaction. The small cross sections reported for the coherent $\gamma d \to d\eta$ reaction [51, 52, 63] established the dominance of the isovector part (see [49] for details).

For heavy mesons like the η or η', due to the relatively large momentum transfers involved, coherent production from even light nuclei is strongly suppressed by the nuclear form factors. Only a few data sets are therefore available and these are mostly for incident photon energies in the immediate neighbourhood of the threshold. In the case of η photoproduction, the situation is particularly unfavourable. For spin $J = 0$ nuclei, such as ^{4}He, coherent photoproduction of pseudoscalar mesons in relative s-wave is forbidden due to spin/parity conservation; even very close to the production threshold only breakup reactions contribute [177, 178]. Furthermore, due to the quantum numbers of the dominating amplitude, which is the isovector component of the E_{0+} multipole (from the excitation of the $S_{11}(1535)$ resonance), there are large cancellations even when $J \neq 0$.

The motivation to measure the coherent reaction comes mainly from the search for η-mesic nuclei

(see discussion in Sec. 7). The basic idea is that η-mesic states that overlap the coherent production threshold should strongly influence the threshold behaviour of the reaction. This concerns the energy dependence of the total cross section as well as the angular distributions. Due to the above constraints, only nuclei with $J, I \neq 0$ are promising candidates for this approach. Among the stable light nuclei this condition is fulfilled for ^{3}He ($I = 1/2, J^\pi = 1/2^+$) and ^{7}Li ($I = 1/2, J^\pi = 3/2^-$).

The reactions have been studied at MAMI, first with the TAPS detector [179] for the ^{3}He target, and later with the Crystal Ball/TAPS setup for ^{3}He [180] and ^{7}Li [147]. The experimental challenge is that the recoil nuclei are stopped in the liquid helium or solid lithium targets so that a direct identification of the coherent process is impossible (active gaseous helium targets provide much too low luminosities). For detectors that cover large solid angles, such as Crystal Ball/TAPS, a significant suppression of the breakup background is achieved by vetoing events where, in addition to the meson-decay photons, a recoil nucleon is detected. However, low energy recoil protons and recoil protons at extreme forward angles escape detection and the detection efficiency for the recoil neutrons is, at best, in the 30 - 40% range.

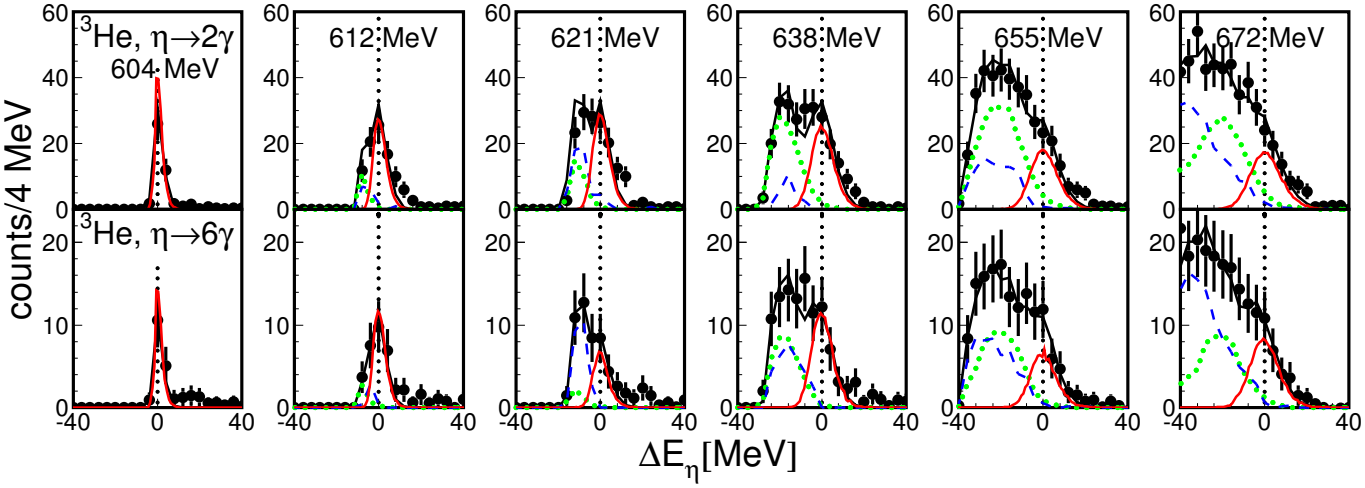

Figure 27: Missing energy spectra for η production off ^{3}He nuclei for different bins of incident photon energy [180]. Top row for the $\eta \to 2\gamma$, bottom row for the $\eta \to 3\pi^0 \to 6\gamma$ decay. Black symbols with error bars: measured data, solid (red) curves: simulated line shapes for the coherent $\gamma^3\text{He} \to \eta^3\text{He}$ reaction, dashed (blue): breakup reaction with recoil taken by a nucleon, dotted (green): recoil taken by a di-nucleon, solid (black): sum of all.

The final separation of breakup and coherent reactions must rely on the reaction kinematics. This is done with a missing-energy analysis, where the measured kinetic energy of the meson in the c.m. frame is compared to that extracted from the incident photon energy for the two-body η - nucleus final state. The missing-energy spectra for the ^{3}He target and both analyzed decay branches of the η-meson are summarized in Fig. 27 [180]; results for the ^{7}Li target [147] are qualitatively similar. While the identification of the η mesons via invariant mass analysis is clean (in particular the $\eta \to 3\pi^0$ decay channel is almost background-free in the near-threshold region, see [147]) residual background from breakup reactions becomes dominant in the ^{3}He case already 40 MeV above threshold. Only the fitting of the simulated line shapes for the coherent and breakup reactions to the experimental data allows the extraction of the coherent part. It is only in the first energy bin, centred around 604 MeV, that a clean coherent signal is visible because this energy is below the threshold for a breakup reaction.

Total cross sections extracted from such analyses are shown in Fig. 28. The agreement between the two MAMI experiments for ^{3}He is reasonable, but the older data [179] show a dip around 625 MeV that

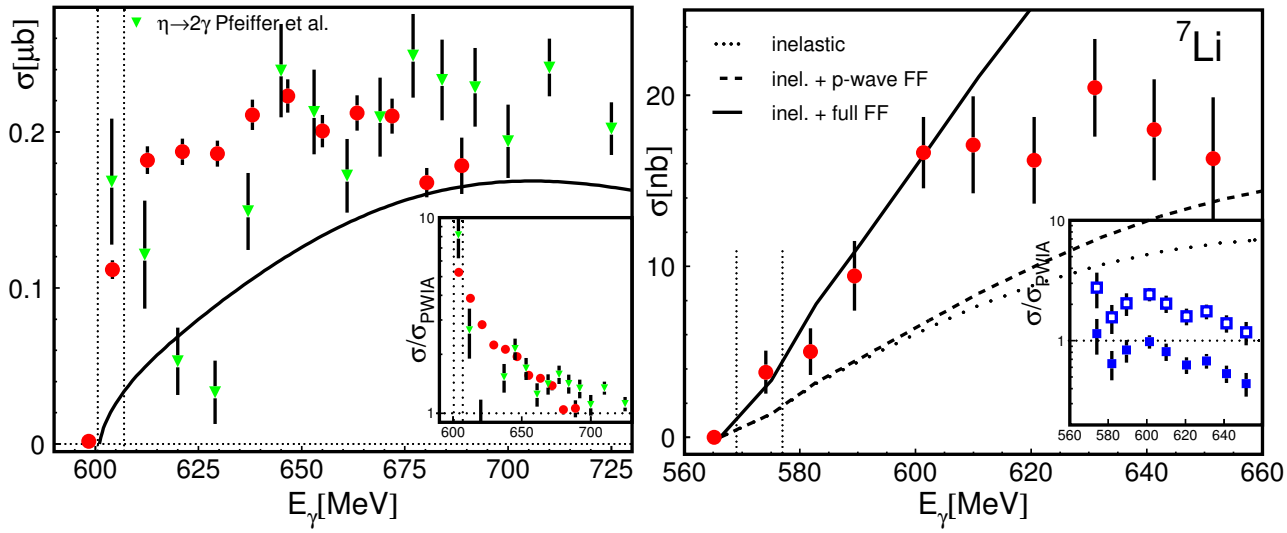

Figure 28: Total cross section for the $\gamma\,^3\mathrm{He} \to \eta\,^3\mathrm{He}$ [180] (left hand side) and $\gamma\,^7\mathrm{Li} \to \eta\,^7\mathrm{Li}$ [147] (right hand side) coherent η-production reactions. The green points for ^{3}He are from [179]. The curves represent PWIA modelling. For the ^{7}Li target the inelastic contribution (excitation of low lying nuclear state) is shown separately and calculations using the full elastic form factor or only the p-wave part are shown. The dotted lines indicate coherent and breakup thresholds. The inserts show the ratio of data to the PWIA prediction; in the ^{7}Li case this is shown separately for the full and p-wave form factor.

was not confirmed in the later experiment. This is in the most critical region as far as the separation of the coherent components and breakup reactions is concerned; at lower photon energies the breakup background is not so important and at higher energies it is better separated from the coherent channel in the missing energy plots. Since the Pfeiffer et al. measurement [179] suffered from significantly larger breakup background than the more recent experiment (the apparatus covered a smaller fraction of the solid angle so that the vetoing of events with recoil nucleons was less efficient), it seems likely that systematic uncertainty in this region was larger. The statistical fluctuations are obviously also much more significant. The ^{7}Li data are so far the only results for coherent production from nuclei heavier than the deuteron or ^{3}He. The cross section is smaller by one order of magnitude than that on ^{3}He and the rise at threshold is less steep (the plateau value of the cross section is reached for ^{3}He within $\approx$ 10 MeV, for ^{7}Li only $\approx$40 MeV above threshold).

The energy dependence of the ^{3}He data is striking. The cross section rises very steeply from the production threshold and then stays almost constant. Already the data point between the coherent and breakup thresholds reaches more than half the plateau value. Here, one should note that the experimental resolution for the incident photon energy is much better than the bin size in the figure [61] so that resolution effects for the slope are negligible. A similar but even more spectacular behaviour has been observed for the $dp \to {}^3\mathrm{He}\,\eta$ reaction measured at COSY [181, 182] (see Fig. 39 and the discussion in Sec. 6.2.1). This has been interpreted as at least a signature of strong FSI effects and possibly some evidence for the formation of a mesic state (the similar and unusual threshold behaviour of reactions with different initial states is most likely due to the FSI). The behaviour of the angular distributions supports this picture. Close to threshold they are almost isotropic and not forward peaked as one would expect from the influence of the nuclear form factor, which becomes significant only at higher energies. The lithium results behave more as one would expect.

For a more quantitative discussion, both data sets have been compared to the predictions of a simple Plane-Wave-Impulse-Approximation (PWIA) using the formalism outlined in [147, 180]. For a given

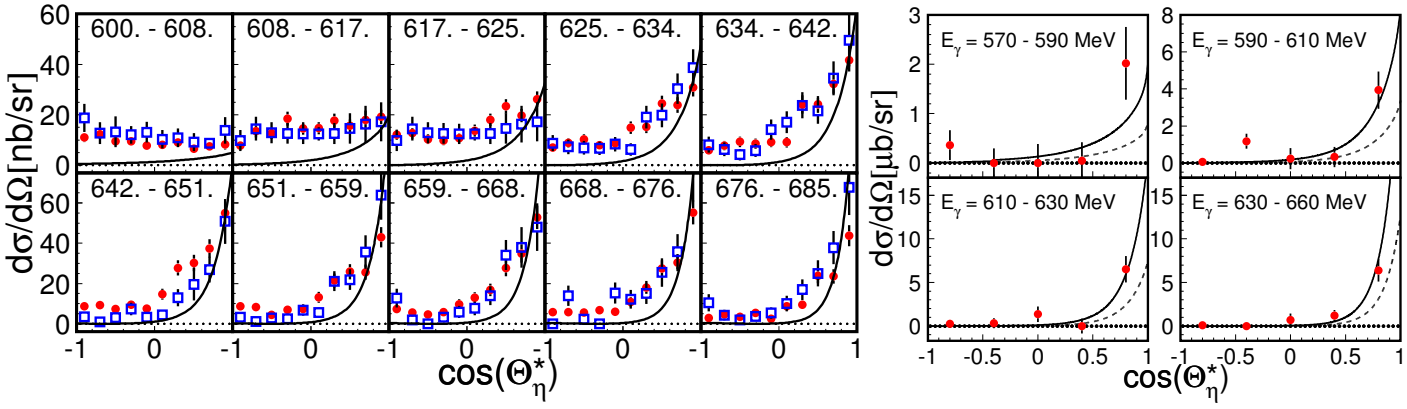

Figure 29: Angular distributions of $\gamma\,^3\mathrm{He} \to {}^3\mathrm{He}\,\eta$ (left hand side) and $\gamma\,^7\mathrm{Li} \to {}^7\mathrm{Li}\,\eta$ (right hand side) for different energy bins. For the helium target, results from $\eta \to 2\gamma$ (red circles) and $\eta \to 6\gamma$ (blue stars) are shown separately. The results for the lithium target have been averaged over both decays. The curves are the predictions from the PWIA approximation (see text). For lithium, the PWIA results are shown for the full form factor (solid) and the p-wave form factor (dotted).

incident laboratory photon energy E_γ (four-momentum P_γ) and an off-shell nucleon moving with three-momentum $\vec{p}_N$ (four-momentum P_N) inside the nucleus the effective total c.m. energy $W = \sqrt{s^{\mathrm{eff}}}$ is obtained from

$$s_{\mathrm{eff}} = (P_\gamma + P_N)^2. \tag{3.7}$$

The nucleon momentum $\vec{p}_N$ is related in the factorization approximation [144] to the momentum transfer $\vec{q}$ to the nucleus (note that the expressions in reference [144] are formulated for the c.m. system while in [147, 180] the laboratory frame has been used)

$$\vec{p}_N = -\left(\frac{A-1}{2A}\right)\vec{q}\,, \tag{3.8}$$

where A is the target mass number. The amplitudes of the elementary reactions are then evaluated at $W(E_\gamma, \vec{q})$. Up to this point there is analogy to the much better studied coherent π^0 photoproduction off (mostly $J = 0$) nuclei [144, 145, 146, 147]. In this case the spin- and isospin-independent components of the elementary amplitude from all nucleons must be coherently added. However, since threshold η-production is dominated by the E_{0+} spin-flip amplitude, only the unpaired nucleon can contribute. For ^{3}He this is (dominantly) the $1s_{1/2}$ neutron and for ^{7}Li the $1p_{3/2}$ proton. This means, of course, that *coherent* η-production does not profit from the A^2 factor resulting from the coherent superposition of scalar amplitudes. This feature, together with the larger momentum transfers, explains the small cross sections observed.

Taking into account the phase-space factors related to the transformation from the photon - nucleon c.m. system to the photon - nucleus c.m. system and the nuclear form factors, the differential cross section can be written as

$$\frac{d\sigma_{\mathrm{PWIA}}}{d\Omega}(E_\gamma, x) = \left(\frac{q_\eta^{(A)}}{k_\gamma^{(A)}} \cdot \frac{k_\gamma^{(N)}}{q_\eta^{(N)}}\right)\left(\frac{F_A(q^2)}{F_p(q^2)}\right)^2 \frac{d\sigma_{\mathrm{elem}}}{d\Omega}, \tag{3.9}$$

where $k_\gamma^{(N)}$ and $q_\eta^{(N)}$ are the photon and η three-momenta in the photon-nucleon c.m. system and $k_\gamma^{(A)}$ and $q_\eta^{(A)}$ the same in the photon-nucleus c.m. frame. We also define $x = \cos\theta_\eta^*$, where $\theta_\eta^\star$ is the polar angle of the η meson in the photon-nucleus c.m. system. The elementary cross section $d\sigma_{\mathrm{elem}}/d\Omega$ is

the (measured) $\gamma n \to n\eta$ cross section for the ^{3}He target and the $\gamma p \to p\eta$ cross section for ^{7}Li. Since meson photoproduction probes the distribution of point-like nucleons in the nucleus, the nuclear form factors F_A must be divided by the nucleon form factor F_p (the charge form factor of the proton is used) to account for the contribution of the finite radii of the nucleons to the nuclear charge form factors. For the ^{3}He target the charge form factor [183] of this nucleus has been used.

The situation is a bit more complicated for the ^{7}Li case. This nucleus has the low lying state ($J^\pi = 1/2^-$, 478 keV excitation energy), corresponding to the excitation of the $1p_{3/2}$ proton to the $1p_{1/2}$ state. This contribution cannot be separated experimentally from the coherent reaction because the missing-energy resolution is by no means good enough and the coincident detection of a 478 keV de-excitation photon is not possible. The form factor that should be used in Eq. (3.9) must therefore include contributions from both the elastic and the inelastic excitation to this state, as given in [184]. Furthermore, since only the $p_{3/2}$ proton contributes, there is some ambiguity whether for the elastic part the full form factor or only the p-wave part is relevant. In [147] the full form was used but here we compare the data also to a model calculation based on the p-wave form factor.

The results of the PWIA calculations are compared to the data in Figs. 28 and 29. In the case of ^{3}He the rise at threshold is much less steep in the model. The ratio of data and PWIA shown in the insert of the figure rises very strongly towards threshold (note the logarithmic scale). The angular distributions in the model show the expected rise to forward angles due to the form factor influence for all energies. However, the measured distributions are almost isotropic in the neighbourhood of the threshold and might even show a slight rise to backward angles for the energy bin between coherent and breakup threshold. This behaviour is interpreted as evidence for strong FSI effects.

The results for the ^{7}Li target are more in line with the PWIA approximation predictions for both the energy dependence of the total cross section and the shape of the angular distributions. Due to the much smaller cross section, the statistical quality of the data is of course inferior to the ^{3}He results so that the angular distributions could only be investigated in coarser energy bins. As shown on the right hand side of Fig. 28, the expected contribution from the excitation of the $1/2^-$ state is substantial and the modelling using the full elastic form factor is in better agreement with the measurement than the ansatz using the p-wave form factor.

In summary, the data for ^{3}He show evidence for strong FSI effects and, in combination with the corresponding COSY data for the $dp \to {}^3\mathrm{He}\,\eta$ reaction [181, 182], make ^{3}He so far the best candidate for the observation of an η-mesic state, although there is no final proof that the system is really quasi-bound. There were also attempts in [179, 180] to observe the decay of the η-mesic $^3_\eta$He state via $\pi^0 - p$ back-to-back emission following the capture of the η by a nucleon into the $S_{11}(1535)$ resonance (see discussion in Sec. 7.2). With this decay channel it is possible to probe also the region below the η threshold. The observation of a peak-like structure at the η threshold was interpreted in [179] as tentative evidence for this decay. However, it was shown later [180] that this structure is an artefact, related to the interplay of the energy and opening-angle dependence of the $p\pi^0$ decay of nucleon resonances, which obscures any possible signal from an η-mesic state.

The data for the ^{7}Li nuclei do not show any unusual behaviour and can be reasonably well reproduced by the PWIA approximation so that there is so far no experimental indication of a heavier η-mesic state. Due to the behaviour of the nuclear form factors and the spin-flip nature of the dominant transition amplitude, most nuclei are excluded as targets for coherent η production. For heavier nuclei one could of course try instead to use the breakup reaction tuned so that the recoil nucleon takes away the momentum of the incident photon and the η is produced (almost) at rest in the nucleus, or to explore the coherent production of $\pi\eta$-pairs discussed below. Such experiments have been proposed but have not yet performed.

3.2.2 Coherent production of $\pi^0\eta$-pairs

As discussed in Sec. 2.1.3, the production of $\eta\pi$ pairs is dominated in the threshold region by the $\gamma N \to D_{33}(1700) \to \eta\Delta(1232) \to \eta\pi N'$ reaction chain. In this reaction the η is emitted in relative s-wave and the pion from the Δ resonance in relative p-wave. A model analysis of the elementary reaction [122] finds comparable spin-dependent and spin-independent contributions to the amplitude, so that the coherent production mechanism is not suppressed for spin $J = 0$ nuclei as it is for single η production. Since, in addition, the electromagnetic excitation of a Δ state involves only isovector photons, there are also no cancellations. Significant cross sections have therefore been predicted for the $\gamma A \to A\pi^0\eta$ reaction off light nuclei such as the deuteron or ^{3,4}He [185]. The predicted total cross sections for ^{3}He are of the same order of magnitude as for coherent η production off this nucleus (although the elementary cross sections differs by roughly one order of magnitude) and for ^{4}He the predicted cross sections are even larger. As a side remark, due to the coherent addition of the amplitudes from all nucleons without cancellations, coherent cross sections from heavier nuclei are probably substantial and might in future be explored for detailed studies of η interactions with nuclear matter.

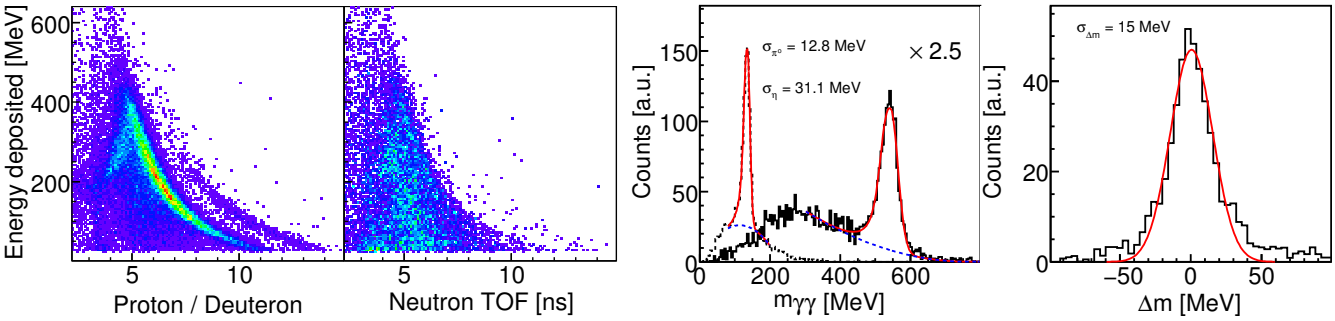

Figure 30: Identification of the coherent $\gamma d \to d\eta\pi^0$ reaction in the CBELSA/TAPS experiment [186]. Left panel: time-of-flight versus energy for charged and neutral non-photon hits in the TAPS forward wall. For charged hits (left most plot), apart from the dominating proton band, a pronounced deuteron band is visible. Right hand side: invariant mass identification of π^0 and η and missing-mass spectrum (after cut on the deuteron band and the π^0 and the η invariant masses). Note the small width of the missing-mass peak. Missing-mass peaks from breakup reactions are broader, due to the Fermi motion.

The only results available so far for coherent $\eta\pi^0$ production are preliminary data for the deuteron target from the CBELSA/TAPS experiment at ELSA [186]. The clean identification of this reaction is demonstrated in Fig. 30. Kinetic energy distributions of the π^0 and η mesons are shown in Fig. 31. These data also clearly support the dominance of the $\Delta^\star \to \Delta(1232)\eta \to N\pi^0\eta$ decay chain. The kinetic energies of the π^0 mesons peak for all incident photon energies close to the value typical for the $\Delta(1232) \to N\pi^0$ decay ($E_\pi^{\rm kin} = 130$ MeV) while the kinetic energies of the η mesons shift to higher values with increasing incident photon energy. The data are in quite good agreement with the results of the model of Egorov and Fix [125], so that their predictions for the γ^4He $\to {}^4$He $\eta\pi^0$ reaction (total cross sections up to 100 nb) are also probably realistic. With the additional degree of freedom from the π^0 meson kinematics, where events can be selected for which the η is slow with respect to the ^{4}He nucleus, it seems that the γ^4He $\to {}^4$He $\eta\pi^0$ reaction may be a promising tool for the search for ${}^4_\eta$He. A corresponding experiment proposal has been accepted for CBall/TAPS at MAMI but the measurement has not yet been undertaken.

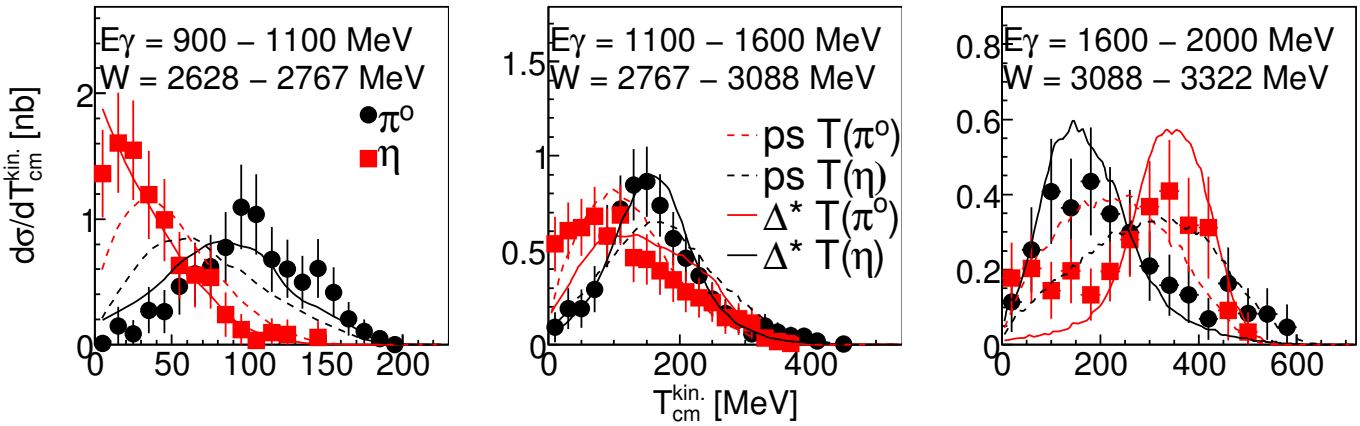

Figure 31: Distributions of the kinetic energies of the π^0 and η mesons from $\gamma d \to d\pi^0\eta$ for three different ranges of incident photon energy. (Black) circles: π^0, (red) squares η mesons. Dashed curves: phase-space simulation, solid curves: simulation assuming the sequential decay of a Δ^* via η emission to the $\Delta(1232)$. Results from [186].

3.2.3 Coherent production of η' mesons

For completeness let us make a short remark on the coherent photoproduction of η' mesons off nuclei, which is so far almost completely unexplored. The cross sections are expected to be very low, mainly because of the large momentum transfers and the small elementary cross sections. Since, just as for η production, this reaction also seems to be dominated in the threshold region by the excitation of an S_{11} partial wave (although probably not so strongly as for η production) it will be also strongly suppressed for spin $J = 0$ targets. So far there are only a few data points for the $\gamma d \to d\eta'$ total cross section [98]. Depending on the analysis assumptions, it seems that these are of the order of a few nb. Model results [98], based on the η'-MAID model, are of a similar order, but the uncertainties in the data are still so large that no definite conclusions can be drawn.

4 Production in pion-nucleus collisions

There have been far fewer measurements of η production from nuclei with low energy pion beams than with photons or nucleons and, of these, only two are really significant.

4.1 The $d(\pi, \eta)NN$ reaction

In quark language, charge symmetry corresponds to the invariance of interactions under the interchange of the u and d quarks. This symmetry requires that the total cross sections for the interaction of π^+ and π^- mesons with the deuteron should be identical. This was tested many years ago for pion laboratory energies between 70 and 370 MeV in a classical transmission experiment [187]. After making corrections for direct Coulomb effects, residual differences of up to 5% were found between $\sigma_{\rm tot}(\pi^+ d)$ and $\sigma_{\rm tot}(\pi^- d)$. These differences could be parameterized in terms of small amounts of charge symmetry breaking (CSB) in the masses and widths of the $\Delta(1232)$ isobar, driven by the u–d mass difference.

The equality of the $\pi^+ d$ and $\pi^- d$ cross sections should also hold for more exclusive reactions and this has been tested through the measurement of the ratio $R = \sigma_{\rm tot}(\pi^+ d \to pp\eta)/\sigma_{\rm tot}(\pi^- d \to nn\eta)$ in the near-threshold region [188], though no attempt was made to extract values of the individual cross sections. Only the η meson was detected through its two-photon decay with the NaI calorimeters that

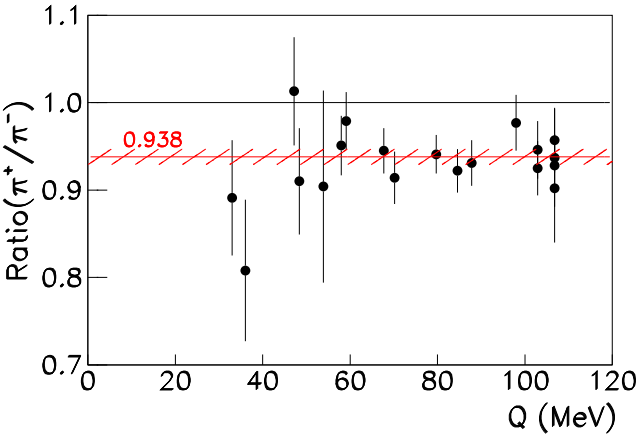

Figure 32: Measurements of the ratio $R = \sigma_{\rm tot}(\pi^+ d \to pp\eta)/\sigma_{\rm tot}(\pi^- d \to nn\eta)$ after adjustment for the n–p mass difference and initial-state Coulomb interaction [188]. The (red) line with hatching represents the mean value and its uncertainty.

formed the central part of the spectrometer used to study the π^{-3}He $\to \eta\,^3$H reaction [189] discussed in the next section.

There are several obvious corrections that have to be made to the ratio R before the results shown in Fig. 32 as a function of the excess energy Q can be fully assessed. These include Coulomb effects, phase-space corrections, and the charge dependence of the $S_{11}(1535)$ mass. The residual contribution to the mean value of the ratio, $\bar{R} = 0.938 \pm 0.009$, was interpreted as being due to charge-symmetry-breaking η–π^0 mixing, with a mixing angle of $1.5^\circ \pm 0.4^\circ$ [188]. This is one contribution to the $dd \to \pi^0\alpha$ reaction, which is the cleanest CSB test because it does not rely on interference effects [190].

4.2 The π^{-3}He $\to \eta\,^3$H reaction

The only measurement of coherent η-production induced by a pion beam is that of π^{-3}He $\to \eta\,^3$H. This was first studied at a single beam momentum for a couple of large angles by identifying the recoil triton [191] and subsequently at five momenta in the forward hemisphere by detecting the $\eta \to \gamma\gamma$ decay products in the LAMPF two-photon spectrometer [189]. The incident pion laboratory momenta between 590 MeV/c and 680 MeV/c corresponded to η c.m. momenta between $\approx$ 78 MeV/c and 278 MeV/c. The shapes of the angular distributions were reasonably well described by DWIA calculations based upon $\pi^- p \to \eta n$ amplitudes dominated by the $N^*(1535)$ isobar but these underestimated the magnitudes of the cross sections by typically a factor of two. This deficit has been ascribed to contributions from two- and three-nucleon mechanisms which increase the magnitudes while affecting the angular distributions far less [192].

Figure 33 shows the forward π^{-3}He $\to \eta\,^3$H differential cross section obtained by extrapolating the measured data using shapes given by the single-nucleon DWIA estimates [189]. However, as shown by the dashed line, this underestimates the absolute magnitudes by about a factor of two. Calculations that include two- and three-nucleon terms (solid curve) lead to a much better description [192].

Unfortunately, the data do not extend down to the near-threshold region where the η^3H final state interaction plays such an important role in other reactions. However, the kinematics are very similar to those of the γ^3He $\to \eta\,^3$He reaction which, away from the FSI region, are well described in impulse approximation [180]. Clearly, if two-step processes with intermediate virtual pions are significant in the

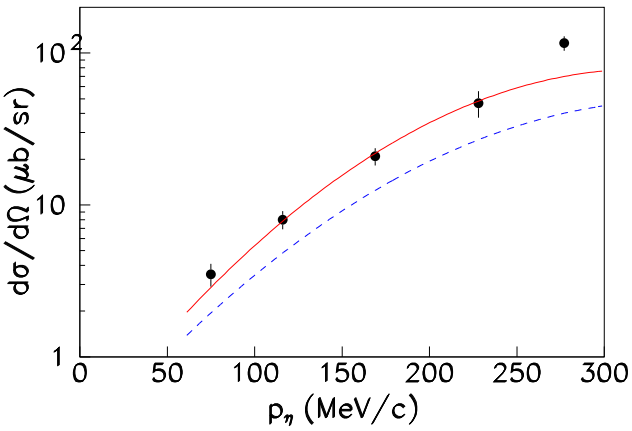

Figure 33: Differential cross section for the $\pi^{-3}\mathrm{He} \to \eta\,{}^3\mathrm{H}$ reaction extrapolated to the forward direction using shapes given by DWIA calculations [189]. The (blue) dashed curve assumes only single-step contributions whereas the solid (red) one includes also two- and three-nucleon mechanisms, though the latter has only a minor effect [192].

(π^-, η) case then it would seem that this should also be true for (γ, η) as well. It might therefore be helpful if the two reactions were analyzed simultaneously.

The LAMPF two-photon spectrometer was also used to measure the inclusive $^{12}\mathrm{C}(\pi^+, \eta)X$ reaction at 680 MeV/c [193] and the limited data set has been analyzed successfully in DWIA approaches [194, 195].

5 Production in nucleon-nucleon collisions

5.1 η production in pp collisions

The total cross section for the $pp \to pp\eta$ reaction has been measured by a variety of groups [196, 197, 198, 199, 200, 201, 202, 203, 204] and the results are shown in Fig. 34 as a function of the excess energy $Q = W - 2m_p - m_\eta$, where W is the total centre-of-mass energy. In most of these experiments the reaction was identified by measuring the two final protons and reconstructing the η through the missing-mass peak in the reaction. However, in the PINOT experiment [196, 203] only the two photons from the η decay were measured in samples of phase space so that these results could be contaminated at the higher energies by the production of an extra pion [203]. The exclusive HADES result at 340 MeV [204], where the η decay products were measured in coincidence with the two final protons, shows that this is probably not a serious concern.

Most of the rapid rise of the total cross section with energy that is apparent in Fig. 34 is merely a reflection of the Q^2 dependence of the non-relativistic three-body phase space. However, if one modifies this with the one-pole approximation to the S-wave proton-proton final state interaction, the near-threshold energy dependence becomes [210]

$$\sigma_T(pp \to pp\eta) = C \left(\frac{Q}{\varepsilon}\right)^2 \Bigg/ \left(1 + \sqrt{1 + Q/\varepsilon}\right)^2, \tag{5.1}$$

where C is constant. Since the Coulomb repulsion has here been neglected, there is some ambiguity in the value to take for the pole position ε and the best fit to the analogous η' production data [198,

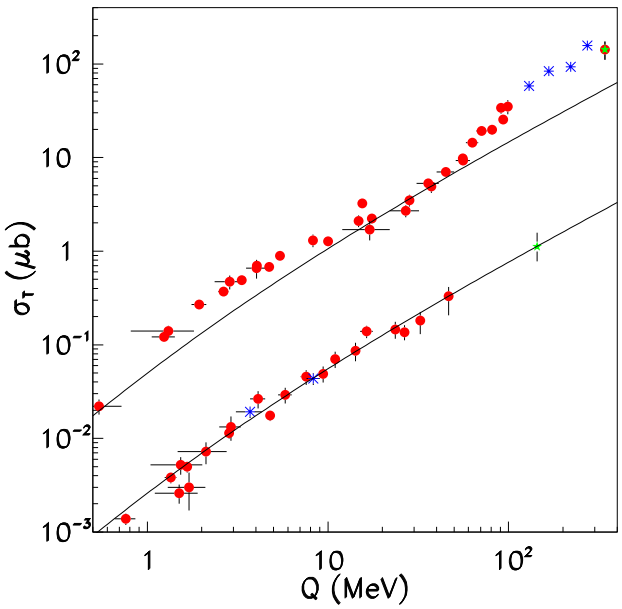

Figure 34: Total cross sections for $pp \to pp\eta$ (upper points) and $pp \to pp\eta'$ (lower points). The η data are taken from Refs. [196, 197, 198, 199, 200, 201, 202] (closed red circles), [203] (blue crosses), and [204] (green star) and the η' data from Ref. [198, 199] (blue crosses), [205] (green star), and [206, 207, 208] (closed red circles). The preliminary η point at much higher energy [209] is not shown. The solid curves are arbitrarily scaled pp FSI predictions of Eq. (5.1).

199, 205, 206, 207, 208] was achieved with $\varepsilon = 0.75^{+0.20}_{-0.15}$ MeV [208], which is quite consistent with the original assumptions [210].

Whereas all the $pp \to pp\eta'$ total cross sections are well described by Eq. (5.1) with $C \approx 0.012$ μb, the same is not true for the analogous η case. If this is normalized to the data at Q = 20-30 MeV, then the curve underpredicts the results at both lower and higher values of Q. In the near-threshold region this is probably due to the neglect of the strong ηp and ηpp FSI and at high energies higher partial waves become important, as can be seen from the differential distributions discussed later.

More detailed information can be obtained from looking at differential distributions of the $pp \to pp\eta$ reaction in data taken at a single energy [212, 213]. The spectrum of the excitation energy E_{pp} in the pp system is shown in Fig. 35a at an excess energy of $Q \approx 15.5$ MeV [201]. What is immediately striking here is the sharp peaking of the experimental data at very low E_{pp} that is due to the dominance of the Ss wave and the very strong final state interaction between the two protons. We are here using the notation $L\ell$ to describe the final state, where L is the orbital angular momentum in the pp system and ℓ that of the η relative to the diproton. There are minor differences in the literature on how the FSI is modeled and the curve shown in Fig. 35a does not include Coulomb repulsion or experimental resolution but it is clear that the model falls well below the data at large E_{pp}. It was suggested that a new approach was needed for FSI models [214]. A more natural assumption is that at large E_{pp} there are contributions associated with Ps final waves [215] and the combination of Ss and Ps final waves describes the data very well.

The most complete exclusive measurements of the $pp \to pp\eta$ reaction were carried out at the CELSIUS ring at Q = 40 MeV and 72 MeV. In addition to measuring the two final protons, the η was identified through either its $3\pi^0$ [216] or 2γ [211] decay. The η angular distributions shown at the two

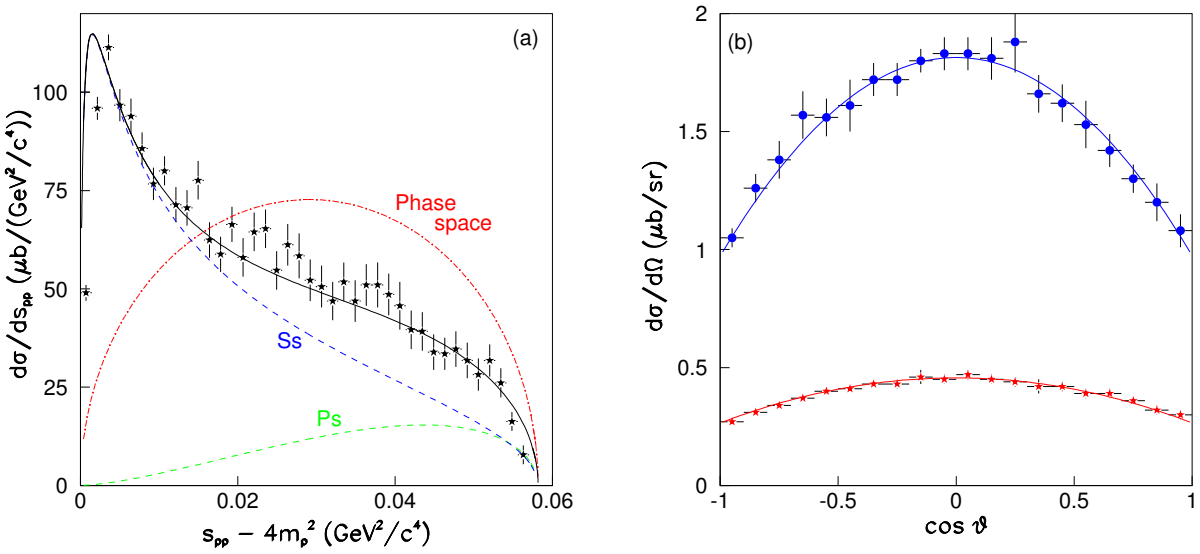

Figure 35: (a) One-dimensional distribution measured in the $pp \to pp\eta$ reaction at $Q = 15.5$ MeV [201]; to a very good approximation the abscissa represents $4m_pE_{pp}$. The (red) chain curve corresponds to a phase space distribution and weighting this arbitrarily with the pp S-wave FSI or a P-wave factor gives the (blue or green) dashed curves. The sum of Ss and Ps contributions (solid black curve) describes well the shape of the data. (b) c.m. angular distribution of the η in the $pp \to pp\eta$ reaction at $Q = 40$ MeV (lower red points) and 72 MeV (upper blue points) [211]. The curves are linear fits in $\cos^2\theta_\eta$.

energies in Fig. 35b deviate significantly from isotropy and, if these are parameterized in the form of $d\sigma/d\Omega_\eta \sim 1 + \alpha\cos^2\theta_\eta$ then one finds that $\alpha = -0.42$ and -0.46 at 40 and 72 MeV, respectively. This was taken as evidence for the importance of Sd or Pp partial waves at these energies [211].

Other evidence for the importance of higher partial waves in the $pp \to pp\eta$ reaction is to be found from inspection of the Dalitz plots measured at 40 and 72 MeV [216, 211]. These show a distinct valley when the invariant mass of one ηp pair has a similar value to that of the other pair, viz. $m(\eta p_1) \approx m(\eta p_2)$. It seems that, as the energy is raised and the Dalitz plot opens out, the η cannot resonate simultaneously with both protons as an $N^*(1535)$. In terms of the partial wave expansion, neither the Sd nor Ps wave can describe such a behaviour, which requires at least a Pp wave [211]. Since at least three sets of higher partial waves are required to parameterize the 40 and 72 MeV data, this brings into question the description of the total cross section given in Fig. 34 by phase space distorted by the proton-proton final state interaction. At low Q there is some evidence for an ηp FSI but it is hard to include this together with the pp FSI in anything other than the factorization approximation [217].

All the one-dimensional spectra extracted from the exclusive $pp \to pp\eta$ measurements at 40 and 72 MeV were described in terms of Ss, Sd, Ds, and Ps partial waves, where the only dynamics included was the pp S-wave FSI [211]. There are, however, nine Pp waves that might potentially contribute and only one of these nine was retained in the description. Though this choice seems adequate for the evaluation of the acceptance of the WASA spectrometer, the authors may not have explored the full range of ambiguity of the parameters. There could, for example, be some conflict of the partial-wave interpretation with the limited $pp \to pp\eta$ data set reported in Ref. [218] at small angles and low E_{pp} and clearly more data would be very useful in the low E_{pp} region.

By taking the amplitudes to be constant, apart from the necessary threshold momentum factors, not only could the data at 40 and 72 MeV be reproduced, but these parameters also describe quantitatively

the pp and ηp invariant-mass distributions measured at $Q = 15.5$ MeV [201]. In particular, the fractional contribution of Ps waves deduced is very similar to that shown in Fig. 35b.

Although there were some measurements of the proton analyzing power in the $\vec{p}p \to pp\eta$ reaction for $Q > 320$ MeV [219], the COSY-11 data at 10 and 36 MeV show very low values for A_y, from which it is hard to draw any firm conclusions [220]. The analysis of a more detailed COSY-WASA experiment is in progress [221, 222].

5.2 η production in pn collisions

The first indication that η production is much stronger in pn than in pp collisions was found from the comparison of the numbers of η mesons originating from pd and pp interactions [223, 224]. Since only the two photons coming from the η decay were detected in the PINOT spectrometer, there was no way of separating the quasi-free $pn \to d\eta$ production from the $pn \to pn\eta$ reaction. Subsequently both the two-body $pn \to d\eta$ [225, 226, 227] and the three-body $pn \to pn\eta$ [228, 229] reactions were measured individually using quasi-free production on the deuteron.

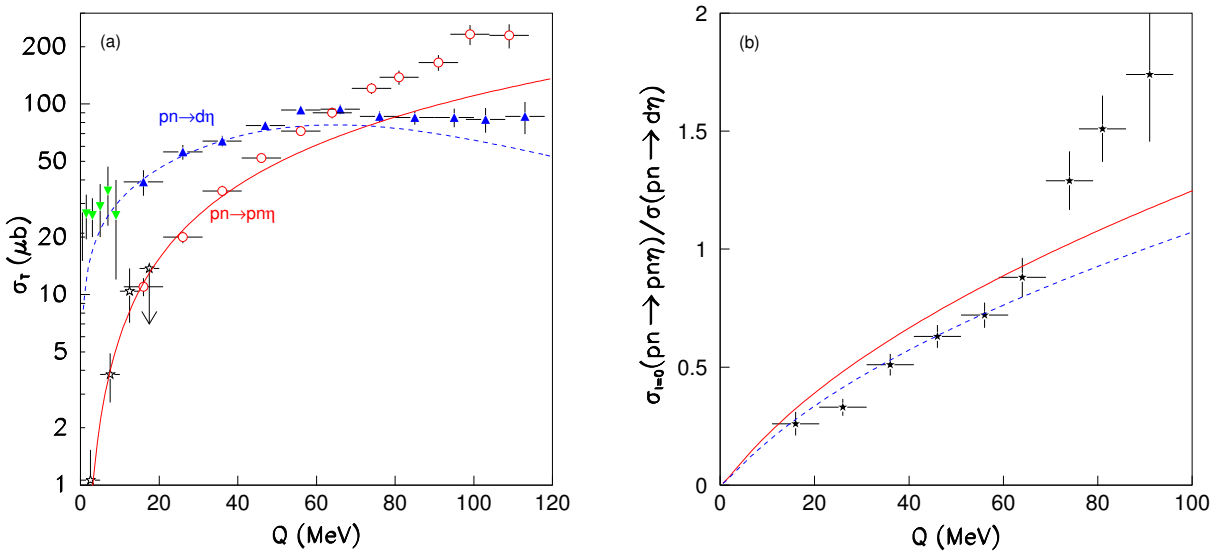

Figure 36: (a) The $pn \to d\eta$ total cross section from Refs. [225, 226] (blue triangles) and [227] (green inverted triangles) and $pn \to pn\eta$ from Refs. [228] (red open circles) and [229] (black open stars). The solid (red) curve represents the shape expected from phase space modified by the $I = 0$ pn final-state interaction whereas the dashed (blue) one is a simple $N^*(1535)$ resonance shape. (b) The ratio of the isoscalar total cross sections for $pn \to pn\eta$ [228] to $pn \to d\eta$ [225, 226]. The solid (red) curve is the final-state-interaction prediction of Eq. (5.2). Arbitrarily scaling this by a factor of 0.85 leads to the (blue) dashed curve.

The comparison of the results shown in Figs. 34 and 36a show that, away from threshold, the total cross section for $pn \to pn\eta$ is about 6.5 times that for $pp \to pp\eta$. Since the pn channel is composed of half isospin 0 and 1, this means that $\sigma_{I=0}(NN \to NN\eta) \approx 12 \times \sigma_{I=1}(NN \to NN\eta)$. In a one-meson-exchange model a large value for the ratio is to be expected if the dominant exchanges are isovector mesons (π and ρ) rather than isoscalar (ω and η) but it seems that a ratio of 12 can only be achieved if the π and ρ exchanges add constructively in the $I = 0$ channel and destructively for $I = 1$ [230].

At low energies the $pn \to d\eta$ cross section is much larger than that for $pn \to pn\eta$ due to the phase spaces being proportional to $\sqrt{Q}$ and Q^2, respectively. In the $pn \to d\eta$ case, there seems to be some evidence for the effects of the $S_{11}(1535)$ resonance because the total cross section quickly changes from the near-threshold $\sqrt{Q}$ behaviour. The points very close to $Q = 0$, which were taken by placing counters to detect deuterons that escaped down the CELSIUS beam pipe [227], show an enhancement that is discussed in Sec. 7.

In the near-threshold region final-state-interaction theory suggests that, if one neglects relativistic corrections, there should be the simple relation between the $pn \to pn\eta$ and $pn \to d\eta$ cross sections [210]:

$$\sigma^{I=0}_{pn\to pn\eta} \approx \frac{1}{4}\left(\frac{Q}{\varepsilon}\right)^{3/2}\left(1+\sqrt{1+Q/\varepsilon}\right)^{-2}\sigma_{pn\to d\eta}, \tag{5.2}$$

where ε is the deuteron binding energy. In the derivation of Eq. (5.2) it is assumed that the η production operator is of short range and that the effects of channel coupling through the np tensor force that gives rise to the deuteron D state can be neglected. In the simplified form presented here, the $pn \to d\eta$ is taken to follow phase space but shape corrections can be introduced [230]. The predictions are only relevant for the $I = 0$ cross section but the small $I = 1$ contribution can easily be subtracted using the data from pp collisions. A more important restriction is that Eq. (5.2) only estimates the cross section where the np emerge in an S wave so that it has to break down at higher values of Q.

The rapid rise from threshold of the $pn \to pn\eta$ cross section in Fig. 36a is rather similar to that in the $pp \to pp\eta$ collisions in Fig. 34. The shape is well described by Eq. (5.2) for $Q \lesssim 40$ MeV. This is examined more quantitatively in Fig. 36b, where the $\sigma^{I=0}_{pn\to pn\eta}/\sigma_{pn\to d\eta}$ cross section ratio is compared to the predictions of Eq. (5.2). The two cross sections were measured simultaneously [225, 226, 228] and so the big luminosity uncertainty cancels but it is not clear if the small deviations between the predictions and the data at low Q are due to an oversimplified theory or to systematic uncertainties in the event identification or the evaluation of Q in the $pn \to pn\eta$ case. Reducing the predictions by 15% gives a much better description of the data. What is, however, very clear is that the sharp rise above $Q = 60$ MeV is likely to be due to higher partial waves in the recoiling pn system.

It has been argued [229] that the difference in the rise of the $pn \to pn\eta$ and $pp \to pp\eta$ total cross sections in the first 10 MeV of excitation energy is due to the different np and pp final state interactions, as described by Eqs. (5.2) and (5.1).

5.3 η' production in pp collisions

Only three groups have studied η' production near threshold through the missing mass in the $pp \to ppX$ reaction and the existing total cross section data [198, 199, 205, 206, 207, 208] are compared to those for η production in Fig. 34. The first thing to notice is that η' production is typically a factor ~ 30 weaker than that of the η so that, for the highest energy point [205], the pp missing-mass criterion had to be supplemented through an $\eta\pi\pi$ selection in order to reduce the background. The even more striking point is that the curve of Eq. (5.1) describes very well all the available data. This indicates that the low-energy interaction of the η' meson with nucleons is far weaker than that of the η. This is not unexpected because there is no strong analogue of the $N^*(1535)$ sitting close to the $\eta' N$ threshold that would boost the interaction.

An interesting by-product of the COSY-11 $pp \to pp\eta'$ studies is a new and direct measurement of the natural width of the η' [231], $\Gamma = (0.226 \pm 0.017 \pm 0.014)$ MeV/c^2. This is by far the most precise value in the PDG tabulation [23] and can be used to normalize the decay widths in the different channels. In order to control the systematic uncertainties, the experiment was performed at five energies close to threshold where the signal-to-background ratio is especially favourable; the phase space for a four-body final state (multipion production) decreases faster than that of the three-body $pp\eta$ as threshold is

approached. For simple kinematic reasons, the missing-mass resolution also gets better at low Q such that in the COSY-11 measurement this was ≈ 0.33 MeV/c^2 at $Q = 0.8$ MeV [231], which is comparable to the line width to be studied.

5.4 The $pp \to pp\eta$ reaction as a source of η mesons

There is typically significantly more background under a missing-mass η peak in the $pp \to pp\eta$ case than for $pd \to {}^3\mathrm{He}\,\eta$. Nevertheless, because of its larger cross section, η production in pp reactions has been used by the COSY-WASA collaboration to study some of the properties of η decays. For example, using 1.2×10^5 identified $\eta \to 3\pi^0$ events, the deviations of the Dalitz plot from isotropy (the α parameter) could be quantified [232]. Though the result is compatible with the current PDG compilation [23], some of the experiments reported there, where the η is produced in γp or e^+e^- collisions, have higher statistics and less hadronic background.

The COSY-WASA tests for the production of the η' meson through the $pp \to pp\eta'$ reaction were less promising since, in the initial runs, no clear η' signal was identified [233]. Multipion production will certainly provide a very significant background [234].

6 Production in proton-nucleus collisions

6.1 Inclusive η production

The measurement of inclusive production of the η meson at 900 MeV and 1 GeV, i.e., well below the threshold in nucleon-nucleon collisions, was undertaken with the PINOT spectrometer at Saclay [235, 236, 237]. This two-arm photon detector, which had a limited energy resolution and very small geometric acceptance, was used to study production on ^{6}Li, B, C, Al, Cu, and Au targets. Even taking into account the much stronger η production in pn compared to pp collisions and a generous interpretation of the kinematics, the folding model, where the NN cross sections are convoluted with the Fermi motion, underpredicts the measured cross section [237] by a factor of two once η absorption is taken into account [238]. There is therefore significant room for two-step production, involving intermediate virtual pions, that seems to be crucial for the coherent $pd \to {}^3\mathrm{He}\,\eta$ reaction discussed in the next section.

6.2 The unpolarized $pd \to {}^3\mathrm{He}\,\eta$ reaction

There have been numerous measurements of the $pd \to {}^3\mathrm{He}\,\eta$ reaction at low energies over the last 30 years, where the ^{3}He nucleus was detected and the η meson identified through the missing mass in the reaction [181, 182, 239, 240, 241, 242, 243, 244, 245, 246, 247, 248]. The statistical precision is generally reasonable but the systematic uncertainties, mainly associated with the overall normalization, range from about 7% in the Saclay measurement [243] up to twice that in most of the other data, except for the large errors at COSY-11 [246].

As seen in Fig. 37, following a very rapid rise from threshold to be discussed in the next section, the total cross section reaches a plateau at relatively low values of the excess energy Q. The threshold cross section is very similar to that of $pd \to {}^3\mathrm{He}\,\pi^0$, despite the much larger momentum transfers [249]. Although very little structure is seen in the total cross section for $Q \gtrsim 10$ MeV, the angular distribution is far from flat, as illustrated by the recent data from COSY-WASA at 49 and 60 MeV [248] shown in Fig. 38. The data in the backward direction (the two-nucleon transfer region) are strongly suppressed and the cross section here falls very rapidly with incident beam energy [240].

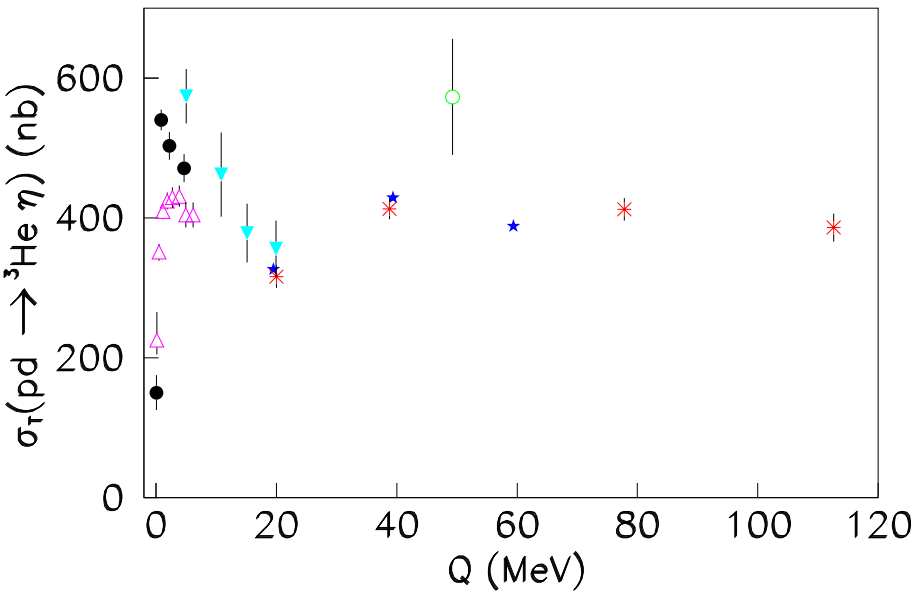

Figure 37: Total cross section for the unpolarized $pd(dp) \to {}^3\mathrm{He}\,\eta$ reaction as a function of the excess energy. The data are taken from Refs. [241] (black filled circles), [243] (open magenta triangles), [244] (open green circle), [245] (red crosses), and [247] (blue stars). Systematic errors are not shown. The near-threshold data are shown in Fig. 39.

It is useful to introduce an angular asymmetry parameter α, defined as

$$\alpha = \frac{d}{d(\cos\theta_\eta)} \ln\left(\frac{d\sigma}{d\Omega}\right)\Bigg|_{\cos\theta_\eta=0} \tag{6.1}$$

to describe the behaviour in the middle of the angular range. Away from the threshold region, α is large and positive.

The data have some similarities to the analogous $pd \to {}^3\mathrm{He}\,\pi^0$ reaction, where the ratio of the forward to the backward cross section increases fast with Q [250]. In this case much of the effect can be understood in a single-scattering model based upon the $pn \to d\pi^0$ with a spectator proton [251]. However, for η production the momentum transfers are so large ($\approx$ 880 MeV/c at threshold) that very high momentum components would be required in the nuclei and the impulse approximation with reasonable values for the $pn \to d\eta$ cross section [227] underestimates the production rate by almost two orders of magnitude [252].

An alternative approach is needed and Kilian and Nann [253] noticed that the threshold kinematics for the $pd \to {}^3\mathrm{He}\,\eta$ reaction fitted well those of the sequential $pp \to d\pi^+$ followed by $\pi^+ n \to \eta p$. The relative momentum between the proton and deuteron produced in this two-step process is very low such that these two particles had a good chance of *sticking* to produce the observed ^{3}He. Although they only made estimates within a semi-classical Monte Carlo approach, using empirical values of the $pp \to d\pi^+$ and $\pi^+ n \to \eta p$ cross sections, they ascribed the large near-threshold cross section to the *magic kinematics*, where the intermediate pion is essentially on-shell, which gives rise to a long-range interaction.

The near-threshold semi-classical estimates were confirmed in a quantum-mechanical implementation of the two-step model [254], though there were also significant contributions where the intermediate pion

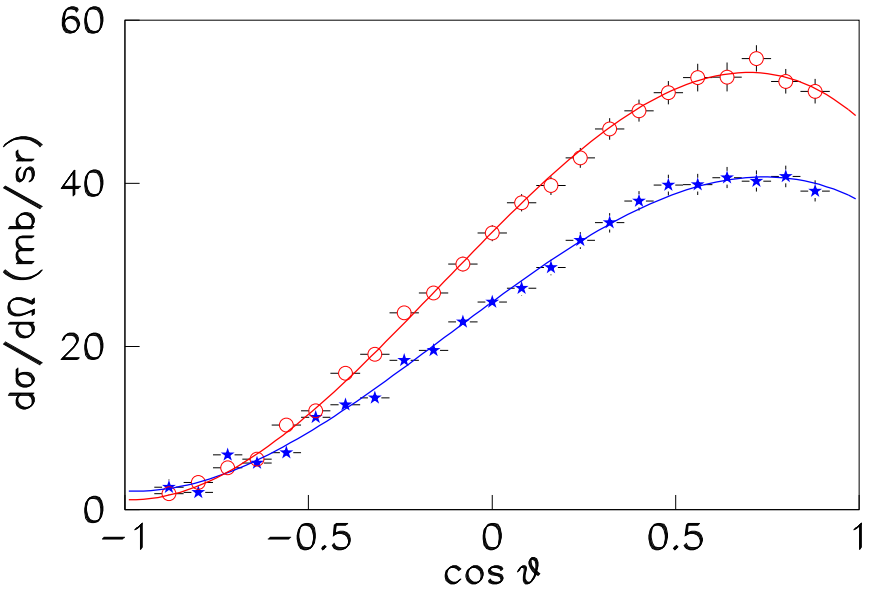

Figure 38: Differential cross section for the unpolarized $pd \to {}^3\mathrm{He}\,\eta$ reaction obtained at WASA-at-COSY [248] at excess energies of 49 (blue filled stars) and 60 MeV (red open circles), respectively. The curves are cubic fits in $\cos\theta$, where θ is the c.m. angle between the incident proton and the outgoing η.

strayed from its mass shell. Although the near-threshold data could indeed be described in terms of $pp \to d\pi^+$ followed by $\pi^+ n \to \eta p$, when this approach was tried at higher energies [255] it predicted differential cross sections that were backward peaked, in complete contrast to the experimental data [244, 245, 248]. The kinematics become less *magic* away from threshold and it is possible that the defect in the model is associated with the neglect of the off-shell behaviour of the $pp \to d\pi^+$ amplitude.

6.2.1 Near-threshold data

Of especial experimental and theoretical interest is the behaviour of the $pd \to {}^3\mathrm{He}\,\eta$ cross section in the very low Q region. Although this had been investigated at a few energies in earlier experiments [241, 243], more detailed measurements were carried out by two groups at COSY [181, 182] using a deuteron beam, where the spectrometer acceptance is enhanced. The two data sets are broadly consistent and only the ANKE results for the total cross section are shown in Fig. 39.

What is absolutely striking here is the fact that the rise to the plateau is achieved within the first 1 MeV. This scale is such that it must reflect the behaviour of the $\eta{}^3\mathrm{He}$ system, i.e., be due to a final-state interaction (FSI) [137]. To investigate this in greater detail, let us evaluate the average amplitude-squared through

$$\overline{|f|^2} = p_d\,\sigma_T(dp \to {}^3\mathrm{He}\,\eta)/4\pi p_\eta, \tag{6.2}$$

where p_d and p_η are the deuteron and η c.m. momenta.

The rapid rise in the cross section shown in Fig. 39 indicates that there must be a pole in the production amplitude near $Q = 0$ and so we parameterize this in the form

$$f_s = \frac{f_B}{(1 - p_\eta/p_1)(1 - p_\eta/p_2)}\,. \tag{6.3}$$

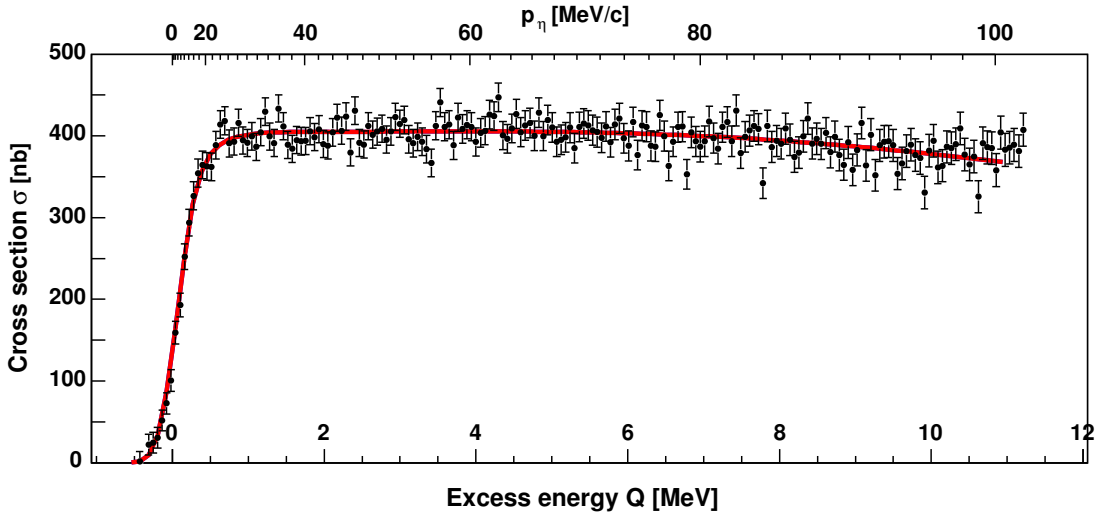

Figure 39: Total cross section for the unpolarized $dp \to {}^3\mathrm{He}\,\eta$ total cross section measured at COSY–ANKE [181] in terms of the excess energy Q and η c.m. momentum p_η. The (red) curve represents the smeared fit of Eq. (6.2) with parameters given in Eq. (6.4).

Here p_1 and p_2 could be expressed in terms of the scattering length and effective range but the p_i parameters are far less coupled in the fits.

After taking into account the momentum distribution in the circulating deuteron beam and the smearing connected with the measuring apparatus, the best fit was achieved with [181]

$$\begin{aligned} p_1 &= [(-5 \pm 7\,^{+2}_{-1}) \pm i(19 \pm 2 \pm 1)]\,\mathrm{MeV}/c \\ p_2 &= [(106 \pm 5) \pm i(75 \pm 12\,^{+1}_{-2})]\,\mathrm{MeV}/c, \end{aligned} \tag{6.4}$$

where the first error is statistical and the second systematic. Note that these data cannot determine the sign of the imaginary parts of the p_i, a point that is critical in the discussion of η-mesic nuclei in Sec. 7. The second pole is an effective one whose position is unstable to changes in the data selection but p_1 represents a genuine singularity which, in the excess energy plane, is situated at $Q_0 = [(-0.36 \pm 0.11 \pm 0.04) \pm i(0.19 \pm 0.28 \pm 0.06)]$ MeV. Therefore, with zero momentum bite and perfect apparatus, the rise in Fig. 39 would be even more precipitous with $|Q_0| \sim 0.4$ MeV.

Further evidence for the pole hypothesis is to be found in the variation of the angular distribution with p_η. There were already indications in the Saclay data [243] that very close to threshold the data were a little stronger in the backward hemisphere, i.e., the parameter α of Eq. (6.1) was slightly negative. This behaviour was confirmed in the two COSY experiments [181, 182] and their results are shown in Fig. 40.

At low Q the parameter α reflects the interference between s and p waves and, if both the magnitude and the phase of the s-wave amplitude vary fast over the first few MeV due to the pole, then this will affect the momentum dependence of α. The best fit in Fig. 40 assuming a constant s-wave phase does not allow α to go negative but, if the phase variation with p_η determined by Eq. (6.3) is taken into account then one can reproduce much better the shape of the α measurements [256]. Therefore it seems that the pole hypothesis in the s-wave production amplitude is on quite firm foundations.

In contrast to the extensive data set available for η production, the only published value of the $pd \to {}^3\mathrm{He}\,\eta'$ cross section was obtained within the context of the threshold study of heavy meson production [257]. It is important to note here the relative weakness of η' production, with the ratio of the squares of the threshold amplitudes being a mere $|f(pd \to {}^3\mathrm{He}\,\eta')|^2/|f(pd \to {}^3\mathrm{He}\,\eta)|^2 \approx 5 \times 10^{-4}$ [257]. In a two-step model, η' production certainly seems to be anomalously weak in this channel compared

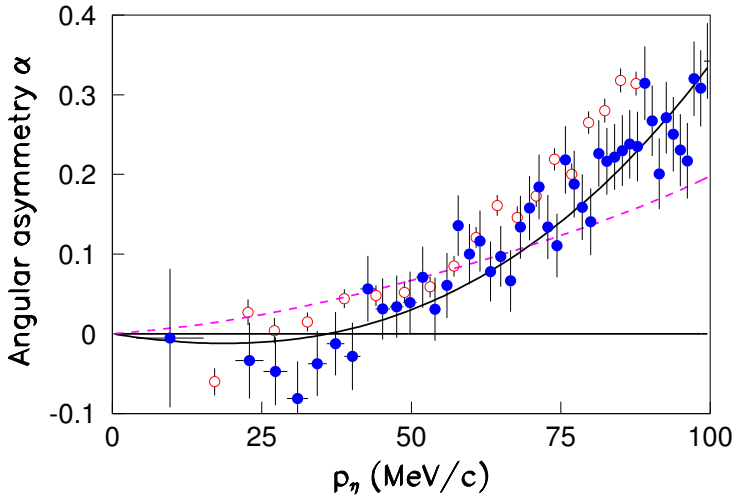

Figure 40: Angular asymmetry parameter α of the $dp \to {}^3\mathrm{He}\,\eta$ reaction defined in Eq. (6.1) measured at COSY-11 [182] (red open symbols) and COSY-ANKE [181] (blue closed symbols). Also shown are the fits to the ANKE data with (solid black line) and without (dashed magenta line) taking the s-wave phase variation into account [256].

to ϕ production [258]. As a consequence the signal/background ratio is likely to be very unfavourable and a value of $\approx 1/40$ was found experimentally at COSY-WASA at $Q \approx 64$ MeV [233], and this makes it doubtful as a source of η' for decay studies. The preliminary total cross section estimate of ≈ 0.6 nb/sr corresponds to $|f(pd \to {}^3\mathrm{He}\,\eta')|^2 \approx 0.2$ nb/sr, which is lower than the threshold value of 0.9 ± 0.2 nb/sr [257].

6.3 The polarized $\vec{d}p \to {}^3\mathrm{He}\,\eta$ reaction

The anomalous energy dependence near threshold of the $dp \to {}^3\mathrm{He}\,\eta$ total cross section, which jumps to its plateau value within the first 1 MeV of excess energy Q [181, 182], is evidence for a strong s-wave $\eta\,{}^3$He final state interaction leading to a pole in the production amplitude for $|Q| < 1$ MeV [137]. If this is indeed true, then the FSI should manifest itself in broadly similar ways for different entrance $\gamma{}^3\mathrm{He} \to \eta{}^3\mathrm{He}$ channels that give rise to the same $\eta\,{}^3$He final state. The recent photoproduction data show a steep increase in the first 4 MeV bin above threshold (see Fig. 28) [180], though the experiment could not determine well the pole position.

In the $dp \to {}^3\mathrm{He}\,\eta$ reaction the s-wave $\eta\,{}^3$He final state can be accessed from either the total spin $S = \frac{3}{2}$ or the $S = \frac{1}{2}$ initial states and the differences will influence the deuteron tensor analyzing power t_{20} in the reaction. The pure s-wave FSI hypothesis would require that t_{20} should remain constant, despite the strange behaviour of the unpolarized cross section.

The tensor analyzing power of the $\vec{d}p \to {}^3\mathrm{He}\,\eta$ total cross section has recently been measured in a missing-mass experiment at COSY from threshold up to $Q \approx 11$ MeV [259]. The results are indeed consistent with a constant value of t_{20}, which offers strong support to the FSI interpretation of the near-threshold energy dependence. It is important to note here that the detection system is independent of the deuteron beam polarization so that many of the systematic effects cancel. The experiment also seems to show that the forward/backward difference in t_{20} is much smaller than for the unpolarized cross section [181] and this, together with the small value found for the vector analyzing power it_{11}, are both useful elements in constraining the amplitude structure near threshold.

6.4 The $pd \to pd\eta$ reaction

Since a two-step model describes much of the near-threshold $pd \to {}^3\mathrm{He}\,\eta$ data, it would be interesting to see if this approach is equally successful for the unbound ^{3}He states, i.e., for the $pd \to pd\,\eta$ reaction. There have been two measurements of the reaction, where the proton and deuteron were detected [260, 261], and the resultant total cross sections are shown in Fig. 41.

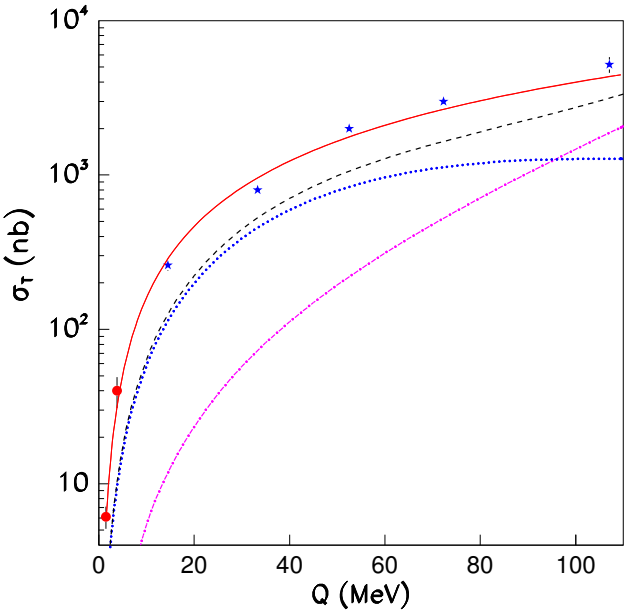

Figure 41: Experimental values of the $pd \to pd\,\eta$ total cross sections from Refs. [260] (red circles) and [261] (blue stars). These are compared with predictions [262] of the pick-up contribution (magenta chain) and the two–step model (blue dotted), and their incoherent sum (black dashed curve). The solid (red) curve is a phenomenological fit on the basis of Eq. (6.5) with $C = 350$ nb.

Near threshold it is predicted [262] that the two-step model, similar to that used to explain the threshold $pd \to {}^3\mathrm{He}\,\eta$ reaction, should dominate but, as Q approaches the threshold in nucleon-nucleon collisions, then the quasi-free $pn \to d\eta$ (pick-up) contribution becomes larger. In all cases the impulse approximation (triangle graph) is negligible. The incoherent sum of these contributions is at least a factor of two too low but this defect is very similar to that found for $pd \to {}^3\mathrm{He}\,\eta$.

There is some evidence from the effective mass distributions measured at $Q \approx 72$ MeV for a significant distortion in the ηd spectrum corresponding to a large ηd scattering length [261]. On the other hand, the spectra do not seem to be affected by the existence of the ^{3}He bound state. Nevertheless, the data are well represented by the phenomenological form [210]

$$\sigma_T(pd \to pd\,\eta) = C\,(Q/\varepsilon)^2 / \left(1 + \sqrt{1 + Q/\varepsilon}\right)^2, \tag{6.5}$$

where $\varepsilon = 5.5$ MeV is the pd binding energy in ^{3}He and the best fit shown in the figure is achieved with $C \approx 350$ nb.

If one neglects spin-quartet production and considers only the ^{3}He pole then one expects that [210]

$$C = \tfrac{1}{4}\sqrt{\varepsilon/Q} \times \sigma_T(pd \to {}^3\mathrm{He}\,\eta)\Big|_{Q=0} \approx 450 \text{ nb}. \tag{6.6}$$

Although the extent of the agreement here may be fortuitous, it does emphasize the close link between the $pd \to {}^3\mathrm{He}$ and $pd \to pd\,\eta$ reactions. Nevertheless, it is clearly a challenge to theory when, as in this case, there are strong final-state interactions in both the pd and $\eta\,d$ channels.

6.5 The η-meson mass

There have been several modern measurements of the η mass that relied on detailed studies of the decay products of the meson [263, 264, 265] but there have also been two recent ones that involved measurements in production reactions [61, 266], and these illustrate contrasting approaches.

The determination of the mass of the η meson, m_η, in any two-body reaction requires the careful measurement of both the beam energy and also the excess energy Q in the reaction. Systematic effects are, however, minimized if the data can be extrapolated to the threshold, i.e., to $Q = 0$. In the study of the $\gamma p \to \eta p$ reaction with the Crystal Ball at MAMI [61], the photon beam energy was determined macroscopically, starting with a precise measurement of the bending radius of the electron beam in the first dipole magnet. A total uncertainty of $\sigma(E_\gamma) = 98$ keV was found. The reaction itself was identified cleanly through both the $\eta \to 2\gamma$ and $\eta \to 3\pi^0 \to 6\gamma$ decay modes, though a very small background, originating from the target windows, had to be subtracted. The threshold energy, E_{thr}, of the reaction was determined by extrapolating the arbitrarily normalized cross section to zero, assuming pure s-wave dominance, viz. $\sigma(E_\gamma) \propto \sqrt{E_\gamma - E_{\mathrm{thr}}}$. Consistent results were obtained from the two decay modes studied and the overall value quoted,

$$m_\eta(\mathrm{MAMI}) = (547.865 \pm 0.031_{\mathrm{stat}} \pm 0.062_{\mathrm{syst}})\ \mathrm{MeV/c^2},$$

agrees well with other modern measurements [263, 264, 265] and with the PDG compilation [23]. The dominant element in the 62 keV/c^2 systematic uncertainty originates from the determination of the beam energy.

In the $pd(dp) \to {}^3\mathrm{He}\,\eta$ reaction near threshold, the meson can be identified through the missing-mass peak in the reaction. However, in the two cases where the beam energy was determined through the measurement of other two-body reactions that fell within the spectrometer acceptances [267, 268], the values obtained for the mass were about 0.5 MeV/c^2 lower than the current PDG average [23].

In a new experiment using the ANKE spectrometer at the COSY storage ring, the internal cluster-jet target had no windows [266]. The momentum of the circulating beam was determined with a relative precision of 3×10^{-5} by using a polarized deuteron beam and inducing an artificial depolarizing resonance, which occurs at a well-defined frequency that depends only upon the particle's speed.

The small background under the η missing-mass peak was estimated reliably using data obtained just below threshold. However, unlike the MAMI $\gamma p \to \eta p$ measurement [61], the extrapolation to threshold was not carried out using the energy dependence of the cross section. Rather, at the 11 points measured above threshold, the excess energy was evaluated from the size of the ^{3}He momentum ellipse in the ANKE focal plane, for which very detailed studies of the spectrometer characteristics had to be undertaken. The result,

$$m_\eta(\mathrm{ANKE}) = (547.873 \pm 0.005_{\mathrm{stat}} \pm 0.027_{\mathrm{syst}})\ \mathrm{MeV/c^2},$$

though agreeing with the PDG average [23], has the best statistical precision of all the experiments and, arguably, the best systematic precision also.

Although it was kinematics rather than cross section that were extrapolated to threshold, a competitive measurement of the η mass was only possible due to the η^3He s-wave FSI such that, as shown in Fig. 39, the cross section plateau is already reached for $Q < 1$ MeV. Thus it would be much harder to extract a reliable value for the π^0 mass from $dp \to {}^3\mathrm{He}\,\pi^0$ data because final-state p-waves are very significant here, even at very low values of Q [249].

6.6 The $p\,^6\mathrm{Li} \to {}^7\mathrm{Be}\,\eta$ reaction

The inclusive cross sections for η production reported in Sec. 6.1 are generally very small and the only hope for measuring an exclusive reaction is in the case of the ^{6}Li target. However, when the $p^6\mathrm{Li} \to {}^7\mathrm{Be}\,\eta$ reaction was identified through the 2γ decay of the η [224] the resolution was not sufficient to decide the relative contributions of the first four or more levels of the ^{7}Be nucleus to a c.m. differential cross section of $d\sigma/d\Omega = 4.8 \pm 3.8$ nb/sr at $\theta_\eta^{c.m.} \approx 25^\circ$. In a later experiment, at a lower value of Q [270], the recoiling ^{7}Be nucleus was detected and the η identified through the missing-mass peak in the reaction. In this case the measured $d\sigma/d\Omega = 0.7 \pm 0.3$ nb/sr must correspond to the production of the ground-state doublet in ^{7}Be because higher states decay via the break-up of the nucleus.

The reaction has been studied in a cluster-model approach [271], where the initial and final nuclear states were described in terms of their αd and $\alpha\tau$ components, respectively. In this model the process is assumed to be driven by $pd \to {}^3\mathrm{He}\,\eta$ with the initial d and final τ in the two nuclei. Apart from the intrinsic crudeness of this approach, the calculations are made much more uncertain by the limited knowledge of cluster wave functions for such a large momentum transfer reaction. Nevertheless, as shown explicitly in Ref. [270], the model is compatible with both data sets and this suggests that it is the excited $L = 3$ doublet that dominates in the final state in the earlier experiment [224]. The relative strengths of the final ^{7}Li states is similarly ambiguous in the $\gamma^7\mathrm{Li} \to \eta^7\mathrm{Li}$ reaction [147].

6.7 The $dd \to {}^4\mathrm{He}\,\eta$ reaction

The third well-identified nuclear state where the s-wave η–nucleus final-state interaction can be usefully investigated is that of ^{4}He. Since the final s-wave is forbidden in the $\gamma^4\mathrm{He} \to \eta^4\mathrm{He}$ reaction, and neither the $p^3\mathrm{H} \to \eta^4\mathrm{He}$ nor $n^3\mathrm{He} \to \eta^4\mathrm{He}$ is experimentally *appealing*, this final state has been studied in a series of measurements of the $dd \to {}^4\mathrm{He}\,\eta$ reaction [272, 273, 274, 275]. It is first important to note that the threshold cross section is about fifty times lower than that of $pd \to {}^3\mathrm{He}\,\eta$, so that its measurement represents much more of a challenge.

Due to the identical nature of the two deuterons in the initial state, there are strong angular momentum constraints on the amplitude structure of this reaction, which can be written in the c.m. frame as:

$$\begin{aligned} M &= A(\vec{\varepsilon}_1 \times \vec{\varepsilon}_2) \cdot \hat{p} + B(\vec{\varepsilon}_1 \times \vec{\varepsilon}_2) \cdot [\hat{p} \times (\vec{p}_\eta \times \hat{p})]\,(\vec{p}_\eta \cdot \hat{p}) \\ &\quad + C\,[(\vec{\varepsilon}_1 \cdot \hat{p})\vec{\varepsilon}_2 \cdot (\vec{p}_\eta \times \hat{p}) + (\vec{\varepsilon}_2 \cdot \hat{p})\vec{\varepsilon}_1 \cdot (\vec{p}_\eta \times \hat{p})]\,, \end{aligned} \tag{6.7}$$

where the $\vec{\varepsilon}_i$ are the polarization vectors of the two deuterons, $\hat{p}$ the direction of one of the incident deuterons, and $\vec{p}_\eta$ the momentum of the final η meson. The three scalar amplitudes A, B, and C are functions of ${p_\eta}^2$, p^2, and $(\vec{p}_\eta \cdot \vec{p})^2 = p_\eta^2 p^2 \cos^2\theta$, where θ is production angle of the η meson.

At threshold ($p_\eta = 0$) the only non-zero contribution comes from the A amplitude and the reaction is then forbidden if the magnetic quantum number of either deuteron is $m = 0$. The Cartesian tensor analyzing power then becomes $A_{xx} = -\frac{1}{2}$. Although the initial SPESIV experiment was carried out with unpolarized deuterons [272], the resolution at the SPESIII spectrometer was insufficient to identify the η peak cleanly [273]. By using a tensor polarized beam and assuming that the background had only a weak analyzing power, they were able to use the $m = 0$ data to model the background and thus extract the $m = \pm 1$ cross section. Since the $m = 0$ cross section is negligible in the near-threshold region, this allowed the unambiguous evaluation of the total cross section and this is confirmed through the comparison of the polarized [273] and unpolarized [272] cross sections at low energies.

Away from threshold the angular distributions are no longer flat [274] but it is not possible from an unpolarized cross section to determine whether this anisotropy arises from the square of the p-wave amplitude, C, or from s–d interference involving the A and B amplitudes. The measurement of A_{xx} away from threshold at $Q = 16.6$ MeV has a large scatter but these data have been interpreted as

suggesting that the p-wave amplitude C is very small [275]. From the values of the fit parameters at 16.6 MeV and assuming that the η d-wave amplitudes vary with threshold factors of p_η^2, it is possible to attempt an extraction of the square of the magnitude of the s-wave amplitude [275], and the results of this are shown in Fig. 42.

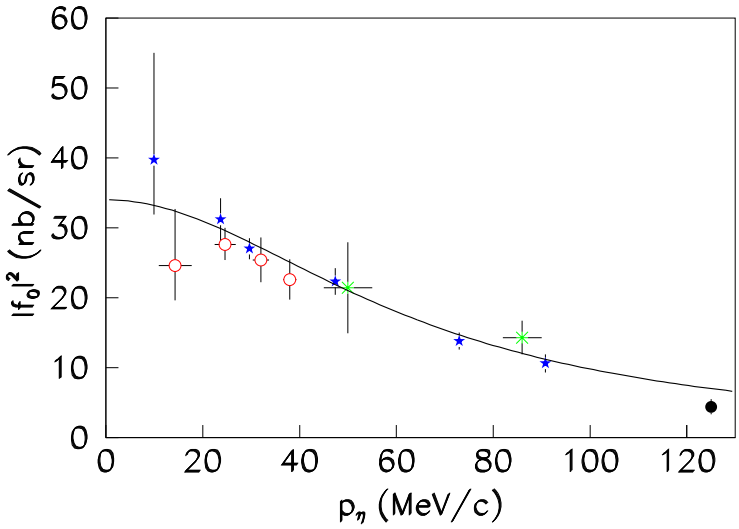

Figure 42: Experimental values of the square of the $dd \to {}^4\mathrm{He}\,\eta$ s-wave amplitude extracted using the methodology presented in Ref. [275]. The data are taken from Refs. [272] (red open circles), [273] (blue stars), [274] (green crosses), and [275] (black closed circle). The curve is a scattering-length fit: $|f_0|^2 = 34/[1 + (p_\eta/64)^2]$ nb/sr, where p_η is measured in MeV/c.

In the scattering-length approximation, only one pole in Eq. (6.3) is considered and the s-wave production amplitude is taken in the form $f_0 = f_B/(1 - p_\eta/p_1)$. The best fits to the data shown in Fig. 42 are achieved with a positive value for the the real part of p_1, which is forbidden by unitarity [181]. Putting this to zero, the curve shown in the figure was obtained with $Im(p_1) = \pm(64 \pm 10)$ MeV/c and $|f_B|^2 = 34 \pm 1$ nb/sr, which corresponds to a pole in the amplitude at an excess energy $|Q_0| = 4.3 \pm 1.3$ MeV [275]. The sign of $Im(p_1)$ cannot be fixed by these real η-production data and this leaves the location of the pole in the complex Q plane even more uncertain, a point that we shall return to in the discussion of possible η-mesic nuclei. The curve does not describe well the highest momentum point but keeping only the first pole in Eq. (6.3), i.e., neglecting the effective range, is clearly a dubious approximation at such high p_η.

6.8 The $pd \to {}^3\mathrm{He}\,\eta$ reaction as a source of η mesons

Since the total cross section for the $pd \to {}^3\mathrm{He}\,\eta$ reaction shown in Fig. 39 reaches a plateau so close to threshold, it means that the multipion background under the η peak at low Q is very limited [181]. It was already suggested at the time of the first near-threshold measurements [241] that this reaction could be a useful source of tagged η-mesons to study their decay properties.

Various decays were indeed studied by the WASA collaboration at both CELSIUS and COSY using this reaction [276, 277, 278]. Although the signal-to-background ratio is much more favourable than for the $pp \to pp\eta$ reaction that was mentioned in Sec. 5.4, the η production rate is not high enough to measure really low branching ratios. Furthermore, when the meson is produced in e^+e^- collisions or

is photoproduced there is little or no hadronic background and the reaction tends to be much cleaner. The production rates are also high. As a consequence, it seems that the parameters in most decay channels are generally better determined at electron accelerators [23].

6.9 The $pd \to {}^3\mathrm{He}\,\eta\,\pi^0$ reaction

The only published measurement of the $pd \to {}^3\mathrm{He}\,\eta\,\pi^0$ reaction [279] was carried out at 1450 MeV using the WASA detector at CELSIUS (Uppsala). At this energy the whole of the $D_{33}(1700)$ discussed in Secs. 2.1.3 and 3.2 could not be scanned. Nevertheless there was some evidence for a cascade decay proceeding via a $\Delta(1232)\eta$ intermediate state. However, when this experiment was repeated using WASA at COSY at higher energy, there was little clear evidence for such a decay chain [280].

7 η-mesic nuclei

Due to the presence of the $N^*(1535)$ overlapping the ηp threshold, the low energy ηp interaction is very strong and attractive [281]. Moreover, since the η is an isoscalar meson, this must also be true for the ηn system. This suggested to Haider and Liu that the attraction might be sufficiently strong as to cause the η meson to bind to a nucleus [282]. The first estimates were based upon the simple $t\rho$ optical potential and, although there is a reasonable consensus as to what to take for the imaginary part of the ηN scattering length $a_{\eta N}$, the same cannot be said for the real part, where values ranging between 0.27 fm and 0.98 fm are to be found in the literature [283]. Part of the difficulty here is that, because of the $N^*(1535)$ resonance, the ηN scattering amplitude has a strong energy dependence and there is uncertainty in how this should be taken into account.

Haider and Liu [282] took a relatively low value for $\mathrm{Re}(a_{\eta N})$ and, as a result, they only found binding for ^{12}C and heavier nuclei. Although there may be poles in the complex energy plane for lighter nuclei, these would correspond to antibound (or virtual) states. Despite not being bound, such poles might still affect nuclear reactions in a similar way to how the antibound $^1S_0$ state may be more important than the bound $^3S_1$ deuteron state in low energy neutron-proton scattering. It is perhaps useful to stress here that, due to the possibility that a mesic nucleus could decay via pion emission, described by the imaginary part of the potential, even for strongly attractive potentials a state is at best quasi-bound.

By increasing the size of the real part of the scattering length $\mathrm{Re}(a_{\eta N})$ from 0.27 fm to 0.51 fm, the simplistic potential model predicts quasi-bound η-mesic nuclei down as far as ${}^4_\eta\mathrm{He}$ [283] but this at the expense of generating states with decay widths in the p-shell nuclei of the order of 10-15 MeV. Since an η would be expected to stick to an excited nuclear level with about the same binding energy as for the ground state [284], the search for such states is clearly made much more difficult when the decay width is larger than the nuclear level spacing.

Several attempts have been made to refine the binding estimates but in the $t\rho$ model one is faced with the choice of energy at which the amplitude t should be evaluated. The value is influenced by the nuclear as well as by the η binding energy and in a recent paper [285] this was estimated in a much more self-consistent way than in earlier approaches. However, even this is not on safe grounds because we don't know how the $N^*(1535)$ itself behaves inside a nucleus. Is it more bound or less bound than a nucleon?

There have been two approaches to the experimental search for η-mesic nuclei. The first involves the study of real η production near threshold, where one attempts to extrapolate in energy to the η-mesic pole. The detection of an emerging η does overcome the large multipion background. This has been partially successful for light nuclei but it is important to note that these above-threshold measurements can never distinguish between a bound and an antibound state. The alternative approach is to look directly in the bound state region, possibly trying to select kinematic regions where the decay of the

η-mesic nucleus might be favoured. Although more direct, this approach faces more severe background problems. We consider these two alternative approaches separately.

7.1 Real η production

The data and the analysis of the near-threshold $dp \to {}^3\mathrm{He}\,\eta$ reaction [181, 182] clearly show that there is a pole in the production amplitude at an excitation energy $Q_0 = [(-0.36 \pm 0.11 \pm 0.04) \pm i(0.19 \pm 0.28 \pm 0.06)]$ MeV which is most likely a property of the η^3He system. The sign of the imaginary part of Q_0, i.e., *bound* or *antibound*, can never be determined from data on real η production. Moreover, the errors on the real and imaginary parts are strongly correlated in fits to the data. The presence of such a pole is also reflected in the rapid rise in the total cross section of the $\gamma^3\mathrm{He} \to \eta\,{}^3\mathrm{He}$ reaction [180]. The angular distributions for producing the η^3He system in dp or γ^3He collisions also show anomalous behaviour near threshold [256, 180] that are consistent with the pole hypothesis.

The s-wave η^3He system can be accessed in the $dp \to {}^3\mathrm{He}\,\eta$ reaction from deuterons with magnetic quantum number $|m| = 1$ or $m = 0$ and, in principle, these different entrance channels could yield poles in different positions in the Q plane. The low value of the tensor analyzing power t_{20} found in the initial Saclay experiment [241] shows that the production from these two initial states is roughly equal so that, if there were two poles, they would be populated with about the same intensity. Fitting them with a single pole model would then give a contribution to the width that was of the same order as the difference in the two pole positions. However, the fits to the data [181, 182] lead to a very small value of $\mathrm{Im}(Q_0)$, which suggests that one could safely dismiss the two-pole hypothesis. A more direct proof of this conclusion is provided by the measurement of t_{20} as a function of energy [259]. One may therefore conclude that the pole in the $dp \to {}^3\mathrm{He}\,\eta$ reaction is indeed a property of the η^3He system.

The s-wave η^4He system cannot be accessed in a two-body photoproduction reaction but several experimental studies have been undertaken in the $dd \to {}^4\mathrm{He}\,\eta$ reaction. However, the cross section is a factor of about 50 lower than that for $dp \to {}^3\mathrm{He}\,\eta$ reaction and so the results are necessarily less precise than in the η^3He case. The exact location of the pole in the complex Q plane is far more uncertain because the data are not very sensitive to the phase of Q_0 and its magnitude has also a comparatively large error, $|Q| = 4.3 \pm 1.3$ MeV [275]. It was argued by Willis et al. [273] that an η would be attracted more to ^{4}He than to ^{3}He because of the extra nucleon and the smaller nuclear radius. Hence, since $|Q_0|$ is bigger for ^{4}He, it would imply that η^4He is quasi-bound. This reasoning has been recently questioned on the grounds that the attraction might be weakened in ^{4}He due to the strong nuclear binding [285].

The quasi-free $pn \to d\eta$ total cross section discussed in Sec. 5.2 was measured in two experiments at CELSIUS [225, 226, 227]. Although the cross section is larger than that for the $pd \to {}^3\mathrm{He}\,\eta$ reaction, the detection of the two photons from the η decay in coincidence with the fast deuteron had a much reduced acceptance and energy resolution. The resolution was better at lower energy when the deuteron and proton from the $dp \to dp\eta$ reaction were measured in coincidence with two photons [261]. In both sets of experiments there is evidence for an enhancement at low ηd invariant masses and, to make this more explicit, the data have been divided by an arbitrarily normalized phase space in Fig. 43. We do not show here the near-threshold data of Ref. [286], where there are uncertainties in the multipion background.

It is possible that the shape of the sub-threshold $pd \to pd\,\eta$ ratios [261] shown in Fig. 43 are distorted by the reaction mechanism such that it is not valid to divide by the three-body phase space. This point will be resolved when the new detailed measurements of the differential and total cross sections of the quasi-free $np \to d\eta$ near threshold become available [288].

Since there are only three particles in the ηnp system, the final state interaction is then theoretically much more tractable and the Alt-Grassberger-Sandhas equations have been resolved for various ηN inputs [287]. Taking $a_{\eta N} = 0.25 + 0.16i$, $0.55 + 0.30i$, and $0.98 + 0.37i$ fm, this group found η-deuteron scattering lengths of $a_{\eta d} = 0.73 + 0.56i$, $1.64 + 2.99i$, and $-4.69 + 1.59i$ fm, respectively. The enhance-

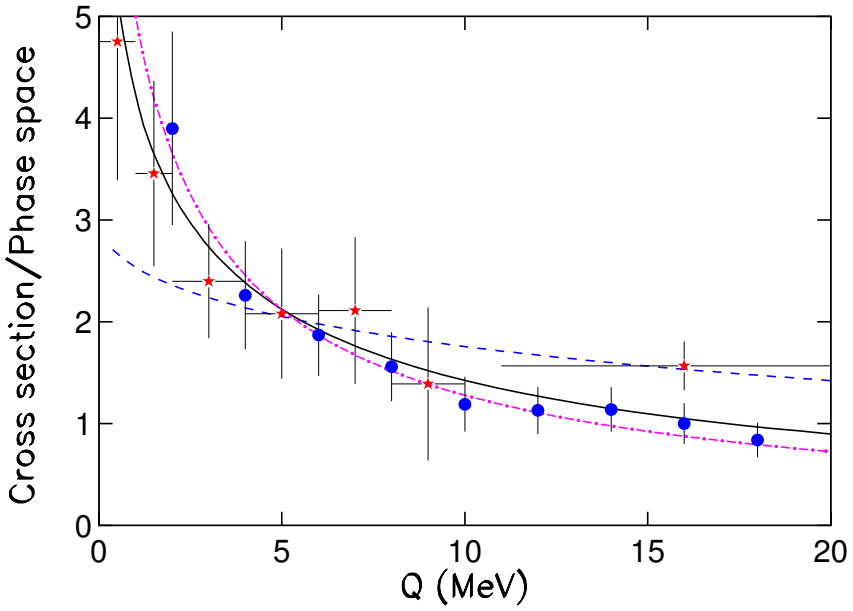

Figure 43: Ratio of the cross section for the production of the $d\,\eta$ system to arbitrarily normalized phase space (red stars) as a function of the energy Q above the ηd threshold [225, 226, 227] and similarly for the $pd \to pd\,\eta$ reaction at 1032 MeV (closed blue circles) [261]. The broken (blue), solid (black) and chain (magenta) curves are the predictions of the scattering length formula with input $a_{\eta d} = 0.73{+}0.56i$, $1.64 + 2.99i$, and $-4.69 + 1.59i$ fm, respectively [287].

ments expected with these scattering lengths are also shown in Fig. 43. The first $a_{\eta N}$ input, which is quite close to that used by Haider and Liu [282], does not give a sharp enough enhancement. The other two can describe the data quite well but, as for the ${}^{3}_{\eta}$He and ${}^{4}_{\eta}$He cases, the results cannot distinguish between the quasi-anti-bound situation, where $\mathrm{Im}[a_{\eta d}] > 0$, and the quasi-bound, where $\mathrm{Im}[a_{\eta d}] < 0$.

The only other cases where the near-threshold production of the η meson from a nucleus was studied involves $A = 7$ final states. The statistics in the $p{}^{6}\mathrm{Li} \to {}^{7}\mathrm{Be}\,\eta$ measurements were paltry [269, 270] and, in the more extensive $\gamma{}^{7}\mathrm{Li} \to \eta{}^{7}\mathrm{Li}$ data [147], the separation of the nuclear levels is ambiguous and the lack of clean results at very low values of Q does not permit the extraction of the associated enhancement factors.

The most straightforward (but not unique) interpretation of the data on light nuclei is that the ηd system is unbound, the $\eta{}^{4}\mathrm{He}$ is bound, but that the $\eta{}^{3}\mathrm{He}$ case is ambiguous. What is remarkable for $\eta{}^{3}\mathrm{He}$ is the small value of the imaginary part of the pole position, $\mathrm{Im}[Q_0] = (0.19{\pm}0.28{\pm}0.06)$ MeV [181]. By adjusting the interaction strength it is possible to get the real part to be close to zero but, in a simple optical potential approach, one only achieves a small imaginary part if the imaginary part of the potential is itself unreasonably weak [289].

7.2 Virtual η production

Since the production of real η mesons can never distinguish between the bound and anti-bound hypotheses, the temptation is to look directly below threshold and search for other decay modes of an η-mesic nucleus. The difficulty in this approach is that, without the η trigger, the multipion background might be hard to overcome. Inspired by the work of Haider and Liu [282], searches were undertaken at Brookhaven [290] and LAMPF [291] using pion beams and measuring the inclusive (π^+, p) reaction on

various nuclei with the hope of finding a missing-mass peak corresponding to a bound η-mesic nucleus. No conclusive signals were identified in either experiment despite, in the LAMPF case [291], detecting in coincidence charged particles from the decay of the supposed η-mesic nucleus.

A significant fraction of the decays of such an exotic nucleus might be through the $\eta N \to \pi N$ reaction and, if one neglects the Fermi motion in the nucleus, the pion and proton should come out back to back in the nuclear rest frame. The searches at the Lebedev Physical Institute of the $\gamma^{12}\mathrm{C} \to \pi^+ nNX$ reaction with correlated back-to-back $\pi^+ n$ pairs did not have a good enough resolution to identify a peak coming from an η-mesic nucleus [292]. A similar experiment that searched for the two-nucleon decay of an η-mesic nucleus has yet to yield conclusive results [293] but it is possible that this branching ratio might have been overestimated [289].

The search for back-to-back $\pi^- p$ pairs was also pursued at JINR using a deuteron beam [294]. A peak was found in the $\pi^- p$ invariant mass just below the ηN threshold but there was no indication that this was associated with an η-mesic nucleus.

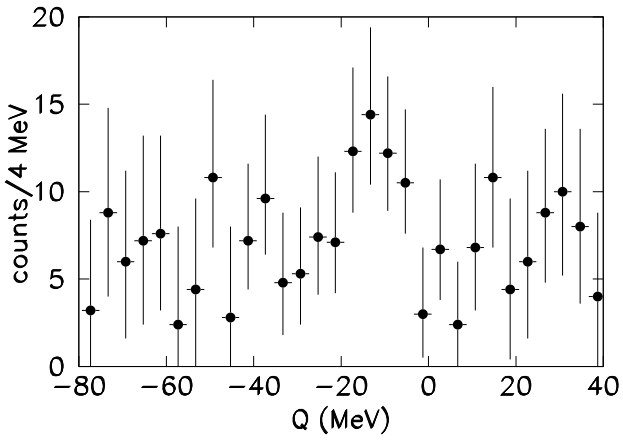

Figure 44: Counts for the $p^{27}\mathrm{Al} \to {}^3\mathrm{He}\, p\, \pi^- X$ reaction as a function of the excess energy in the $\eta^{25}\mathrm{Mg}$ system [295].

The strongest claim for the discovery of a peak arising from the production of an η-mesic nucleus was made by the COSY-GEM collaboration after measuring the $p^{27}\mathrm{Al} \to {}^3\mathrm{He}\, p\, \pi^- X$ reaction [295]. The kinematics were cunningly chosen such that, for a weakly bound state, the η was produced almost at rest so that it had a higher chance of *sticking* to the residual nucleus. As in the Russian experiments, the emerging proton and pion were detected close to the back-to-back region. The resulting spectrum is shown in Fig. 44 as a function of the excess energy in the ${}^{25}_{\eta}\mathrm{Mg}$ system. The authors suggest that the excess of events for $Q \approx -13$ MeV with a width FWHM of ≈ 10 MeV might be a signal for a ${}^{25}_{\eta}\mathrm{Mg}$ bound state. If this were indeed the case, then the production cross section for this state is estimated to be $0.46 \pm 0.16(\mathrm{stat}) \pm 0.06(\mathrm{syst})$ nb. If, on the other hand, it is a statistical fluctuation, this result should be interpreted rather as an upper limit.

The initial measurements of the $\gamma^3\mathrm{He} \to \pi^0 pX$ reaction [179] were very encouraging since, for back-to-back $\pi^0 p$ pairs, an enhancement was found in the total centre-of-mass energy just below the $\eta^3\mathrm{He}$ threshold. Although the significance of this peak was questioned at the time [296], this did seem like *prima facie* evidence for the decay of ${}^3_{\eta}\mathrm{He}$ into the $\pi^0 p(pn)$ channel. As already mentioned in Sec. 3.2, the later and more detailed study of this reaction [180] looked at events with different ranges of $\pi^0 p$ opening angles and found that for each angular range there were similar oscillations as a function of the c.m. energy but that these were displaced with respect to each other. It therefore seems accidental

that the maximum in the back-to-back data is close to the η^3He threshold. The newer measurements did not therefore support the claim for the photoproduction of a quasi-bound system decaying via pion emission.

Back-to-back πp pairs were also measured in deuteron-deuteron collisions, where evidence was sought for the $dd \to {}^4_\eta\mathrm{He} \to \pi^- p\,{}^3\mathrm{He}$ reaction [297]. No unambiguous signal was found for this decay, for which the upper limit put on the total cross section was ≈ 20 nb, depending upon the width of the state [297]. Simple estimates that start from data on the production of real η mesons suggest that the total cross section for $dd \to \pi^- pX$ passing through the ${}^4_\eta$He state might be of the order of 30 nb [289], but the X here refers to all three-nucleon states and not just the ^{3}He measured at COSY-WASA [297]. An upper limit of about 270 nb was found for the $pd \to {}^3_\eta\mathrm{He} \to \pi^- ppp$ [298] compared to a phenomenological estimate of about 80 nb [289], though it is far from certain that the ${}^3_\eta$He pole lies in the quasi-bound region [181].

The calculations in Refs. [289] and [299] are crude but a crucial point that both stress is that data on virtual η production should not be treated in isolation from the data on real η production.

7.3 Possible η' nuclei

The transparency experiments discussed in Sec 3 seem to show that the imaginary part of the η'-nucleus potential is quite small, though these measurements were carried out for an η' momentum $\approx$1.05 GeV/c [153]. Model-dependent estimates of the real part of the η'-nucleus potential from measurements of inclusive η' photoproduction from a ^{12}C target suggest an attraction of depth $\approx$37 MeV [168]. These arguments were behind the proposal to search for η' mesons bound in a nucleus [20, 300].

A counter argument would point to the COSY11 measurements of the $pp \to pp\eta'$ total cross section [206, 207, 208]. As is very evident in Fig. 34, the near-threshold data show no sign of any significant η'-proton interaction and any model dependence here is very limited. Furthermore, the production of η' in the $pd \to {}^3\mathrm{He}\,\eta'$ reaction near threshold is about three orders of magnitude weaker than for the η [257]. As a consequence, searches for η'-mesic nuclei might be even less fruitful than those for the η.

8 Conclusions and outlook

We have reviewed the production of η and η' mesons and $\eta\pi$ pairs with both photon and hadron beams. Reactions on free protons and quasi-free protons and neutrons bound in light nuclei were treated, as well as events where the whole nucleus played a more intrinsic role. Though electroproduction was not explicitly considered, it is abundantly clear that, due to the limited availability of pion beams, most of the important information in the ηN and $\eta' N$ sectors will come from electromagnetic probes. This is already true with the existing data set but it will be reinforced by the abundant data for single and double polarization observables still under analysis or yet to be taken. A careful analysis of these data will certainly cast more light on the *missing* $I = \frac{1}{2}$ $N^\star$ resonances. Furthermore, also the investigation of the decays of this mesons in view of their transition form factors and fundamental symmetries is shifting from hadron induced reactions to electromagnetic production; but this would be the topic of a different review.

The low energy ηN system, accessed with either photon or pion beams, clearly shows evidence for the dominance of the $S_{11}(1535)$ isobar. This sits close to the threshold and it has roughly 50% branching ratios into both ηN and πN channels. This ensures that the low energy η-nucleon interaction is strong (and attractive). The strength is also reflected in the energy dependence of the $pp \to pp\eta$ total cross section and, most spectacularly, in the dependence of the $\eta\,{}^3$He yields near threshold in both $\gamma\,{}^3$He and dp collisions. The variation of the angular shape and the spin dependence all suggest that there is a quasi-bound or quasi-virtual state very close by. However, none of the experiments that detect a

real η-meson emerging can ever separate these two possibilities. On the other hand, experiments that searched for other decay modes of the mesic nuclei below threshold have been rather negative or, at best, inconclusive.

Experiments to study the η' have been hampered by its much smaller production cross section and the lack of such a clean decay signal to identify the meson. It is, however, clear that there is no equivalent of the $S_{11}(1535)$ isobar to dominate the low-energy $\eta' N$ system. Though there are attempts to search for η' bound to nuclei, such experiments will certainly be *challenging*.

Surprisingly, in the threshold region photoproduction of $\eta\pi$ pairs is already much better understood than production of η' mesons. In a sense, the $\eta\pi$ final state is more similar to η production because it is also clearly dominated by the excitation of one single nucleon resonance, namely the $D_{33}(1700)$, which decays for example via the $\Delta(1700) \to \eta\Delta(1232) \to \eta N\pi$ chain. This is reflected in the Dalitz plots of the reaction, angular distributions, kinetic energy spectra of the mesons, and also the isopin dependence of the reaction.

The production of the $\eta\pi$ system might be more interesting for the mesic nucleus hunt and the $\gamma\, ^4\mathrm{He} \to \pi^0\eta\, ^4\mathrm{He}$ reaction might allow one to investigate the low energy $\eta\, ^4\mathrm{He}$ system to compare with the data extracted from the $dd \to \eta\, ^4\mathrm{He}$ reaction. However, in both these cases a real η meson is produced and so neither will give an unambiguous result regarding the possible binding to the nucleus.

More data is likely to appear from proton-induced reactions. Some new data for pion-induced reactions may also arise from, for example, the HADES experiment at GSI. However, over the next few years it will still be information from electron machines that is likely to dominate the database because several of the facilities and experiments will undergo upgrades. We look forward to this with anticipation!

Many people have helped us over the years to research this material and it would be invidious to pick any out. However, we would like to remember two workers in the field, Ben Nefkens and Sven Kullander, who left us earlier this year.

9 Appendix A: Comparison of conflicting $\gamma n \to n\eta$ results

As mentioned in Sec. 2.1.1, the kinematically reconstructed results from the ELSA [43] and MAMI [44, 50] experiments for quasi-free η-production off the deuteron differ in absolute scale. At the left hand side of Fig. 45, the quasi-free results without kinematic reconstruction are shown as functions of the incident photon energy E_γ. In contrast to the kinematically reconstructed data, they are in excellent agreement for protons and in reasonable agreement (within systematic uncertainties) for neutrons.

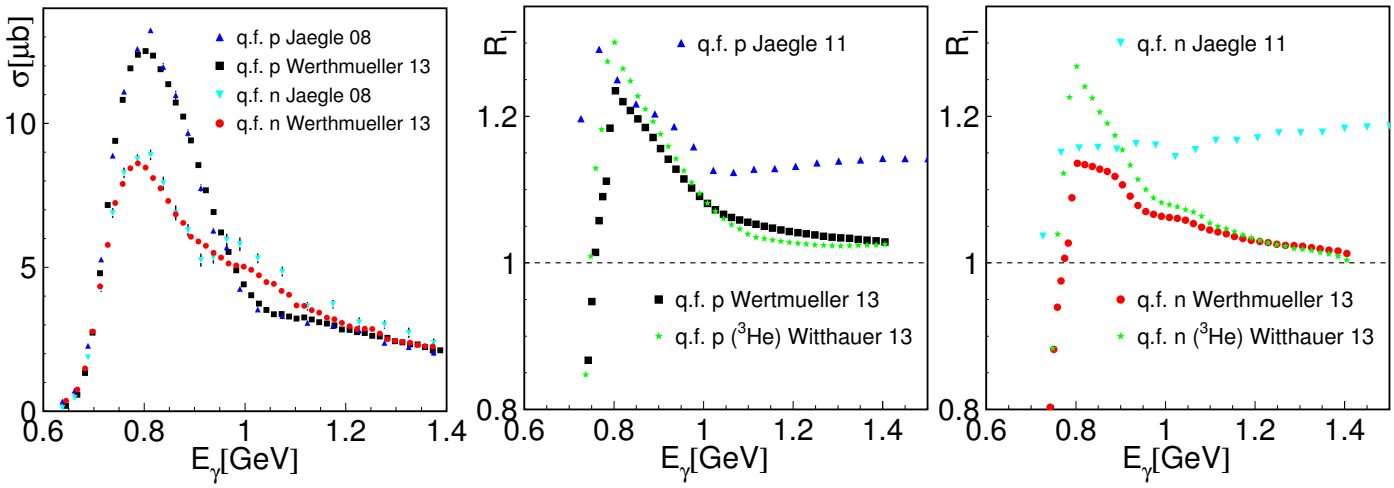

Figure 45: Left: comparison of quasi-free $\gamma N \to N\eta$ data for deuteron targets from ELSA [56] and MAMI [44, 50]. Centre: comparison of the $R_I(E_\gamma)$ factors (see text) for quasi-free protons [43, 44, 45]. Right: the same comparison for quasi-free neutrons.

Since the kinematic reconstruction removes only the effects from Fermi motion, it may change the shape of the observed cross section, but the integral over energy should be conserved (there could be small effects from the finite range of integration but, since the cross section is small and rather flat at the high energy limit, these effects cannot be important). Consequently, the Fermi-smeared cross section $\sigma(E_\gamma)$ and the cross section $\sigma(W)$ from kinematic reconstruction as function of W should be related by:

$$\int_{E_\gamma^{(1)}}^{E_\gamma^{(2)}} \sigma(E_\gamma)\, dE_\gamma \approx \int_{W^{(1)}}^{W^{(2)}} \sigma(W)\, \frac{\delta E_\gamma}{\delta W}\, dW \tag{9.1}$$

for $E_\gamma^{(1)}$ below the η production threshold and $E_\gamma^{(2)} >> E_\gamma^{(1)}$. Since $W = \sqrt{2E_\gamma m_N + m_N^2}$, this means that

$$\int_{E_\gamma^{(1)}}^{E_\gamma^{(2)}} \sigma(E_\gamma)\, dE_\gamma \approx \frac{1}{m_N} \int_{W^{(1)}}^{W^{(2)}} \sigma(W)\, W\, dW \tag{9.2}$$

and thus

$$R_I \equiv (1/m_N) \int \sigma(W)\, W\, dW \Big/ \int \sigma(E_\gamma)\, dE_\gamma \to 1 \tag{9.3}$$

for $E_\gamma >> E_\gamma^{\rm thr}$. It is shown in Fig. 45 that the MAMI deuteron [44, 50] and ^{3}He [45] experiments approximately respect this relation for quasi-free protons and neutrons, while the ELSA deuteron data [56, 43] behave differently. This implies that there is some inconsistency between the absolute normalization of the Fermi-smeared and the kinematically reconstructed data for the ELSA deuteron experiment.

References

[1] G. Fäldt, T. Johansson, C. Wilkin, *Physica Scripta* T99 (2002) 146.

[2] P. Moskal, M. Wolke, A. Khoukaz, W. Oelert, *Prog. Part. Nucl. Phys.* 49 (2002) 1.

[3] N.G. Kelkar, K.P. Khemchandani, N.J. Upadhyay, B.K. Jain, *Rep. Prog. Phys.* 76 (2013) 066301.

[4] H. Machner, *J. Phys.* G (*in press*).

[5] B. Krusche, *Eur. Phys. J. Special Topics* 198 (2011) 199.

[6] E. Aker et al., *Nucl. Instr. and Meth.* A 321 (1992) 69.

[7] A.R. Gabler et al., *Nucl. Instr. and Meth.* A 346 (1994) 168.

[8] W. Hillert, *Eur. Phys. J.* A 28 (2006) 139.

[9] B.A. Mecking et al., *Nucl. Instr. Meth.* A 503 (2003) 513.

[10] O. Bartalini et al., *Eur. Phys. J.* A 26 (2005) 399.

[11] A. Starostin et al., *Phys. Rev.* C 64 (2001) 055205.

[12] K.-H. Kaiser et al., *Nucl. Instr. Meth.* A 593 (2008) 159.

[13] M. Sumihama et al., *Phys. Rev.* C 73 (2006) 035214.

[14] H. Yamazaki et al., *Nucl. Instr. Meth.* A 536 (2005) 70.

[15] M. Unverzagt et al., *Eur. Phys. J.* A 39 (2009) 169.

[16] S. Prakhov et al., *Phys. Rev.* C 79 (2009) 035204.

[17] P. Aguar-Bartolomé et al., *Phys. Rev.* C 89 (2014) 044608.

[18] B.M.K. Nefkens et al., *Phys. Rev.* C 90 (2014) 025206.

[19] B. Bantes et al., *Int. J. Mod. Phys. Conf. Ser.* 26 (2014) 1460093-1.

[20] M. Nanova et al., *ELSA proposal: ELSA/3-2012-BGO* (2012).

[21] V. Credé, W. Roberts, *Rep. Prog. Phys.* 76 (2013) 076301.

[22] C. Amsler, B. Krusche, T. DeGrand (Quark Model review),
in J. Beringer et al., *Phys. Rev.* D 86 (2012) 010001.

[23] J. Beringer et al. (Particle Data Group), *Phys. Rev.* D 86 (2012) 010001 and 2013 partial update for the 2014 edition.

[24] S. Agostinelli et al., *Nucl. Instr. Meth.* A 506 (2003) 250.

[25] B. Krusche et al., *Eur. Phys. J.* A 6 (1999) 309.

[26] E.M. Darwish, H. Arenhövel, M Schwamb, *Eur. Phys. J.* A 16 (2003) 111.

[27] V.E. Tarasov et al., *Phys. Rev.* C 84 (2011) 035203.

[28] M. Dieterle et al., *Phys. Rev. Lett.* 112 (2014) 142001.

[29] B. Krusche, *EPJ Web of Conf.* 72 (2014) 00012.

[30] B. Krusche et al., *Phys. Rev. Lett.* 74 (1995) 3736.

[31] F. Renard et al., *Phys. Lett.* B 528 (2002) 215.

[32] M. Dugger et al., *Phys. Rev. Lett.* 89 (2002) 222002.

[33] V. Credé et al., *Phys. Rev. Lett.* 94 (2005) 012004.

[34] T. Nakabayashi et al., *Phys. Rev.* C 74 (2006) 035202.

[35] O. Bartalini et al., *Eur. Phys. J.* A 33 (2007) 169.

[36] M. Williams et al., *Phys. Rev.* C 80 (2009) 045213.

[37] V. Credé et al., *Phys. Rev.* C 80 (2009) 055202.

[38] E.F. McNicoll et al., *Phys. Rev.* C 82 (2010) 035208.

[39] W.-T. Chiang, S.N. Yang, L. Tiator, D. Drechsel, *Nucl. Phys.* A 700 (2002) 429.

[40] W.-T. Chiang et al., *Phys. Rev.* C 68 (2003) 045202.

[41] A.V. Anisovich et al., *Eur. Phys. J.* A 48 (2012) 15.

[42] A.V. Anisovich et al., *Eur. Phys. J.* A 48 (2012) 88; `pwa.hiskp.uni-bonn.de`.

[43] I. Jaegle et al., *Eur. Phys. J.* A 47 (2011) 89.

[44] D. Werthmüller et al., *Phys. Rev. Lett.* 111 (2013) 232001.

[45] L. Witthauer et al., *Eur. Phys. J.* A 49 (2013) 154.

[46] V.A. Anisovich et al., *Eur. Phys. J.* A 49 (2013) 67.

[47] O. Bartholomy et al., *Eur. Phys. J.* A 33 (2007) 133.

[48] M. Sumihama et al., *Phys. Rev.* C 80 (2009) 052201(R).

[49] B. Krusche, S. Schadmand, *Prog. Part. Nucl. Phys.* 51 (2003) 399.

[50] D. Werthmüller et al., *Phys. Rev.* C 90 (2014) 015205.

[51] B. Krusche et al., *Phys. Lett.* B 358 (1995) 40.

[52] P. Hoffmann-Rothe et al., *Phys. Rev. Lett.* 78 (1997) 4697.

[53] J. Weiß et al., *Eur. Phys. J.* A 16 (2003) 275.

[54] V. Kuznetsov et al., *Phys. Lett.* B 647 (2007) 23.

[55] F. Miyahara et al., *Prog. Theor. Phys. Suppl.* 168 (2007) 90.

[56] I. Jaegle et al., *Phys. Rev. Lett.* 100 (2008) 252002.

[57] V. Shklyar, H. Lenske, U. Mosel, *Phys. Rev.* C 87 (2013) 015201.

[58] B. Saghai, Z. Li, *Eur. Phys. J.* A 11 (2001) 217.

[59] B. Krusche, N.C. Mukhopadhyay, J.-F. Zhang, M. Benmerrouche, *Phys. Lett.* B 397 (1997) 171.

[60] B. Krusche et al., *Z. Phys.* A 351 (1995) 237.

[61] A. Nikolaev et al., *Eur. Phys. J.* A 50 (2014) 58.

[62] R. Thompson et al., *Phys. Rev. Lett.* 86 (2001) 1702.

[63] J. Weiß et al., *Eur. Phys. J.* A 11 (2001) 371.

[64] A. Fantini et al., *Phys. Rev.* C 78 (2008) 015203.

[65] A. Bock et al., *Phys. Rev. Lett.* 81 (1998) 534.

[66] L. Tiator, D. Drechsel, G. Knöchlein, C. Bennhold, *Phys. Rev.* C 60 (1999) 035210.

[67] C.S. Akondi et al., *Phys. Rev. Lett.* 113 (2014) 102001.

[68] H. Denizli et al., *Phys. Rev.* C 76 (2007) 015204.

[69] R.G. Moorhouse, *Phys. Rev. Lett.* 16 (1966) 772.

[70] V. Shklyar, H. Lenske, U. Mosel, *Phys. Lett.* B 650 (2007) 172.

[71] D. Diakonov, V. Petrov, M.V. Polyakov, *Z. Phys.* A 359 (1997) 305.

[72] M.V. Polyakov, A. Rathke, *Eur. Phys. J.* A 18 (2003) 691.

[73] R.A. Arndt et al., *Phys Rev.* C 69 (2004) 035208.

[74] Y.I. Azimov et al., *Eur. Phys. J.* A 25 (2005) 325.

[75] A.V. Anisovich et al., *Phys. Lett.* B 719 (2013) 89.

[76] R. Shyam, O. Scholten, *Phys. Rev.* C 78 (2008) 065201.

[77] V.A. Anisovich et al., *Eur. Phys. J.* A 41 (2009) 13.

[78] M. Döring, K. Nakayama, *Phys. Lett.* B 683 (2010) 145.

[79] Ki-Seok Choi, Seung-Il Nam, Atsuhi Hosaka, Hyun-Chul Kim, *Phys. Lett.* B 636 (2006) 253.

[80] A. Fix, L. Tiator, M.V. Polyakov, *Eur. Phys. J.* A 32 (2007) 311.

[81] M. Shrestha, D.M. Manley, *Phys. Rev.* C 86 (2012) 045204, *idem* 86 (2012) 055203.

[82] J. Ajaka et al., *Phys. Rev. Lett.* 81 (1998) 1797.

[83] D. Elsner et al., *Eur. Phys. J.* A 33 (2007) 147.

[84] A.V. Anisovich et al., *arXiv:1402.7164 [nucl-ex]* (2014)

[85] S. Capstick, *Phys. Rev.* D 46 (1992) 2864.

[86] V.D. Burkert et al., *Phys. Rev.* C 67 (2003) 035204.

[87] W.T. Chiang, F. Tabakin, *Phys. Rev.* C 55 (1997) 2054.

[88] A.V. Anisovich et al., *Eur. Phys. J.* A 25 (2005) 427.

[89] J. Ahrens et al., *Eur. Phys. J.* A 17 (2003) 241.

[90] B.T. Morrison, M. Dugger, B.G. Ritchie, *AIP Conf. Proc.* 1432 (2012) 421.

[91] I.S. Barker, A. Donnachie, J.K. Storrow, *Nucl. Phys.* B 95 (1975) 347.

[92] K. Nakayama, H. Haberzettl, *Phys. Rev.* C 73 (2006) 045211.

[93] ABBHHM collaboration, *Phys. Rev.* 175 (1968) 1669.

[94] W. Struczinski et al., *Nucl. Phys.* B 108 (1976) 45.

[95] J.-F. Zhang, N.C. Mukhopadhyay, M. Benmerrouche, *Phys. Rev.* C 52 (1995) 1134.

[96] R. Plötzke et al., *Phys. Lett.* B 444 (1998) 555.

[97] M. Dugger et al., *Phys. Rev. Lett.* 96 (2006) 169905.

[98] I. Jaegle et al., *Eur. Phys. J.* A 47 (2011) 11.

[99] Ch. Elster, A. Sibirtsev, S. Krewald, J. Speth, *AIP Conf. Proc.* 717 (2004) 837.

[100] Xian-Hui Zhong, Qiang Zhao, *Phys. Rev.* C 84 (2011) 065204.

[101] F. Huang, H. Haberzettl, K. Nakayama, *Phys. Rev.* C 87 (2013) 054004.

[102] F.N. Afzal, *EPJ Web of Conf.* 73 (2014) 04005.

[103] P. Levi Sandri et al., *arXiv:1407.6991* (2014).

[104] W. Roberts, T. Oed, *Phys. Rev.* C 71 (2005) 055201.

[105] A.V. Sarantsev et al., *Phys. Lett.* B 659 (2008) 94.

[106] F. Zehr et al., *Eur. Phys. J.* A 48 (2012) 98.

[107] V.L. Kashevarov et al., *Phys. Rev.* C 85 (2012) 064610.

[108] I. Keshalashvili, A. Käser, *J. Phys. Conf. Ser.* 503 (2014) 012023.

[109] J. Ajaka et al., *Phys. Rev. Lett.* 100 (2008) 052003.

[110] V.L. Kashevarov et al., *Eur. Phys. J.* A 42 (2009) 141.

[111] E. Gutz et al., *Eur. Phys. J.* A 50 (2014) 74.

[112] I. Horn et al., *Phys. Rev. Lett.* 101 (2008) 202002.

[113] I. Horn et al., *Eur. Phys. J.* A 38 (2008) 173.

[114] E. Gutz et al., *Eur. Phys. J.* A 35 (2008) 291.

[115] E. Gutz et al., *Phys. Lett.* B 687 (2010) 11.

[116] V.L. Kashevarov et al., *Phys. Lett.* B 693 (2010) 551.

[117] A. Fix, H. Arenhövel, *Phys. Rev.* C 83 (2011) 015503.

[118] S. Strauch et al., *Phys. Rev. Lett.* 95 (2005) 162003.

[119] D. Krambrich et al., *Phys. Rev. Lett.* 103 (2009) 052002.

[120] M. Oberle et al., *Phys. Lett.* B 721 (2013) 237.

[121] M. Oberle et al., *Eur. Phys. J.* A 50 (2014) 54.

[122] A. Fix, V.L. Kashevarov, A. Lee, M. Ostrick, *Phys. Rev.* C 82 (2010) 035207.

[123] M. Döring, E. Oset, D. Strottman, *Phys. Lett.* B 639 (2006) 59.

[124] M. Döring, E. Oset, D. Strottman, *Phys. Rev.* C 73 (2006) 045209.

[125] A. Fix, *private communication* (2013)

[126] B. Krusche, *Acta Phys. Pol.* B 45 (2014) 639.

[127] F. Bulos et al., *Phys. Rev. Lett.* 13 (1964) 486.

[128] W. Deinet et al., *Nucl. Phys.* B 11 (1969) 495.

[129] W.B. Richards et al., *Phys. Rev.* D 1 (1970) 10.

[130] D.M. Binnie et al., *Phys. Rev.* D 8 (1973) 2789.

[131] N.C. Debeham et al., *Phys. Rev.* D 12 (1975) 2545.

[132] J. Feltesse et al., *Nucl. Phys.* B 93 (1975) 242.

[133] R.M. Brown et al., *Nucl. Phys.* B 153 (1979) 89.

[134] R.D. Baker et al., *Nucl. Phys.* B 156 (1979) 93.

[135] S. Prakhov et al., *Phys. Rev.* C 72 (2005) 015203.

[136] D.E. Bayadilov et al., *Phys. Atom. Nuclei* 75 (2012) 923.

[137] C. Wilkin, *Phys. Rev.* C 47 (1993) R938.

[138] H.H. Landolt, R. Börnstein, *New Series, Springer* vol I/12a (1988).

[139] R.K. Rader et al., *Phys. Rev.* D 6 (1972) 3059.

[140] A. Starostin et al., *Phys. Rev.* C 72 (2005) 015205.

[141] R.A. Arndt, W.J. Briscoe, I.I. Strakovsky, R.L. Workman, *Phys. Rev.* C 74 (2006) 045205; `http://gwdac.phys.gwu.edu`.

[142] S. Leupold, V. Metag, U. Mosel, *Int. J. Mod. Phys.* E 19 (2010) 147.

[143] B. Krusche, *Prog. Part. Nucl. Phys.* 55 (2005) 46.

[144] D. Drechsel, L. Tiator, S.S. Kamalov, S.N. Yang, *Nucl. Phys.* A 660 (1999) 423.

[145] B. Krusche et al., *Phys. Lett.* B 526 (2002) 287.

[146] B. Krusche, *Eur. Phys. J.* A 26 (2005) 7.

[147] Y. Maghrbi et al., *Eur. Phys. J.* A 49 (2013) 38.

[148] C.M. Tarbert et al., *Phys. Rev. Lett.* 112 (2014) 242502.

[149] C.M. Tarbert et al., *Phys. Rev. Lett.* 100 (2008) 132301.

[150] B. Krusche et al., *Eur. Phys. J.* A 22 (2004) 277.

[151] M. Röbig-Landau et al., *Phys. Lett.* B 373 (1996) 45.

[152] T. Mertens et al., *Eur. Phys. J.* A 38 (2008) 195.

[153] M. Nanova et al., *Phys. Lett.* B 710 (2012) 600.

[154] M. Kotulla et al., *Phys. Rev. Lett.* 100 (2008) 192302.

[155] N. Bianchi et al., *Phys. Rev.* C 54 (1996) 1688.

[156] H. Geissel, et al., *Phys. Rev. Lett.* 88 (2002) 122301.

[157] T. Ishikawa et al., *Phys. Lett.* B 608 (2005) 215.

[158] T. Yorita et al., *Phys. Lett.* B 476 (2000) 226.

[159] T. Kinoshita et al., *Phys. Lett.* B 639 (2006) 429.

[160] O. Buss et al., *Phys. Reports* 512 (2012) 1.

[161] A. Hombach, A. Engel, S. Teis, U. Mosel, *Z. Phys.* A 352 (1995) 223.

[162] M. Effenberger, A. Hombach, S. Teis, U. Mosel, *Nucl. Phys.* A 614 (1997) 501.

[163] J. Lehr, M. Effenberger, U. Mosel, *Nucl. Phys.* A 671 (2000) 503.

[164] J. Lehr, U. Mosel, *Phys. Rev.* C 64 (2001) 042202.

[165] E. Hernández, E. Oset, *Z. Phys.* A 341 (1992) 201.

[166] V.K. Magas, L. Roca, E. Oset, *Phys. Rev.* C 71 (2005) 065202.

[167] M. Kaskulov, E. Hernandez, E. Oset, *Eur. Phys. J.* A 31 (2007) 245.

[168] M. Nanova et al., *Phys. Lett.* B 727 (2013) 417.

[169] E.Ya. Paryev, *J. Phys.* G 40 (2013) 025201.

[170] R. Nasseripour et al., *Phys. Rev. Lett.* 99 (2007) 262302.

[171] M.H. Wood et al., *Phys. Rev.* C 78 (2008) 015201.

[172] M. Thiel et al., *Eur. Phys. J.* A 49 (2013) 132.

[173] J. Weil, U. Mosel, V. Metag, *Phys. Lett.* B 723 (2013) 120.

[174] D. Jido, H. Nagahiro, S. Hirenzaki, *Phys. Rev.* C 85 (2012) 032201.

[175] H. Nagahiro et al., *Phys. Rev. Lett.* 94 (2005) 232503.

[176] E. Oset, A. Ramos, *Phys. Lett.* B 704 (2011) 334.

[177] V. Hejny et al., *Eur. Phys. J.* A 6 (1999) 83.

[178] V. Hejny et al., *Eur. Phys. J.* A 13 (2002) 493.

[179] M. Pfeiffer et al., *Phys. Rev. Lett.* 92 (2004) 252001; *idem* 94 (2005) 049102.

[180] F. Pheron et al., *Phys. Lett.* B 709 (2012) 21.

[181] T. Mersmann et al., *Phys. Rev. Lett.* 98 (2007) 242301.

[182] J. Smyrski et al., *Phys. Lett.* B 649 (2007) 258.

[183] J. S. McCarthy, I. Sick, R. R. Whitney, *Phys. Rev.* C 15 (1977) 1396.

[184] L. Lichtenstadt et al., *Phys. Lett.* B 219 (1989) 394.

[185] M. Egorov, A. Fix, *Phys. Rev.* C 88 (2013) 054611.

[186] I. Jaegle, *Chinese Phys.* C 33 (2009) 1340.

[187] E. Pedroni et al., *Nucl. Phys.* A 300 (1978) 321.

[188] W.B. Tippens et al., *Phys. Rev.* D 63 (2001) 052001.

[189] J.C. Peng et al., *Phys. Rev. Lett.* 63 (1989) 2353.

[190] E.J. Stephenson et al., *Phys. Rev. Lett.* 91 (2003) 142302.

[191] J.C. Peng et al., *Phys. Rev. Lett.* 58 (1987) 2027.

[192] L.C. Liu, *Phys. Lett.* B 288 (1992) 18.

[193] J.C. Peng, in *Production and decay of light mesons*, Ed. P. Fleury (World Scientific, 1988) p. 102.

[194] M. Kohno, H. Tanabe, *Nucl. Phys.* A 519 (1990) 755.

[195] B.V. Krippa, J.T. Londergan, *Phys. Lett.* B 286 (1992) 216.

[196] E. Chiavassa et al., *Phys. Lett.* B 322 (1994) 270.

[197] H. Calén et al., *Phys. Lett.* B 366 (1996) 39.

[198] A.M. Bergdolt, et al., *Phys. Rev.* D 48 (1993) R2969;

[199] F. Hibou et al., *Phys. Lett.* B 438 (1998) 41.

[200] J. Smyrski et al., *Phys. Lett.* B 474 (2000) 182.

[201] P. Moskal et al., *Phys. Rev.* C 69 (2004) 025203.

[202] P. Moskal et al., *Eur. Phys. J.* A 43 (2010) 131.

[203] N. de Marco, *private communication* (2001).

[204] G. Agakishiev et al., *Eur. Phys. J.* A 48 (2012) 74.

[205] F. Balestra et al., *Phys. Lett.* B 491 (2000) 29.

[206] P. Moskal et al., *Phys. Rev. Lett.* 80 (1998) 3202.

[207] P. Moskal et al., *Phys. Lett.* B 474 (2000) 416.

[208] E. Czerwiński, P. Moskal, M. Silarski, *Acta Phys. Polon.* B 45 (2014) 739.

[209] K. Teilab, *Int. J. Mod. Phys.* A 26 (2011) 694.

[210] G. Fäldt, C. Wilkin, *Phys. Lett.* B 382 (1996) 209.

[211] H. Petrén et al., *Phys. Rev.* C 82 (2010) 055206.

[212] H. Calén et al., *Phys. Lett.* B 458 (1999) 190.

[213] M. Abdel-Bary et al., *Eur. Phys. J.* A 16 (2003) 127.

[214] A. Deloff, *Phys. Rev.* C 69 (2004) 035206.

[215] K. Nakayama, J. Haidenbauer, C. Hanhart, J. Speth, *Phys. Rev.* C 68 (2003) 045201.

[216] C. Pauly, Ph.D. thesis, Hamburg University, 2006.

[217] V. Bernard, N. Kaiser, U.-G. Meißner, *Eur. Phys. J.* A 4 (1999) 259.

[218] S. Dymov et al., *Phys. Rev. Lett.* 102 (2009) 192301.

[219] F. Balestra et al., *Phys. Rev.* C 69 (2004) 064003.

[220] R. Czyżykiewicz et al., *Phys. Rev. Lett.* 98 (2007) 122003.

[221] P. Moskal, M. Hodana, *J. Phys. Conf. Ser.* 295 (2011) 012080.

[222] M. Hodana, P. Moskal, I. Ozerianska, M.J. Zieliński, *Acta Phys. Pol.* B 45 (2014) 697.

[223] E. Chiavassa et al., *Phys. Lett.* B 337 (1994) 192.

[224] E. Scomparin, PhD thesis, University of Turin (1993).

[225] H. Calén et al., *Phys. Rev. Lett.* 79 (1997) 2642.

[226] S. Häggström, PhD thesis, *Acta Universitatis Upsaliensis* 13 (1997).

[227] H. Calén et al., *Phys. Rev. Lett.* 80 (1998) 2069.

[228] H. Calén et al., *Phys. Rev.* C 58 (1998) 2667.

[229] P. Moskal et al., *Phys. Rev.* C 79 (2009) 015208.

[230] G. Fäldt, C. Wilkin, *Physica Scripta* 64 (2001) 427.

[231] E. Czerwiński et al., *Phys. Rev. Lett.* 105 (2010) 122001.

[232] C. Adolph et al., *Phys. Lett.* B 677 (2009) 24.

[233] J. Złomańczuk, PrimeNet Workshop, Bonn (2009);
`http://www.itkp.uni-bonn.de/~kubis/PrimeNet/Program.html`.

[234] M.J. Zieliński, P. Moskal, A. Kupsc, *Eur. Phys. J.* A 47 (2011) 93.

[235] E. Chiavassa et al., *Zeit. Phys.* A 342 (1992) 107.

[236] E. Chiavassa et al., *Zeit. Phys.* A 344 (1993) 345.

[237] E. Chiavassa et al., *Nuovo Cim.* 107 A (1994) 1195.

[238] E. Vercellin et al., *Nuovo Cim.* 106 A (1993) 861.

[239] J. Banaigs et al., *Phys. Lett.* 45B (1973) 394.

[240] P. Berthet et al., *Nucl. Phys.* A 443 (1985) 589.

[241] J. Berger et al., *Phys. Rev. Lett.* 61 (1988) 919.

[242] T. Kirchner, PhD thesis, Université de Paris-Sud, (1993).

[243] B. Mayer et al., *Phys. Rev.* C 53 (1996) 2068.

[244] M. Betigeri et al., *Phys. Lett.* B 472 (2000) 267.

[245] R. Bilger et al., *Phys. Rev.* C 65 (2002) 044608.

[246] H.-H. Adam et al., *Phys. Rev.* C 75 (2007) 014004.

[247] T. Rausmann et al., *Phys. Rev.* C 80 (2009) 017001.

[248] P. Adlarson et al., *Eur. Phys. J.* A 50 (2014) 100.

[249] V.N. Nikulin et al., *Phys. Rev.* C 54 (1996) 1732.

[250] C. Kerboul et al., *Phys. Lett.* B 181 (1986) 28.

[251] J.-F. Germond, C. Wilkin, *J. Phys.* G 16 (1990) 381.

[252] J.-F. Germond, C. Wilkin, *J. Phys.* G 15 (1989) 437.

[253] K. Kilian, H. Nann, *AIP Conf. Proc.* 221 (1991) 185.

[254] G. Fäldt, C. Wilkin, *Nucl. Phys.* A 587 (1995) 769.

[255] K.P. Khemchandani, N.G. Kelkar, B.K. Jain, *Phys. Rev.* C 68 (2003) 064610.

[256] C. Wilkin et al., *Phys. Lett.* B 654 (2007) 92.

[257] R. Wurzinger et al., *Phys. Lett.* B 374 (1996) 283.

[258] G. Fäldt, C.Wilkin, *Phys. Lett.* B 354 (1995) 20.

[259] M. Papenbrock et al., *Phys. Lett.* B 734 (2014) 333.

[260] F. Hibou et al., *Eur. Phys. J.* A 7 (2000) 537.

[261] R. Bilger et al., *Phys. Rev.* C 69 (2004) 014003.

[262] U. Tengblad, G. Fäldt, C. Wilkin, *Eur. Phys. J.* A 25 (2005) 267.

[263] A. Lai et al., *Phys. Lett.* B 533 (2002) 196.

[264] F. Ambrosino et al., *J. High Energy Phys.* 12 (2007) 73.

[265] D.H. Miller et al., *Phys. Rev. Lett.* 99 (2007) 122002.

[266] P. Goslawski et al., *Phys. Rev.* D 85 (2012) 112011.

[267] F. Plouin et al., *Phys. Lett.* B 276 (1992) 526.

[268] M. Abdel-Bary et al., *Phys. Lett.* B 619 (2005) 281.

[269] E. Scomparin et al., *J. Phys.* G 19 (1993) L51.

[270] A. Budzanowski et al., *Phys. Rev.* C 82 (2010) 041001 (R).

[271] J.S. Al-Khalili, M.B. Barbaro, C. Wilkin, *J. Phys.* G 19 (1993) 403.

[272] R. Frascaria, et al., *Phys. Rev.* C 50 (1994) 537 (R).

[273] N. Willis, et al., *Phys. Lett.* B 406 (1997) 14.

[274] A. Wrońska et al., *Eur. Phys.* J. A 26 (2005) 421.

[275] A. Budzanowski et al., *Nucl. Phys.* A 821 (2009) 193.

[276] C. Bargholtz et al., *Phys. Lett.* B 644 (2007) 299.

[277] M. Berłowski et al., *Phys. Rev.* D 77 (2008) 032004.

[278] P. Adlarson et al., *Phys. Lett.* B 707 (2012) 243.

[279] K. Schönning et al., *Phys. Lett.* B 685 (2010) 33.

[280] M. Büscher, P. Fedorets, *private communication* (2011).

[281] R.S. Bhalerao, L.C. Liu, *Phys. Rev. Lett.* 54 (1985) 865.

[282] Q. Haider, L.C. Liu, *Phys. Lett.* B 172 (1986) 257, *idem* 174 (1986) 465E.

[283] Q. Haider, L.C. Liu, *Phys. Rev.* C 66 (2002) 045208.

[284] Q. Haider, *private communication* (2010).

[285] E. Friedman, A. Gal, J. Mareš, *Phys. Lett.* B 725 (2013) 334.

[286] F. Plouin, P. Fleury, C. Wilkin, *Phys. Rev. Lett.* 65 (1990) 690.

[287] N.V. Shevchenko et al., *Phys. Rev.* C 58 (1998) 3055 (R).

[288] A. Khoukaz, D. Schroer, COSY proposal #211 (2012), `http://collaborations.fz-juelich.de/ikp/anke/proposal/Proposal_211_pndeta.pdf`.

[289] C. Wilkin, *Acta Phys. Pol.* B 45 (2014) 603.

[290] R.E. Chrien et al., *Phys. Rev. Lett.* 60 (1988) 2595.

[291] J.B. Lieb, in *Proc. Int. Conf. Nucl. Phys.*, Sao Paulo, Brazil (1988).

[292] G.A. Sokol et al., *Part Nucl. Lett.* 102 (2000) 71.

[293] V.A. Baskov et al., *PoS (Baldin ISHEPP XXI)* (2012) 102.

[294] S.V. Afanasiev et al., *Nucl. Phys. B (Proc. Suppl.)* 219-220 (2011) 255.

[295] A. Budzanowski et al., *Phys. Rev.* C 79 (2009) 012201 (R).

[296] C. Hanhart, *Phys. Rev. Lett.* 94 (2005) 049101.

[297] P. Adlarson et al., *Phys. Rev.* C 87 (2013) 035204.

[298] P. Moskal, J. Smyrski, *Acta Phys. Pol.* B 41 (2010) 2281.

[299] S. Wycech, W. Krzemień, *Acta Phys. Pol.* B 45 (2014) 745.

[300] K. Itahashi et al., *Prog. Theor. Phys.* 128 (2012) 601.